공학박사학위논문

플라즈마 원자막 증착 이트리아 안정화 지르코니아 및 고체산화물 연료전지에의 적용

Plasma Enhanced Atomic Layer Deposition of Yttria-stabilized Zirconia and Its Application to Solid Oxide Fuel Cells

2016년 2월

서울대학교 대학원

기계항공공학부

조 구 영

Plasma Enhanced Atomic Layer Deposition of Yttria-Stabilized Zirconia and Its Application to Solid Oxide Fuel Cells

by

Gu Young Cho

A Dissertation Submitted in Partial Fulfillment

of the Requirements for the Degree of

DOCTOR OF PHILOSOPHY

Department of Mechanical and Aerospace Engineering

Seoul National University

February 2016

ABSTRACT

Plasma Enhanced Atomic Layer Deposition of Yttria stabilized Zirconia and Its Application to Solid Oxide Fuel Cells

Gu Young Cho

Department of Mechanical and Aerospace Engineering

Seoul National University

Student number: 2009-20723

Thin film solid oxide fuel cells (TF-SOFCs) are considered as promising next generation energy conversion devices due to its many advantages. Because of nanometer class thin film electrolyte and electrodes, TF-SOFCs can operate at low temperature (usually lower than 500 °C) compared with typical SOFCs (usually above 700 °C). This low operation temperature of TF-SOFCs allows unique strong points, such as fast start up, mitigated thermal degradation and relaxed thermal stress. Also, TF-SOFCs have fuel flexibility, high efficiency, and no requirement of water management. TF-SOFCs are fabricated by using many thin film techniques such as sputtering, pulsed laser deposition (PLD), and atomic layer deposition (ALD). Among various thin film techniques, ALD is

adopted to fabricate thin film electrolyte of TF-SOFCs due to its dense and pin-hole free nature. In addition, ALD shows many strong points, such as low temperature process (generally lower than 400 °C), precise thickness control, superior step coverage, and good uniformity because of surface limited reaction. Thus, ALD Y_2O_3 stabilized ZrO_2 (YSZ) thin film electrolyte is widely used as a thin film electrolyte for TF-SOFCs. However, ALD generally shows poor crystallinity (due to low operation temperature), very low growth rate, and contamination problems (dependent on oxidant).

Plasma enhanced atomic layer deposition (PEALD) or plasma assisted atomic layer deposition (PAALD) is a kind of energy enhanced ALD method. Because of utilization of plasma, PEALD shows unique advantages compared with typical ALD, such as, improved growth rate, enhanced crystallinity, negligible impurities, flexibility of precursor, and expansion of process temperature. In spite of above strong points, to the best of our knowledge, PEALD YSZ and PEALD YSZ based TF-SOFCs are not studied anywhere. Therefore, in this study, investigations of PEALD YSZ thin films and PEALD YSZ based TF-SOFCs are carried out.

First, effects of preparation process on properties of YSZ films are evaluated. Sputter, thermal ALD, and PEALD YSZ films are compared. Thermal ALD YSZ films show lots of carbon impurities due to poor reactivity of oxygen gas as an oxidant. PEALD YSZ and sputter YSZ show polycrystalline structure, but thermal ALD YSZ film show almost amorphous or nanocrystalline structure. Open circuit voltages (OCVs) of TF-SOFC based on sputter YSZ films are measured very low value under 500 nm thick compared with

thermal ALD or PEALD YSZ thin film electrolyte cell. Interestingly, thermal ALD YSZ cell show almost identical OCVs (~0.8V) regardless of electrolyte thickness due to internal leakage current caused by carbon impurities. In contrast, PEALD YSZ cell show higher OCV (1.09 V) and maximum power density (168.2 mW/cm^2) at 500 °C. TEM analysis also shows that amorphous structure of thermal ALD YSZ and polycrystalline structure of PEALD YSZ. To improve low OCV of thermal ALD YSZ cell, various after treatments are carried out. Surface oxygen plasma treatment, addition of PEALD YSZ layer (30nm), and addition of sputter YSZ layer (150nm) improved OCVs at 500 °C (more than 1.0 V).

After comparison of effects of preparation method, properties of PEALD YSZ thin films were characterized. Influence of plasma power and duration on properties of PEALD YSZ films is systematically studied. Chemical composition of PEALD YSZ films has no relation with plasma conditions. Also, because of superior reactivity of plasma species, all PEALD YSZ films show negligible carbon impurities. Interestingly, in-plane conductivities of YSZ films are improved as the plasma power and duration were increased. TEM analysis shows that higher plasma power and duration induced almost epitaxial growth of YSZ films and less grain boundaries. Finally, electrochemical characteristics of 200 W-16 s PEALD YSZ based TF-SOFC are carried out at 450 °C (95.4 mW/cm^2) and 550 °C (217.5 mW/cm^2).

After characterization, optimization of Y_2O_3 concentration of PEALD YSZ thin film electrolyte is carried out. Y_2O_3 concentration is controlled by changing ZrO_2 : Y_2O_3 ratio in the YSZ supercycle.

Regardless of very similar surface morphology, cross-sectional structure, and degree of crystallinity, higher Y_2O_3 concentrated PEALD YSZ cell (10.73 mol. % Y_2O_3) show the best performance (180 mW/cm^2) compared with other cells (32.4 mol. % - 27 mW/cm^2, 7. 24 mol. % - 143 mW/cm^2, and 4.95 mol. % - 83 mW/cm^2) at 450 °C due to higher density of oxygen vacancies at the cathode-electrolyte interface.

In addition, ZrO_2 is considered as a promising high k material. In order to use various strong points of ZrO_2 for temperature sensitive substrates, such as polymers or metal foils, low temperature (100 °C) PEALD ZrO_2 deposition process is developed, and then, chemical, physical, and electrical properties of LT PEALD ZrO_2 thin films are characterized. Impurities in LT PEALD ZrO_2 films are negligible due to superior reactivity of plasma species despite of low temperature. As the plasma power and duration are increased, crystal structure, leakage current characteristics, capacitance characteristics of LT-PEALD ZrO_2 films are improved. Dielectric constants of LT PEALD ZrO_2 films are calculated from capacitance characteristics.

Lastly, PEALD Y_2O_3 thin film deposition process is also developed, and then, chemical, physical and electrical characteristics of PEALD Y_2O_3 thin films are investigated. Regardless of deposition temperature of Y_2O_3 films, all Y_2O_3 films show negligible carbon contaminations compared with thermal Y_2O_3 films with O_2 reactant because of superior reactivity of oxygen plasma. Degree of crystallinity and film density of PEALD Y_2O_3 thin films are improved as the deposition temperature is increased. Dielectric constant of

PEALD Y_2O_3 thin films are calculated by using capacitance characteristics measured by metal-insulator-metal (MIM) structure.

This study is devoted to investigate properties of PEALD YSZ and characterize TF-SOFCs based on PEALD YSZ thin film electrolyte. By evaluation of influence of plasma power and duration on properties of PEALD YSZ, comparison between thermal ALD YSZ and PEALD YSZ, and optimization of Y_2O_3 concentration of PEALD YSZ for TF-SOFCs are systematically carried out. The results of this study may help to expand the utilization of PEALD and TF-SOFCs for various applications.

Key words: Thin film solid oxide fuel cells, plasma enhanced atomic layer deposition, atomic layer deposition, yttria-stabilized zirconia, thin film, anodized aluminum oxide.

CONTENTS

LIST OF FIGURES

LIST OF TABLES

CHAPTER 1 INTRODUCTION

1.1 Motivation

Fuel cells are considered as the next generation power solutions because of their inherent many strong points. Fuel cells produce electricity by using electrochemical reactions which allows direct conversion from chemical energy of fuel to electrical energy without any complex and inefficient mid-process steps. This is the origin of many strong points of fuel cells and the most obvious difference from internal combustion power sources which use hydrocarbon fuel such as gasoline or diesel. In terms of utilization of electrochemical reactions, fuel cells are more similar to batteries than internal combustion power sources. In contrast, fuel cells can produce electricity as long as the fuel is supplied like internal combustion engines. [1-3] In summary, fuel cells have advantage of both batteries (direct production of electricity from fuel by using electrochemical reactions) and internal combustion engines (production of electricity as long as the fuel is supplied).

In addition, fuel cells have more interesting advantages. [1] Compared with the internal combustion engines, because of direct conversion from chemical energy to electrical energy

by electrochemical reactions, fuel cells are generally more efficient. In addition, fuel cells usually have no mechanical moving components. It implies that fuel cells are absolutely silent, long-lasting, and reliable than internal combustion power generators. Moreover, typical fuel cells generate almost zero emissions such as CO_x, NO_x and SO_x when H_2 is used as a fuel. Compared with the batteries, fuel cells usually have higher energy density and are generally recharged shortly by re-fueling. Also, fuel cells have scalability in power and capacity from watt class (portable recharger of smart devices) to megawatt class (power plant or stationary power unit). [1-3]

	PEMFC	PAFC	AFC	MCFC	SOFC
Electrolyte	Polymer membrane	Liquid H_3PO_4	Liquid KOH	Morten carbonate	Ceramic
Charge carrier	H^+	H^+	OH^-	CO_3^{2-}	O^{2-}
Operating temperature	80˚C	200˚C	60-220˚C	650˚C	600-1000˚C
Catalyst	Platinum	Platinum	Platinum	Nickel	Perovskite (ceramic)
Cell components	Carbon based	Carbon based	Carbon based	Stainless based	Ceramic based
Fuel compatibility	H_2, methanol	H_2	H_2	H_2, CH_4	H_2, CH_4, CO

Table 1.1. Description of fuel cell types [1]

In general, fuel cells are categorized by their electrolytes or

operation temperature. [1] Table 1.1. shows major fuel cells, phosphoric acid fuel cells (PAFCs), polymer electrolyte membrane fuel cells (PEMFCs), alkaline fuel cells (AFCs), molten carbonate fuel cells (MCFCs), and solid oxide fuel cells (SOFCs)) classified in their electrolytes and operation temperature. Among fuel cells listed in table 1.1, SOFCs, kind of high temperature fuel cells (HTFCs), use stabilized (or doped) oxide electrolytes such as Y_2O_3 stabilized ZrO_2 (YSZ), Gd_2O_3 doped CeO_2 (GDC), Y_2O_3 doped CeO_2 (YDC), Sc_2O_3 stabilized ZrO_2 (ScSZ), and yttrium doped barium zirconate (BZY). [1,2,4–84]

Typical SOFCs are generally operated at high temperature (> 700 °C) due to temperature dependent ion conductivity of ceramic electrolyte, i.e. poor ionic conductivity at low temperature. In SOFCs, fundamental electrochemical reactions are as follows using H_2 as a fuel. [1,2]

$$\text{(Anode) } 2H_2 + O^{2-} \rightarrow H_2O + 2e^-$$

$$\text{(Cathode) } \frac{1}{2}O_2 + 2e^- \rightarrow O^{2-}$$

SOFCs have been researched due to their unique strong points compared with other fuel cells because of their high operation temperature (> 700 °C). [1,2,4–86] SOFCs generally show high efficiency, especially in the form of

combined heat power generation. [85,86] Because of oxide electrolyte, there is no fuel cross-over problem through electrolyte which is a crucial problem of PEMFCs or direct methanol fuel cells (DMFCs). SOFCs have no water management problem which is also the most critical problem in PEMCs or DMFCs due to high operation temperature. Also, because of high operation temperature, SOFCs have no requirement of noble metal catalyst such as platinum (Pt), palladium (Pd), or Ruthenium (Ru) to enhance electrochemical reactions. In addition, there is no CO poisoning problems which is also one of the most critical problems in PEMFCs. Moreover, SOFCs can use hydrocarbon fuels directly such as methane and butane due to high operation temperature. (fuel flexibility)

This high operation temperature of SOFC causes not only many advantages but also many crucial problems. [1,2,4–84] SOFCs usually require high cost thermal resist materials to compose power generation systems. SOFCs also have sealing problem, thermal degradation problems of materials, severe thermal stress problems caused by mismatch of thermal expansion coefficient between components. [1,2,4–84]

In order to mitigate these problems caused by high operation temperature of SOFCs, there have been many researches to lower the operation temperature of SOFCs. [4–84] The ohmic resistance mainly caused by ionic conduction

through electrolyte is calculated by a followed equation.

$$R = \rho \times \frac{L}{A} = \frac{1}{\sigma} \times \frac{L}{A}$$

Where R is a resistance, ρ is a resistivity, σ is a conductivity, L is a length (thickness of electrolyte), and A is an cross sectional area.

According to the above equation, there are two main research approaches to compensate poor ionic conductivity (severe ohmic resistance) of solid oxide electrolyte at low temperature. [1,2] The one method is to develop new materials with high ionic conductivity (increase σ) at reduced temperature such as GDC, YDC, and BZY. [6,12,26,30,39,87–93] The other approach is to apply semiconductor thin film techniques such as pulsed laser deposition (PLD), sputter, spray pyrolysis, chemical solution deposition (CSD), chemical vapor deposition (CVD), atomic layer deposition (ALD), and plasma enhance atomic layer deposition (PEALD) to minimize the thickness of electrolyte (reduce L). [4–84] Thin film electrolyte prepared by above mentioned thin film techniques can reduce the ionic path about nanometer scale between anode and cathode, and then, minimize the ohmic resistance caused by electrolyte and achieve high performance at low temperature. [4–84] In terms of utilization of thin film

facilities, display or semiconductor production facilities, i.e. thin film technique facilities – sputter, CVD and ALD, can be used to fabricate thin film solid oxide fuel cells (TF-SOFCs) composed of thin film electrodes and electrolyte. This implies that TF-SOFCs are much favorable to mass production than typical SOFCs fabricated by wet process such as sol-gel or screen printing methods due to fast and precise characteristics of semiconductor thin film techniques. Because of these reasons, intensive researches have been conducted about TF-SOFCs operated at low temperature (< 550 °C), recently. [4-84]

Y_2O_3 stabilized ZrO_2 (YSZ) or Y_2O_3 doped ZrO_2 (YDZ) is the most well-known and reliable oxygen ion conducting material for SOFCs, oxygen pumps, and oxygen membranes because of its relatively high oxygen ion conductivity at high temperature, low electron conductivity, and superior chemical stability for both reducing and oxidizing environment. [1,2,5,21,94] Because of above strong points of YSZ, YSZ is used or studied for many applications, such as a gate oxide for dynamic random access memories, thermal barrier coatings, bonding coatings, buffer layers for high temperature superconducting, and ferroelectric films. [94-99] However, most of all, YSZ is usually used as an oxygen ion conducting electrolyte for typical SOFCs or TF-SOFCs. In prior studies of TF-SOFCs, YSZ thin film electrolytes are prepared by various thin film

techniques such as PLD, magnetron reactive / radio frequency (RF) sputtering, CSD, CVD, ALD, PEALD and etc. [4–84,100–107]

In TF–SOFCs, quality of thin film electrolyte such as defects, stoichiometry, and contaminations is the critical issue to ensure high performance – voltage, maximum power density – of fuel cells at low temperature. Especially, pin–hole like defects in thin film electrolyte can cause internal short circuit or break gas tightness between anode and cathode, and then, can reduce the performance of TF–SOFCs. [1,36,72,81] Interestingly, considering requirements of thin film electrolyte, ALD or PEALD are quite appropriate to deposit thin film electrolyte compared with aforementioned various thin film techniques. ALD is a kind of chemical vapor deposition method. Different from CVD, precursor (source) pulsing step and oxidant (reactant) pulsing step are perfectly separated by purging steps. Because of this separated process, ALD generally shows superior step coverage and uniformity of thin films. Moreover, it is widely known that thin films prepared by ALD have no pinhole like defects. [108–112] This indicates that ALD process is clearly suitable for fabrication of TF–SOFCs, especially thin film electrolyte which needs strict requirements about pinhole free and gas tightness. Consequently, extensive researches on TF–SOFCs based on ALD have been carried out. [4,17,19,21,28] PEALD,

a kind of energy enhanced ALD method, also have fundamental advantages of typical ALD. In addition, thin films prepared by PEALD usually show enhanced crystallinity, less impurities, and improved stoichiometry compared with the typical thermal ALD because of superior reactivity of plasma species such as activated atoms, ions, and electrons. Because of these advantages, researches about thin films including oxides and pure metals prepared by PEALD have been gradually increased recent years. [108,110,112] However, to the best of our knowledge, there have been no researches about TF-SOFCs based on PEALD.

Therefore, TF-SOFCs based on thin film YSZ electrolyte prepared by PEALD, as a promising power generation devices combined with the next generation thin film techniques, become attractive research subject.

1.2 Background Studies

1.2.1 Thin Film Solid Oxide Fuel Cells

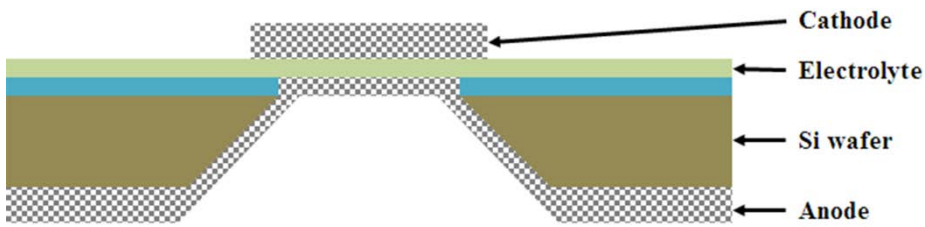

Figure 1.1. Schematics of free-standing TF-SOFCs

TF-SOFCs are categorized in two different types according to their substrate structure. The one is the free-standing TF-SOFCs. Figure 1.1. shows schematics of free-standing TF-SOFCs. By combining microelectromechanical system (MEMS) process (e.g. deep reactive ion etching process and photolithography process) and thin film techniques (sputter and ALD), most of free-standing TF-SOFCs have tens of nanometer scale thin film electrolyte.[46–52,54–60] Furthermore, MEMS process allows 3-dimensional structure of TF-SOFCS such as corrugated structure and pyramid structure. [28,32] In prior research about the flat free standing TF-SOFCs, ~ 1.0 V open circuit voltages (OCVs)

and 155 mW/cm2 ~ power density were measured at 510 °C by using sputtered 54 nm thick YSZ thin film electrolyte. [57] In other studies about the flat free standing TF-SOFCs, 1.02 V ~ 1.10V open circuit voltages (OCVs) and 28 mW/cm^2 ~ 270 mW/cm^2 power density are measured in the temperature range from 265 °C ~ 350 °C by using 60 nm thick ALD YSZ thin film electrolyte. [21] Improved charge transfer kinetics of ALD YSZ caused by nano-crystalline YSZ films is speculated by enhancement of performance. In spite of high power density of flat free-standing TF-SOFCs, its total power output (W) is too small to apply in practical use because of limited electrochemical active area of fuel cells. Electrochemical active areas of typical flat free standing TF-SOFCs are usually hundreds of square nanometer due to thermos-mechanical stability. [46–52,54–60] In order to overcome this limited active area, aforementioned various 3-dimensional nano-structuring methods are applied to free-standing TF-SOFCs. [28,32] Corrugated 3-dimensional structure composed of cup-shapes by deep reactive ion etching is applied to free-standing TF-SOFCs. [32] This corrugated free standing TF-SOFCs shows 677 mW/cm^2 at 400 °C with 70 nm thick ALD YSZ thin films electrolyte which is almost 1.9 times higher perk power density than flat free-standing TF-SOFCs. Also, 3-dimensional pyramid structure of free standing TF-SOFCs is prepared by using

nano-sphere lithography method to enlarge the electrochemical active area and ALD YSZ thin film electrolyte (~50 nm). [28] Including Y_2O_3 doped CeO_2 (YDC) cathode functional layer which helps oxygen reduction reactions (ORRs), 3-dimensional free-standing TF-SOFCs show 1.34 W/cm^2 at 450 °C.

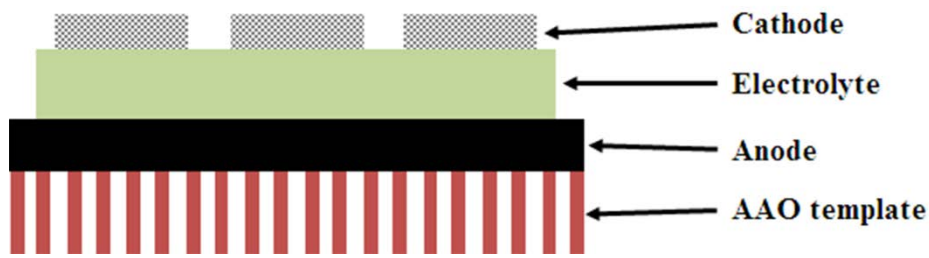

Figure 1.2. Schematics of AAO-based TF-SOFCs

The other is the nano-porous template based TF-SOFCs such as anodic aluminum oxide (AAO) based TF-SOFCs. [4,6,9–11,13–15,17,19,25,64,113] Figure 1.2. illustrates the schematics of AAO-based TF-SOFCs. Nano-porous substrates such as AAO provide both superior thermo-mechanical stability and effective gas (fuel) supply to electrode at the same time. This superior thermo-mechanical stable nano-porous supporting structure allows the enlargement of electrochemical active area in square centimeter scale. [11] Nano-porous template based TF-SOFCs is also relatively easy and simple to fabricate by using

thin film techniques compared with free-standing TF-SOFCs which require complex MEMS process such as reactive ion etching and photolithography patterning. Moreover, sandwich structure of electrode between oxide template and electrolyte helps to mitigate thermal degradation of bottom electrode. Because of above advantages of nano-porous templates, researches about nano-porous substrate based TF-SOFCs are intensively carried out recently. [4,6,9–11,13–15,17,19,25,64,113] Park et al. shows influence of anode structure on electrochemical characteristics of AAO based TF-SOFCs. [15] Porous and thick anode helps to increase triple phase boundaries (TPBs) where electrochemical reactions are occurred between anode and electrolyte interface and to reduce in-plane electronic resistance at bottom electrode, and then, enhance the performance of TF-SOFCs. Park et al. reported that 450 nm thick porous Pt anode (using sputtering, prepared at 12 Pa of Ar) showed 165 mW/cm^2 at 500 °C with 500 nm thick sputtered YSZ thin film electrolyte which is 2.8 times higher than 450 nm dense Pt anode (80 nm diameter AAO, using sputtering, prepared at 0.67 Pa of Ar) Ji et al. reported that TF-SOFCs based on same templates with 20 nm thick GDC anode functional layer which was inserted between bottom electrode and electrolyte showed 120 mW/cm^2 at 500 °C with 500 nm thick sputtered YSZ thin film electrolyte [10] Ji et al. also reported that ALD

YSZ – sputtered GDC bilayer thin film electrolyte on identical AAO templates measured 110 mW/cm^2 at 450 °C with dense Pt ALD cathode catalyst layer with porous Pd cathode. [9] Ha et al. reported that results of ALD YSZ – sputter YSZ hybrid thin film electrolyte based high performance TF–SOFCs – 180 mW/cm^2 at 450 °C. [19] In addition, S. Ji et al. reported results of AAO based PEALD YSZ thin film electrolyte TF–SOFCs with 70 nm thick PEALD YSZ thin film electrolyte – 175 mW/cm^2 at 500 °C. [17]

However, because of inherent relatively rough surface, AAO based TF–SOFCs are usually trouble with pinholes or defects problems in thin film electrolyte. [113] In order to minimize the possibility of formation of pinholes during fabrication of thin film electrolyte and mitigate the roughness of surface of anode, AAO based TF–SOFCs usually have hundreds of nanometer thick dense anode structure on supporting templates and hundreds of nanometer thick electrolyte. [4,6,9–11,13–15,17,19,25,64,113] Most of prior studies based on 80 nm diameter pore AAO used from 150 nm to 450 nm thick Pt anode. [4,6,9–11,13–15] In addition, insertion of blocking layer to prevent growth of pinholes or defects by using dense and pinhole free nature of ALD thin films. [113,114] Kwon et al, used ALD Al_2O_3 functional layer to prevent growth of pinhole in YSZ thin film electrolyte prepared by PLD. TF–SOFCs with Al_2O_3 functional layer cell

showed 350 mW/cm^2 at 500 °C. Yu et al, also used PEALD YSZ functional layer for same purpose – the defect blocking layer. TF-SOFCs with PEALD YSZ functional layer and GDC cathode functional layer showed at 172 mW/cm^2 at 500 °C.

In summary, there are two types of TF-SOFCs – free-standing TF-SOFCs and nano-porous template based TF-SOFCs. Free-standing TF-SOFCs usually shows superior maximum power density even at low temperature. However, free-standing TF-SOFCs are generally troubled with thermo-mechanical problems due to their mechanically unstable structure and insufficient electrochemical active area (total power output). In contrast, nano-porous template based TF-SOFCs, e.g. AAO based TF-SOFCs, shows slightly lower power density compared with free-standing TF-SOFCs. Nevertheless, because of fully supporting structure, AAO based TF-SOFCs generally shows superior thermo-mechanical stability and much larger electrochemical active area compared with free-standing TF-SOFCs. Therefore, the use of nano-porous templates (AAOs) as the supporting microstructure for the TF-SOFCs allows the preparation of thin (sub-micrometer thick), denes, mechanically stable electrolyte of high ionic conductive and minimum thickness to maximize the performance of TF-SOFCs. If ALD or PEALD methods are applied to fabricate or modify thin film electrolytes, the thickness of electrolyte can be minimized.

1.2.2 Atomic Layer Deposition

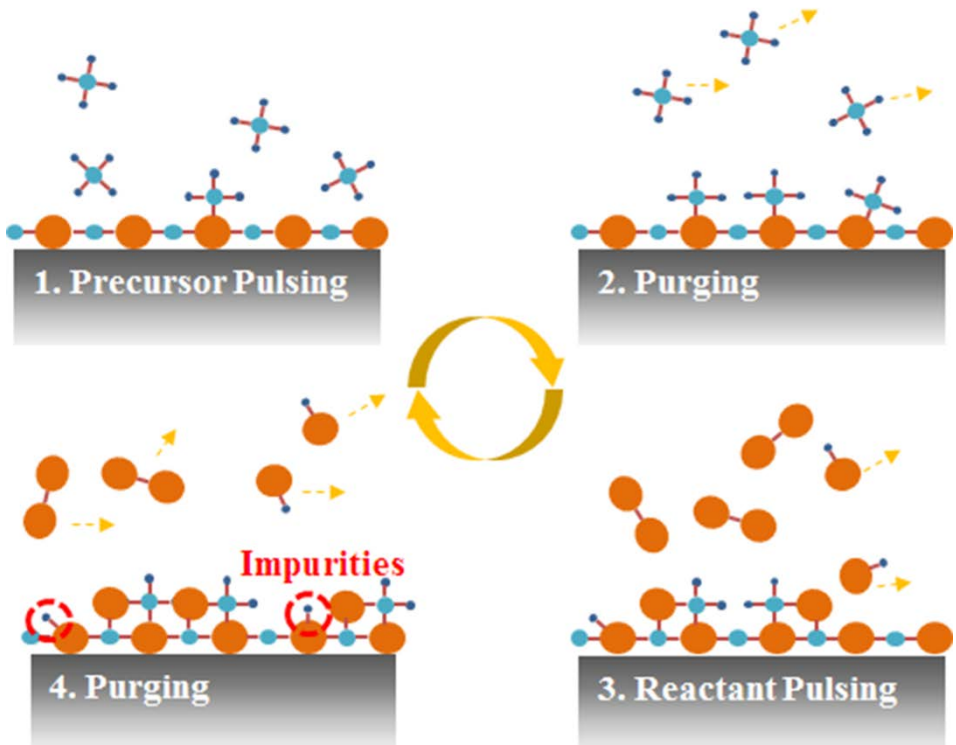

Figure 1.3. Sequential process steps of the thermal ALD cycle

As mentioned above, atomic layer deposition (ALD) or atomic layer epitaxy (ALE) is a kind of modified chemical vapor deposition. Figure 1.3. shows sequential process steps of the thermal ALD cycle. As seen in figure 1.3., one ALD process is composed of four different steps, as follows: 1) first precursor (source) pulsing: gas state precursor molecules are introduced into reaction chamber where the substrate is positioned at specific temperature.

Physisorption or chemisorption of precursor molecules are happened – 2) purging un-reacted excessive precursor: in order to prevent gas state reactions between excessive reactant molecules (not physisorbed or chemisorbed molecules) and oxidant molecules which will be introduced next step, remaining precursor molecules are removed. – 3) reactant (oxidant) pulsing and chemical reactions: gas state reactant molecules are introduced to reaction chamber and chemical reactions are occurred between first precursor molecules and reactant molecules. – 4) purging un-reacted remaining reactant: similar to step 2), in the same manner, un-reacted reactant molecules are removed. Because of this unique process which is perfectly separated precursor pulsing and reactant pulsing by purging steps, surface self-limited reactions are occurred. Thus, ALD has distinct strong points compared with other thin film techniques including CVD. Thin films fabricated by ALD generally show good uniformity with smooth surface. Also, precise thickness control (theoretically from angstrom to nanometer scale) of target thin film is available. In addition, superior step coverage and conformality of thin films on complex 3-dimensional structure is possible.

Because of above many strong points, ALD YSZ is intensively applied as a functional layer of SOFCs or thin film electrolyte of TF-SOFCs. Also, intensive studies about physical, chemical, and electrochemical characteristics of ALD YSZ films have been carried out. [4,6,19,21,28,32,36,38,41,43,45] As mentioned above, Shim et al. prepared ALD YSZ thin films by using custom-made thermal ALD and applied as a thin film electrolyte of free-standing TF-

SOFCs. [21] In order to deposit 8 mol. % Y_2O_3 in YSZ thin films which is generally known the best conductivity, ratio between ZrO_2 vs. Y_2O_3 in the YSZ supercycle was maintained 7 during deposition. The fuel cell showed 28 mW/cm^2 ~ 270 mW/cm^2 in the temperature range from 265 °C ~ 350 °C, respectively. Because of pinhole free nature of ALD, only 60 nm thick YSZ thin film successfully acted as electrolyte (prevent formation of short circuit, maintain gas tightness, and oxygen ion conductivity). The fuel cell with ALD YSZ thin film electrolyte showed much higher performance than the cell with sputter YSZ thin film electrolyte. It was speculated that nanocrystalline characteristics of ALD YSZ thin films are the reason of this high performance. ALD YSZ thin films also used as a thin film electrolyte of 3-dimensional free standing TF-SOFCs because of superior step coverage and comformality. Su et al. reported that corrugated free standing TF-SOFCs with ALD YSZ thin film electrolyte. [32] The cell showed 677 mW/cm^2 and 861 mW/cm^2 at 400 °C and 450 °C, respectively. In addition, An et al. also reported three dimensional pyramid structured free-standing TF-SOFCs based on ALD YSZ and PVD YDC bilayer thin film electrolyte. (1.3 W/cm^2 at 450 °C) Interestingly, Son et al. investigated influence of Y_2O_3 concentration of ALD YSZ thin films on in-plane conductivity. [115] Different from generally known results (8 mol. % Y_2O_3 concentration shows best ionic conductivity in bulk YSZ), 10.9 mol. % of Y_2O_3 concentrated YSZ thin film showed best in-plane oxygen ion conductivity. Inhomogeneous Y_2O_3 doping was believed to the reason of the difference of optimal Y_2O_3 concentration between bulk YSZ and ALD YSZ. Notably, Chao

et al. reported that effects of Y_2O_3 concentration on cathode functional layered of ALD YSZ. [41,43] Similar to results of in-plane conductivity of ALD YSZ thin films, highly Y_2O_3 concentrated ALD YSZ (11~14 mol. % Y_2O_3) thin films showed best performance enhancement. It was considered that high Y_2O_3 concentration in the ALD YSZ films increases the oxygen vacancies at the surface of electrolyte which helps the oxygen incorporation reactions at cathode-electrolyte interface.

1.2.3 Plasma Enhance Atomic Layer Deposition

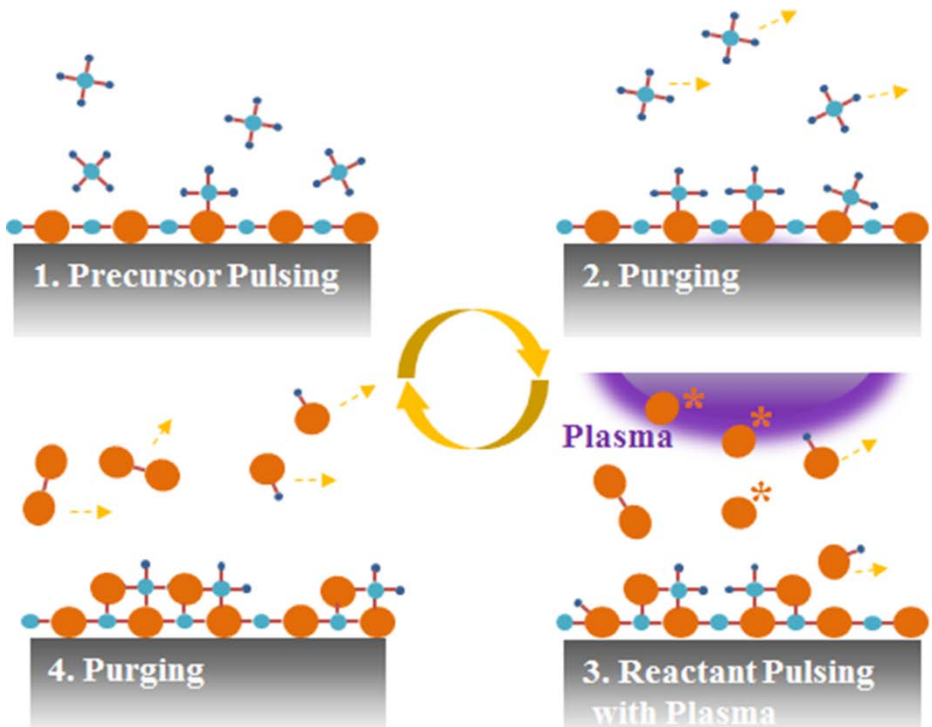

Figure 1.4. Sequential process steps of the PEALD cycle

Plasma enhance atomic layer deposition (PEALD), or plasma assisted atomic layer deposition (PAALD) is a type of energy enhance atomic layer deposition method. [108,110,112] PEALD is basically identical with typical thermal ALD except utilization of plasma power source. Figure 1.4. shows the sequential process steps of the PEALD cycle. As seen in figure 1.4., the most obvious difference of the PEALD for thermal ALD is that plasma generation

at reactant step which means utilization of the superior reactivity of plasma species – activated atoms, ions, and electrons as a reactant. Because of superior reactivity of plasma species compared with typical reactant of thermal ALD – O_2, O_3, or deionized water, PEALD shows exclusive strong points compared with thermal ALD. Based on typical thermal ALD's advantages, PEALD generally shows higher growth rate than typical thermal ALD. Moreover, by using PEALD, high quality thin films can be achievable such as improved crystallinity (supply of additional energy by bombardment of plasma species), increased film density (supply of additional energy by bombardment of plasma species) less impurities (superior reactivity of plasma species), improved stoichiometry (superior reactivity of plasma species), flexibility of precursor (superior reactivity of plasma species), and expansion of ALD window to low temperature area (superior reactivity of plasma species). [108,110,112] Because of above strong points, there have been intensive researches about thin films prepared by PEALD, including high k oxide material thin films to apply semiconductor or display. [108,110,112] However, to the best of author's knowledge, there are no earlier researches about application of PEALD to fabricate YSZ thin films and TF-SOFCs. As a result, characterization of PEALD YSZ and application of PEALD YSZ to TF-SOFCs will provide significant insights in the design of high performance TF-SOFCs.

1.3 Thesis Outlines

This thesis concentrates on characteristics of PEALD YSZ and utilization of PEALD YSZ as oxygen ion conducting thin film electrolytes of AAO based TF-SOFCs. The main body of this dissertation composed of 6 chapters. Each chapter organizes as follows:

Chapter 2 describes the properties of PEALD YSZ thin films. Influences of plasma power and plasma duration on chemical, physical and electrochemical characteristics of the PEALD YSZ thin films are investigated. First, chemical and physical characterizations of PEALD YSZ (chemical composition, crystallinity, surface morphology, and ionic conductivity) were carried out. In addition, electrochemical characterization of PEALD YSZ was carried out as a thin film electrolyte of AAO based TF-SOFCs.

Chapter 3 describes effects of preparation techniques on properties of YSZ thin films. Sputter, thermal ALD, and PEALD YSZ thin films were compared. Chemical and physical characteristics of YSZ thin films were measured. Finally, in order to investigate electrochemical properties of YSZ thin films, AAO based TF-SOFCs were used.

Chapter 4 describes optimization of Y_2O_3 doping in PEALD YSZ thin film electrolyte for TF-SOFCs. Various YSZ thin films with

different Y_2O_3 concentration were fabricated by controlling Y_2O_3 vs ZrO_2 process ratio in the YSZ supercycle. Chemical, physical, electrochemical properties of various YSZ thin films with different Y_2O_3 concentration were evaluated to clarify optimization of Y_2O_3 concentration of YSZ thin film electrolyte for TF-SOFCs..

Chapter 5 describes properties of ZrO_2 thin films prepared by PEALD at low temperature (100 °C). In order to apply to low temperature flexible material (polymers and metal foils), low temperature (LT) PEALD ZrO_2 process was developed. Chemical (chemical composition), physical (crystallinity and crystal structure, surface morphology), and electrical properties (leakage current vs. applied voltage and capacitance vs. applied voltage) of LT PEALD ZrO_2 thin films were investigated.

Chapter 6 describes characteristics of Y_2O_3 thin films prepared by PEALD. Similar to PEALD YSZ, there have been no previous studies about properties of PEALD Y_2O_3 thin films. In this chapter, therefore, PEALD Y_2O_3 thin film process was developed. Similar to chapter 5, chemical, physical, and electrical characteristics of PEALD Y_2O_3 films were systematically examined.

CHAPTER 2 EFFECTS OF PREPARATION PROCESS ON CHARACTERISTICS OF YSZ THIN FILMS

2.1 Introduction

Recently, there have been many researches about TF-SOFCs using YSZ thin film electrolyte prepared by various thin film techniques such as PLD, sputter, CSD, CVD, ALD, and PEALD. [4-84]

PLD, one of the most well-known physical vapor deposition (PVD) techniques, is widely utilized to deposit thin films such as compounds and alloys with controlled stoichiometry of chemical composition. By using pulse of high power laser, atoms or clusters are ablated or evaporated from the target surface, and then, deposited on the surface of substrates. PLD has relatively simple system design and can use many forms of targets - powder, single crystal, and polycrystalline pellets with complex chemical composition. However, limitation of uniform area which is the most critical and severe problem of PLD prevents industrial application of PLD. [122]

Sputter uses bombardments of energetic ions on the surface of target material (collision between energetic ions and surface atoms) to eject required atoms from the target surface and deposits thin

films on substrates. Sputter can fabricate almost any materials such as pure metal, alloy, oxide, and nitrides. Also, process conditions are highly reliable due to inherent simple structure. However, like PLD, limitation of uniformity and poor step coverage are also critical problems for industrial utilization. [122]

ALD and PEALD, advanced CVD methods, have exclusive characteristics compared with PLD or sputter. Because of self-limited, perfectly separated process, thin films fabricated by ALD or PEALD show better uniformity, superior step-coverage, controllability of thickness in nanometer scale, defect free, and nanocrystalline characteristics. [108,110,112]

Considering aforementioned unique characteristics of each thin film techniques, one can imagine that characteristics of nano-thin YSZ films are affected easily by preparation methods. Actually, chemical composition, crystallinity, and microstructures of films straightly affect on their characteristics and performance of devices such as YSZ thin film electrolyte based TF-SOFCs. [39,103,105,118–120] However, there are no intensive studies about influence of preparation methods on properties of YSZ thin films at the fuel cell level.

Therefore, in this chapter, characteristics of YSZ thin films which are prepared by different thin film techniques – sputter (physical vapor deposition, well-known PVD method, easy to handling), thermal ALD (chemical vapor deposition, precise thickness control, low degree of crystallinity, carbon contamination), and PEALD (chemical vapor deposition, negligible impurities, high degree of crystallinity, negligible impurity) – are compared and investigated

before application of YSZ thin film electrolyte of TF-SOFCs. After analysis of characteristics of YSZ thin films, YSZ thin film electrolytes are applied to TF-SOFCs to evaluate influence of fabrication methods on electrochemical characteristics.

2.2 Experimental

As mentioned above, YSZ thin films were prepared by sputter, thermal ALD, and PEALD methods.

For sputter YSZ films, a commercial sputtering system with RF power source (A-tech Korea) and a commercial Y-Zr metal alloy (16 atomic % Y, Adventech Korea, Korea) target was used. Fabrication of sputter YSZ film was carried out with 200 W of RF power at 0.67 Pa of Ar/O_2 mixing gas (20 vol. % O_2).

For thermal ALD YSZ and PEALD YSZ films, a commercial showerhead type direct PEALD system with capacitively coupled plasma power source was used (Atomic premium, CN1, Korea). High purity oxygen gas (99.999%, Shinjin gas, Korea) was used as an oxidant for thermal ALD YSZ and oxygen plasma was used as an oxidant for PEALD YSZ. The commercial tetrakis-(dimethylamino) zirconium precursor (TDMAZ, Sigma Aldrich, USA) and the tris-(methylcyclopentadienyl) yttrium (Strem chemicals, USA) were utilized as a source of ZrO_2 and Y_2O_3, respectively. The temperature of stainless steel canisters were maintained at 50 °C for Zr and 150 °C for Y, respectively. Stainless steel lines which connected between canisters and the reaction chamber were also maintained at 70 °C for Zr line and 165 °C for Y line to prevent condensation of precursor. Preparation of thermal ALD YSZ and PEALD YSZ were conducted at 250 °C which is well known ALD window of above precursors. [4–6,12,17,19,21,28,32,36,38,41,43,114,123]

The thermal ALD ZrO_2 process cycle was composed of as followed steps: 1) Zr pulse (3 s) – 2) Ar purging (40 s) – 3) O2 pulse (10 s) – 4) Ar purging (40 s). The thermal ALD Y_2O_3 process cycle was composed of similar steps: 1) Y pulse (3 s) – 2) Ar purging (75 s) – 3) O2 pulse (10 s) – 4) Ar purging (75 s). Because of the poor reactivity of O_2 gas for ALD process, O_2 pulse time was maintained 10 s to reduce impurities as much as possible. For PEALD, the PEALD ZrO_2 process cycle was also composed of several steps: 1) Zr pulse (3 s) – 2) Ar purging (40 s) – 3) O_2 pulse (1 s) – 4) O_2 pulse with plasma (3 s) – 5) Ar pulse (40 s). Also, the PEALD Y_2O_3 process cycle was composed of as followed steps: 1) Y pulse (3 s) – 2) Ar purging (75 s) – 3) O_2 pulse (1 s) – 4) O_2 pulse with plasma (3 s) – 4) Ar purging (75 s). In order to stabilize the oxygen partial pressure before plasma generation, 1 second of O_2 pulse step was inserted before O_2 plasma step. To prepare YSZ thin films with proper Y_2O_3 concentration, YSZ was prepared by combination of ZrO_2 process and Y_2O_3 process – YSZ supercycle. In this study, like various prior studies, 1 YSZ supercycle was composed of 7 ZrO_2 process and 1 Y_2O_3 process for both thermal ALD and PEALD to secure enough Y_2O_3 concentration (7~9 mol % Y_2O_3). [4–6,12,17,19,21,28,32,36,38,41,43,114,123]

Pieces of (100) Si wafer (LG siltron, Korea) were used for characterization of YSZ films. Before YSZ film deposition, wafer pieces were cleaned with acetone, ethanol, and deionized water for 10 minutes at 40 °C by using ultrasonic bath. Chemical compositions of YSZ films were measured by x-ray photoelectron spectroscopy (XPS, Theta probe base system, spot diameter: 400 μ

m, Al Kα (1486.6 eV), Thermo Fisher Scientific, USA). 150 eV Ar ion etching was conducted for 15 s before measurement to remove surface impurities. Crystal structures of YSZ thin films on Si wafer were analyzed by using x-ray diffraction (XRD, X' pert Pro, PANalytical, Netherlands, Cu Kα source) Detailed Cross-sectional structure of thermal ALD YSZ and PEALD YSZ thin film electrolyte based TF-SOFCs were evaluated by high resolution transmission electron microscopy (HRTEM, JEM-2100F, JEOL, Japan) with 200 keV operation voltage.

In order to characterize electrochemical characteristics of YSZ films, nano-porous AAO based TF-SOFCs were prepared with YSZ thin film electrolyte deposited by sputter, thermal ALD, and PEALD. First, dense Pt anode film was deposited on a bare AAO template to make smooth and flat surface for thin film electrolyte. 200 W of DC sputtering power was applied to pure Pt target at 0.67 Pa of Ar working pressure. After preparation of anode, YSZ thin film electrolyte was fabricated by various methods. Finally, porous Pt cathode was deposited on the top of YSZ thin film electrolyte to maximize triple phase boundaries (TPBs). Similar to anode, 100 W of DC power was used at 12 Pa of Ar pressure. Electrochemical characteristics were carried out at 500 °C with 30 sccm of pure H_2 by using custom-made experimental set-up. OCV, current density - voltage behavior, and EIS characteristics of TF-SOFCs were measured by using Solartron 1287/1260 (Solartron, UK). EIS measurements were conducted in the frequency range from 2 MHz to 2 Hz.

2.3 Results and Discussion

First, in order to examine influence of fabrication techniques on chemical composition of YSZ thin films, XPS analysis was carried out. Deposition conditions and chemical compositions of YSZ films were summarized at table 2.1.

Name (atom. %)	Sputter YSZ	Thermal ALD YSZ	PEALD YSZ
Deposition conditions	RF 200 W Ar/ O_2 (20%) 25 ˚C	O_2 (10s) Zr: 50 ˚C, Y: 150 ˚C 250 ˚C	O_2 plasma (50 W-3s) Zr: 50 ˚C, Y: 150 ˚C 250 ˚C
Zr	28.98	20.9	34.81
Y	7.15	3.1	4.87
O	63.29	62.2	58.8
C	0.59	13.8	1.51
Y_2O_3 mol. %	11.5	7	7.7

Table 2.1. Deposition condition and chemical composition of YSZ thin films

As seen in table 2.1., Y_2O_3 mol. % of sputter YSZ was higher value (~11.5 mol. %) than generally known value (~8 mol. %). It is because that high Y contents in Y/Zr alloy target (16 at. %). Chemical composition of thin films fabricated by sputtering methods is directly dependent on chemical composition of sputtering target. [121] Interestingly, in spite of long reactant step (10 s), thermal

ALD YSZ film presents very high concentration of carbon impurities (~14 at. %) compared with other YSZ films. In prior studies, there have been no reports about carbon impurities due to usage of deionized water. [21,28,32,38] It is widely known that oxygen gas used as oxidant in this study has poor reactivity as a reactant gas for ALD reactions. Oxygen gas can't remove efficiently contaminations such as carbon or nitrogen of precursor molecules. [112] Therefore, it was speculated that carbon impurities within thermal ALD YSZ films was formed during deposition due to un-sufficient reactivity of oxygen gas to remove contaminations. However, in spite of very short plasma duration (3 s), concentration of carbon contamination was very low (1.51 at. %) compared with ALD YSZ because of superior reactivity of plasma species. [108,110,112]

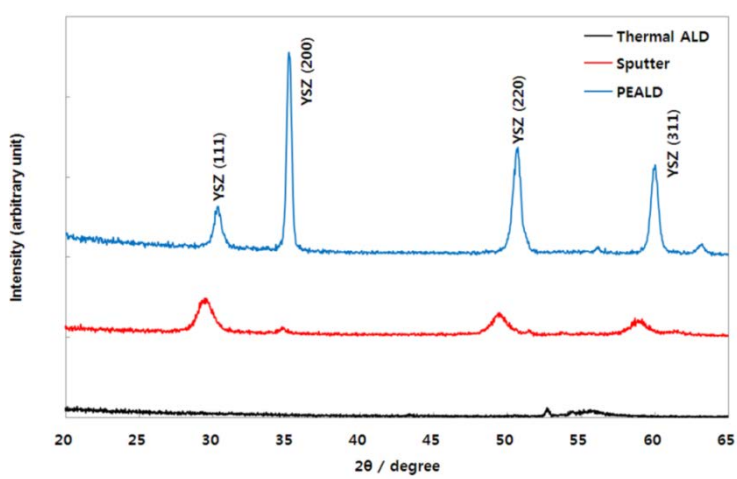

Figure 2.1. Crystal structure of YSZ thin films on Si substrate

Figure 2.1. shows crystal structure of as-deposited YSZ films on Si substrate. Thermal ALD YSZ film presents almost amorphous or very weak crystallized structure. It indicates that thermal energy of deposition temperature was not enough to form polycrystalline structure. Sputter YSZ film also shows low and broad peak of crystal structures due to weak and partially crystallized polycrystalline structure. In contrast, PEALD YSZ showed clear and sharp peaks of YSZ crystal structure compared with other YSZ films. Considering the identical deposition temperature between ALD and PEALD, this XRD result of PEALD YSZ implies that additional energy to form polycrystalline structure was provided by plasma steps – bombardment of plasma species. [108,110,112]

After film characterizations, YSZ films were applied as a thin film electrolyte of AAO-based TF-SOFCs. For thin film electrolyte, formation of pin-hole like defects and gas-tightness problems due to nanometer scale level electrolyte are very crucial issues to ensure high performance of fuel cells (OCVs and maximum power density). Therefore, in this study, OCVs of TF-SOFCs were measured as the thickness of YSZ thin film electrolytes was changed to confirm mechanical stability of YSZ thin film electrolytes. Figure 2.2. illustrates OCV results of TF-SOFCs based on YSZ thin film electrolyte prepared by sputter, thermal ALD, and PEALD.

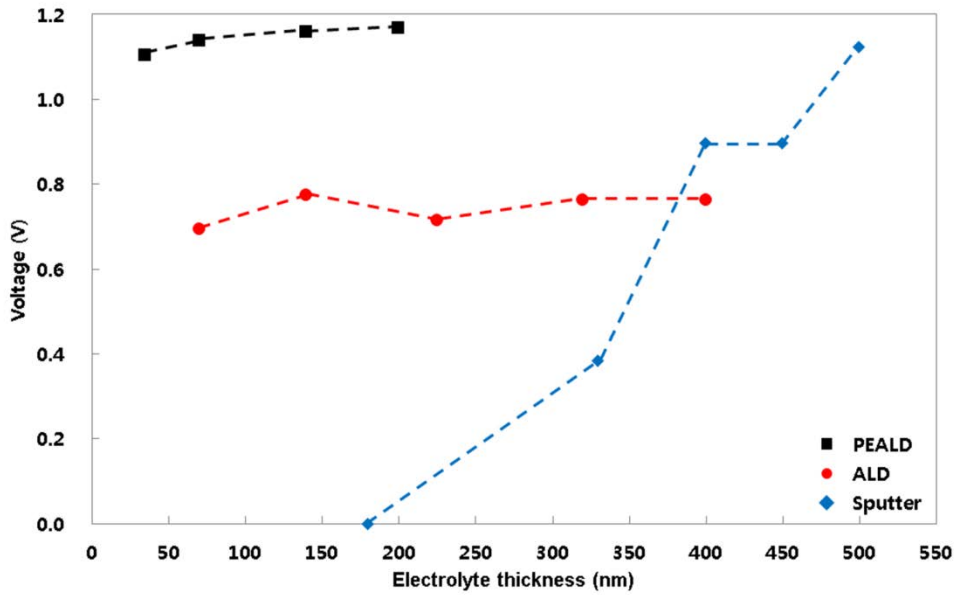

Figure 2.2. OCVs of TF-SOFCs based on YSZ thin film electrolyte formed by PEALD, thermal ALD, and sputter at 500 °C

YSZ thin film electrolytes showed noticeable OCV results depends on fabrication process. As seen in figure 2.2., TF-SOFC based on sputter YSZ electrolyte presented drastic OCV results compared with other cells, from 0 V (electrically short circuit) to above 1.0 V. 180 nm thick sputtered YSZ thin film electrolyte was not enough to ensure gas-tightness and pin-hole (defects) free. It is generally known that thin films prepared by PVD methods such as sputter and PLD have a columnar structure. [11,19,113] Also, thin films deposited on rough surface usually have many defects deposited by PVD methods. [113] Therefore, in prior researches, thin film electrolytes prepared by PVD on rough substrates, fuel cells have

hundreds of nanometer scale (submicron scale) thick electrolyte to prevent formation of electrical short circuit. [11,15,113] In the same manner, sputter YSZ cell shows over 1.0 V of OCV at 500 nm thick sputter YSZ thin film electrolyte. Interestingly, thermal ALD YSZ cells shows almost identical OCVs regardless of thickness of thin film electrolyte. From 80 nm to 400 nm thick of ALD YSZ thin film electrolyte, OCVs of ALD YSZ cells were measured from 0.7 V to 0.78 V. We speculate that these similar OCV results were caused by formation of internal short circuit in YSZ films due to high concentration of carbon contaminations. Because of internal short circuit form by carbon contaminations, OCV of ALD YSZ cell didn't increase above 1.0 V as the thickness of ALD YSZ cell was increased to 400 nm in spite of defect free thin film nature of ALD characteristics. In contrast, PEALD YSZ based fuel cells, which showed almost 0 carbon impurity concentration (< 2.0 at. %), presented superior OCVs compared with other YSZ thin film electrolyte even at very thin electrolyte (1.10 V at 35 nm YSZ thin film electrolyte). We think that this high OCVs of PEALD YSZ based TF-SOFCs caused by negligible impurities, pin-hole free and dense thin film nature of PEALD characteristics.

In order to confirm dense and pin-hole free ~140 nm thick YSZ thin film electrolyte formed by ALD and PEALD, surface morphology of YSZ electrolyte was measured by using FESEM. Figure 2.3. presents surface morphology of YSZ electrolyte.

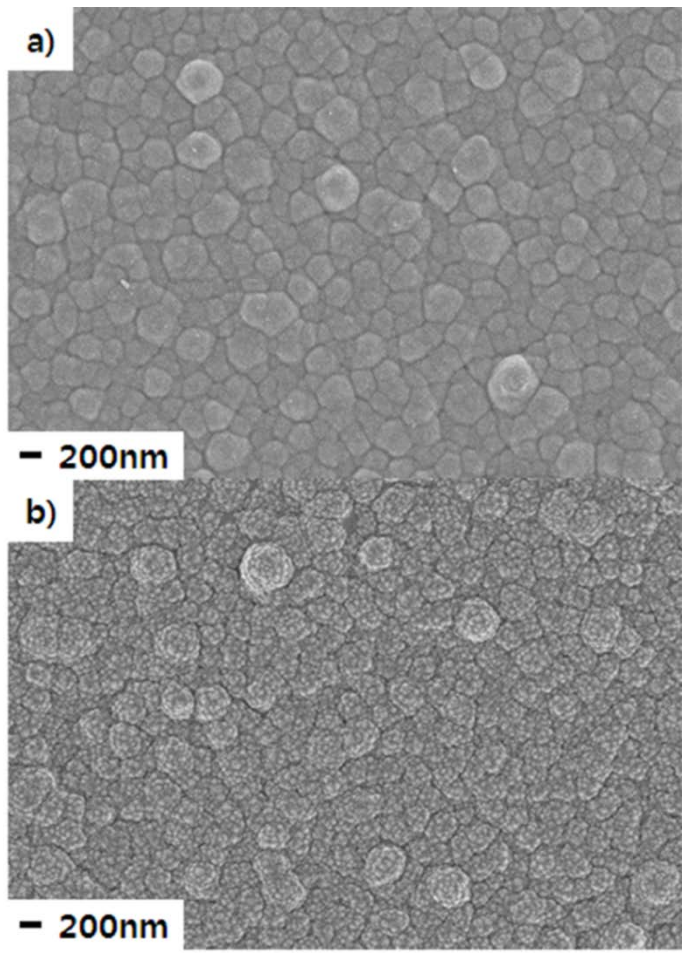

Figure 2.3. Surface morphology of ALD-YSZ and PEALD-YSZ thin film electrolyte. a) Surface morphology of ALD-YSZ thin film electrolyte. b) Surface morphology of PEALD-YSZ thin film electrolyte

As seen in figure 2.3., YSZ electrolytes showed dense, pin-hole free surface morphology regardless of deposition process. Interestingly, in figure 2.3. b), PEALD YSZ looked rougher than

ALD YSZ thin film electrolyte in figure 2.3. a). We speculated that rougher surface of PEALD YSZ was occurred by growth of facets of films at PEALD process. [124,125] Therefore, low OCV ALD YSZ thin film electrolyte cell was caused by internal leakage current through carbon impurities.

To clarify detailed investigation of YSZ electrolytes, TEM analysis was carried out. Figure 2.4., shows TFM images of YSZ electrolyte of TF-SOFCs.

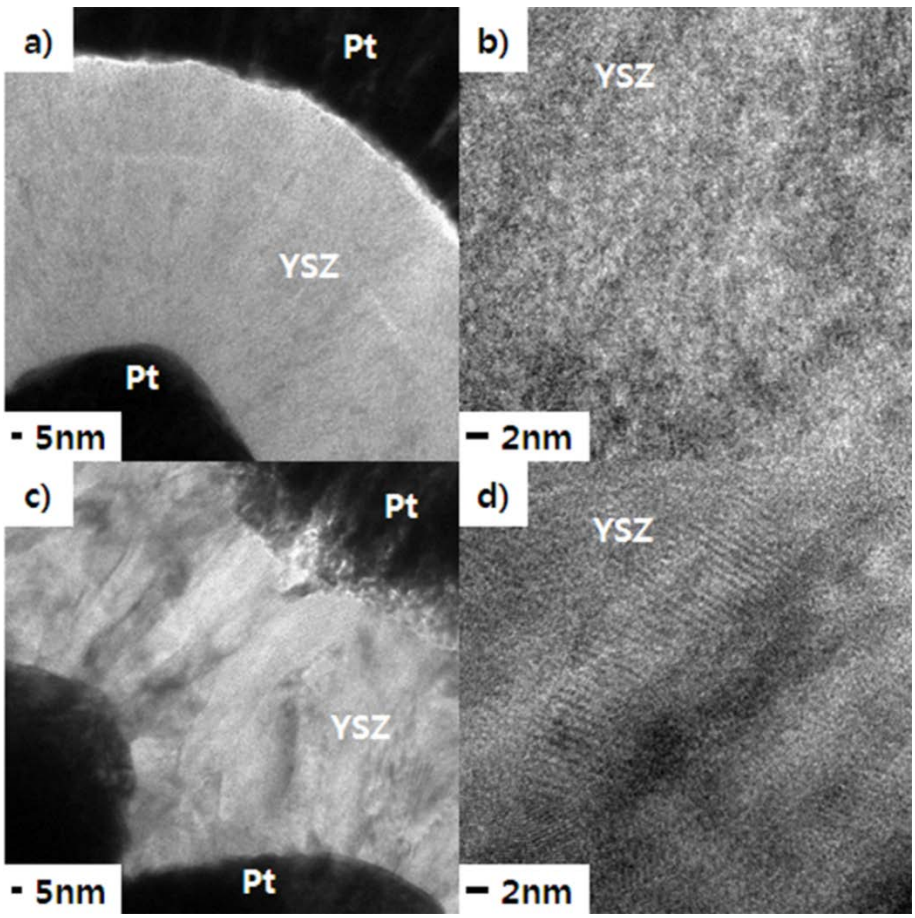

Figure 2.4. TEM images of YSZ electrolyte of TF-SOFCs. a) TEM images of ALD YSZ thin film electrolyte of TF-SOFCs. b) HRTEM images of ALD YSZ thin film electrolyte. c) TEM images of PEALD YSZ thin film electrolyte of TF-SOFCs. d) HRTEM images of PEALD YSZ thin film electrolyte.

As shown in figure 2.4., ALD YSZ and PEALD YSZ thin film electrolyte showed obvious difference. ALD YSZ, in figure 3.4. a), showed almost amorphous structure. There was no clear evidence of crystallization in whole measurement area. This TEM results was coincided with XRD results of ALD YSZ in figure 3.1. – amorphous or very weak polycrystalline structure. In contrast, in spite of low plasma power (50 W) and short duration (3 s), PEALD YSZ thin film electrolyte in figure 3.4. c) and d) showed clear polycrystalline structure. We think that this polycrystalline structure caused by superior reactivity and bombardment of plasma species. [108,110,112]

After measurements of TF-SOFCs by TEM and FESEM, electrochemical characterization was carried out at 500 °C with 30 sccm H_2 at anode side. Figure 3.5. presents polarization curves of TF-SOFCs with ALD YSZ thin film electrolyte and TF-SOFCs with PEALD YSZ thin film electrolyte.

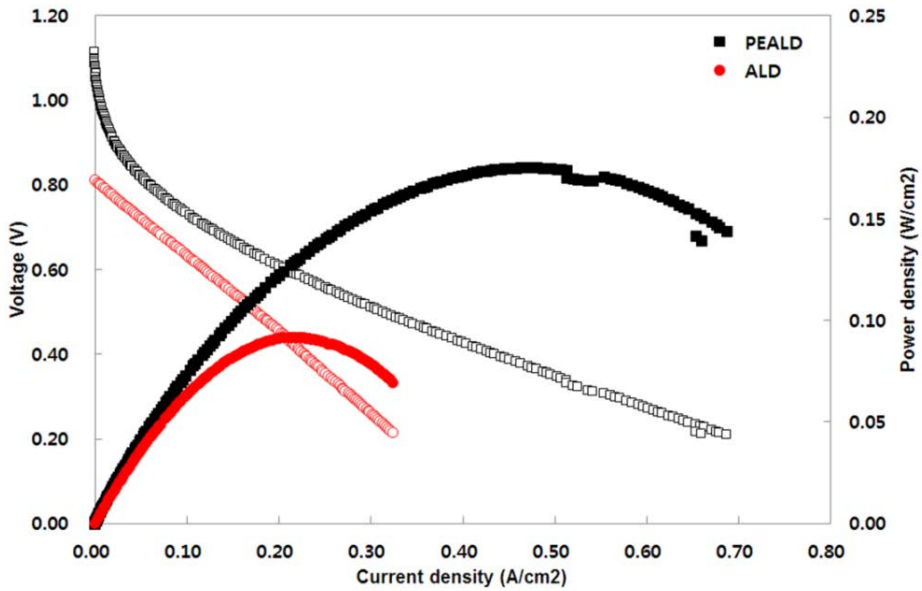

Figure 2.5. Polarization curves of TF-SOFCs

As shown in figure 2.5., a fuel cell with ALD YSZ thin film electrolyte showed lower OCV result (0.81 V), i.e. Y axis intercept point, than OCV of PEALD YSZ cell (1.09 V). Therefore, a fuel cell with ALD YSZ electrolyte cell showed lower maximum power density (91.8 mW/cm^2) than PEALD YSZ cell (168.2 mW/cm^2). Interestingly, ALD YSZ cell showed almost zero activation loss which generally showed in low current density region compared with PEALD YSZ cell. Also, in spite of similar thickness of electrolyte, ohmic resistance of ALD YSZ (grade of polarization curve, voltage-current density) seemed larger than PEALD YSZ. We speculate that carbon impurities in ALD YSZ film have great influence on activation loss and on the oxygen ion conduction.

Detailed investigations have been conducted in our group.

In order to find out detailed behavior of fuel cells, EIS measurements were carried out. Figure 3.6. illustrates EIS results of fuel cells.

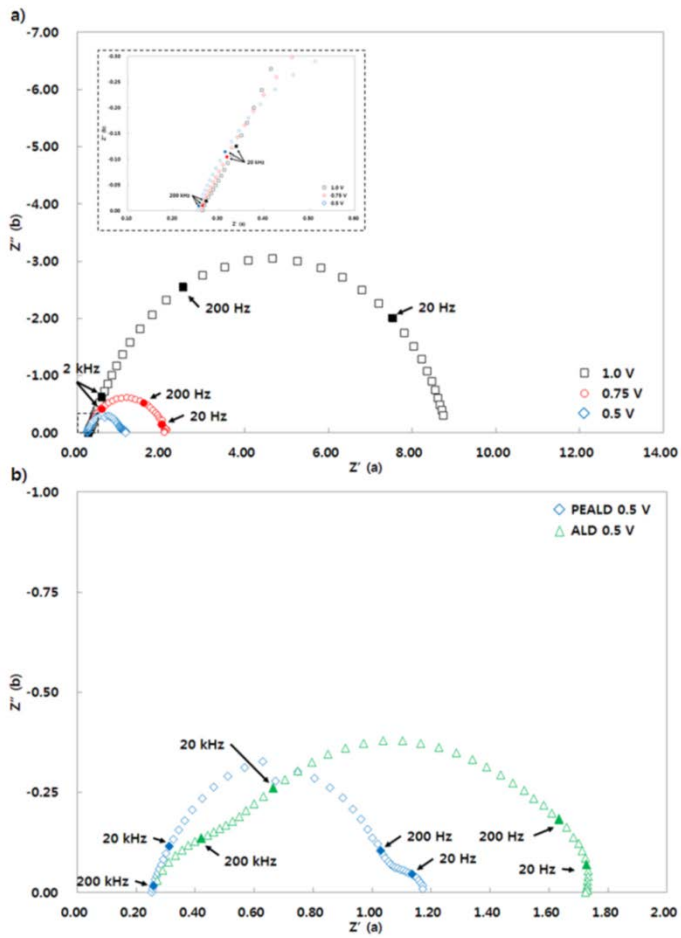

Figure 2.6. EIS results of fuel cells. a) EIS results of PEALD YSZ cell measured at 1.0 V, 0.75 V and 0.5 V. b) EIS results of ALD YSZ cell and PEALD YSZ cell at 0.5 V.

Figure 2.6. a) shows EIS results of PEALD YSZ cell measured at 1.0 V, 0.75 V and 0.5 V. The in-set showed high frequency region of EIS results to confirm the ohmic resistance of a cell. As seen in figure 3.6. a) and inset of figure 3.6. a), X-axis intercept points were very similar (0.265 $\Omega \cdot cm^2$ at 1.0 V, 0.262 $\Omega \cdot cm^2$ at 0.75 V and 0.255 $\Omega \cdot cm^2$ at 0.5 V) regardless of voltage conditions. It implies that X-axis intercept point was thought to be the ohmic resistance of a fuel cell. [1,2] Also, in PEALD YSZ cell, radius of low frequency arc was clearly decreased as the voltage was decreased. It is generally known that cathodic polarization resistance related with oxygen reduction reactions are highly affected by the cell voltage. [1,2,33,34,37,38,72,126] Therefore, cathodic polarization resistance was the main reason of decrease of fuel cell's power density due to sluggish oxygen reduction reactions at low temperature. Figure 2.6. b) shows EIS results of ALD YSZ cell and PEALD YSZ cell which were measured at 0.5 V. Unfortunately, because of low OCV of ALD YSZ cell, there was only one EIS results measured at 0.5 V. Therefore, we can't determine ohmic resistance of ALD YSZ cell. However, we can conclude that total resistance of ALD YSZ cell – total value of ALD YSZ cell was larger than PEALD YSZ cell. As mentioned above, we think that carbon contaminations in ALD YSZ films had adverse effects on electrode process and ion conduction process. More detailed

investigations have been carried out.

Finally, in order to increase OCV of ALD YSZ cell, additional treatments were carried out. Figure 2.7. shows schematics of additional treated cell to improve OCV of ALD YSZ based cell.

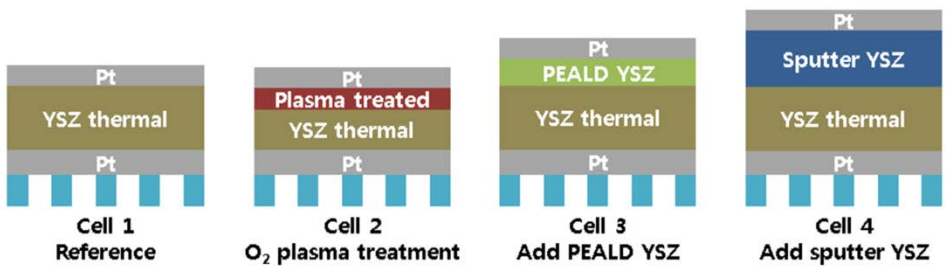

Figure 2.7. Schematics of additional treatment of TF-SOFCs with ALD YSZ thin film electrolyte.

As mentioned above, we think that carbon contaminations within ALD YSZ thin film electrolyte cause leakage current by formation of electrical circuit. Therefore, in order to prevent leakage current through ALD YSZ electrolyte, 5 minutes and 50 W of oxygen plasma treatment (cell-2), addition of 30 nm of PEALD YSZ thin film (cell-3), and addition of 150 nm of sputter YSZ thin film (cell-4) were carried out. OCV results of each cells measured at 500 °C were summarized at figure 3.8.

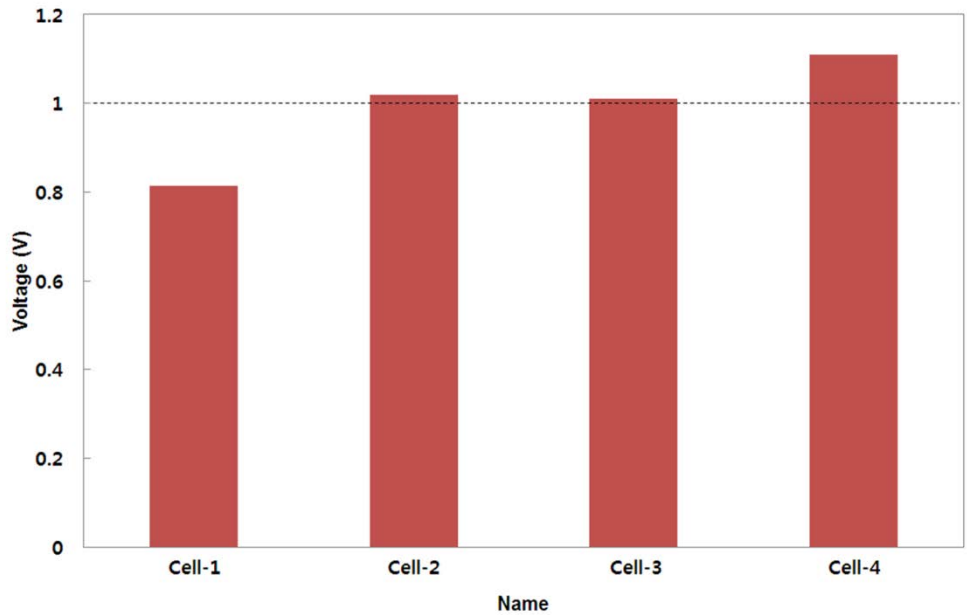

Figure 2.8. OCVs of additional treated ALD YSZ cell.

As shown in figure 2.8., OCVs of all fuel cells were obviously increased (above 1.0 V) by additional treatment. Both removal of surface carbon impurities by oxygen plasma (cell-2) and insertion of carbon free YSZ thin films (cell-3 and cell-4) worked effectively to improve OCVs. These results – improved OCVs by additional treatment – support that low OCV of ALD YSZ cell was caused by carbon contaminations in YSZ thin film electrolyte.

2.4 Conclusions

In this study, properties of YSZ thin films prepared by sputter, thermal ALD, and PEALD were characterized and compared. XPS results showed that ALD YSZ had high carbon contaminations compared with sputter or PEALD due to poor reactivity of oxygen gas. Also, ALD YSZ film showed almost amorphous or very weak polycrystalline structure. In contrast, PEALD YSZ and sputter YSZ films showed clear polycrystalline structure.

After film characterization, application of YSZ film as a thin film electrolyte of TF-SOFCs. Due to columnar structure and inherent defects of sputter YSZ films on porous substrate, TF-SOFCs required more than 500 nm thick of sputter YSZ thin film electrolyte to secure reasonable OCVs - more than 1.0 V at 500 °C. However, PEALD YSZ and ALD YSZ thin film electrolyte fuel cells showed much higher OCVs at thinner electrolyte (< 150 nm). Especially, PEALD YSZ showed higher OCVs near the theoretical value due to defects free and negligible electronic conductivity. However, ALD YSZ fuel cell showed about ~0.8 V regardless of ALD YSZ thickness. This low OCV of ALD YSZ was caused by higher carbon impurity concentration which formed electrical circuit and occurred leakage current. Therefore, TF-SOFC with ALD YSZ

showed lower OCV and maximum power density than OCV and maximum power density of PEALD YSZ cell at 500 ° C.

Finally, additional treatment was carried out to improve OCVs of ALD YSZ cell. After oxygen plasma treatment on surface on ALD YSZ thin film electrolyte to remove surface carbons and insertion of carbon free YSZ films to prevent formation of electrical circuit and leakage current were conducted. All above after treatments effectively improved OCVs of ALD YSZ cells.

CHAPTER 3 Properties of PEALD YSZ thin films

3.1 Introduction

As mentioned in chapter 1, there have been no prior intensive researches about PEALD YSZ thin films and TF-SOFCs based on PEALD YSZ thin film electrolyte. However, considering unique characteristics of PEALD caused by superior reactivity (related with chemical composition of films) and bombardment of plasma species (related with crystallinity and surface roughness of films), it is very significant to investigate about properties of PEALD YSZ. As a result, in this chapter, chemical, physical, and electrochemical properties of PEALD YSZ thin films are systematically studied. After characterization, PEALD YSZ thin films are applied as a thin film electrolyte of AAO based TF-SOFCs (AAO template - Pt anode - PEALD YSZ - Pt cathode structure) to examine electrochemical characteristics of PEALD YSZ.

In the first part of this chapter, preparation process of PEALD YSZ thin films is described. Especially, influence of plasma power and duration on properties of PEALD YSZ thin films is systematically studied. Chemical composition of YSZ films and physical properties (cross-sectional structure, degree of crystallinity, and in-plane oxygen ion conductivity) of PEALD YSZ

thin films prepared by different power and duration on single crystal MgO (100) are investigated.

In the second part of this chapter, electrochemical properties of PEALD YSZ thin films are studied as a thin film electrolyte of AAO based TF-SOFCs. As aforementioned above, nano-porous AAO supporting structure - dense Pt anode - PEALD YSZ thin films electrolyte - porous Pt cathode structure is used to evaluate electrochemical properties of PEALD YSZ thin films in the temperature range from 450 °C to 550 °C.

3.2 Experimental

A commercial showerhead type direct PEALD (Atomic premium, CN1, Republic of Korea) with capacitively coupled plasma power source was used to fabricate PEALD YSZ thin films. The commercial tetrakis (dimethylamino) zirconium precursor (TDMAZ, Sigma Aldrich, USA) and the tris (methylcyclopentadienyl) yttrium (Strem chemicals, USA) were used as a source of Zr and Y, respectively. High pure Ar gas (99.999%) and O_2 gas (99.999%) were used as a carrier gas and a source of O_2 plasma. The temperature of Zr and Y stainless steel canister were maintained at 50 °C and 150 °C during deposition, respectively. Also, the temperature of stainless line was kept at 70 °C for Zr canister – reaction chamber and 165 °C for Y canister to reaction chamber to prevent condensation of precursors. Preparation of YSZ thin films were carried out at 250 °C which is well-known ALD window temperature for both precursors. [4-6, 9, 12, 17, 21, 28, 32, 36, 38, 43, 116, 117]

1 YSZ supercycle was composed of 7 ZrO_2 cycles and 1 Y_2O_3 cycle in order to contain proper Y_2O_3 concentration in YSZ films. The ZrO_2 cycle was composed of followed several process steps: 1) Zr pulse (3 s) – 2) Ar purging (40 s) – 3) O_2 pulse (1 s) – 4) O_2 pulse with plasma (controlled) – 5) Ar pulse (40 s). Similarly, the Y_2O_3 cycle was also composed of followed process steps: 1) Y

pulse (3 s) – 2) Ar purging (75 s) – 3) O_2 pulse (1 s) – 4) O_2 pulse with plasma (controlled) – 4) Ar purging (75 s). In order to stabilize the oxygen partial pressure before plasma generation, 1 second of O_2 pulse step was inserted before O_2 plasma step. Plasma duration (3 s, 8 s, and 16 s) and plasma power (50 W, and 200 W) were systematically changed to investigate influence of plasma power and duration on properties of YSZ films.

Commercial 1 cm X 1 cm and 500 μm thick one side polished single crystal MgO (100) substrates (MTI Co., USA) were used to measure in-plane ionic conductivity of PEALD YSZ thin films. Also, commercial Si wafer (LG Siltron, Republic of Korea) pieces were used as substrates to investigate characteristics of PEALD YSZ thin films. All substrates were cleaned in ultrasonic bath with acetone, ethanol and deionized water sequentially before deposition to remove surface contaminations. Oxygen ion conductivity of PEALD YSZ thin films on single crystal MgO, electrical impedance spectroscopy (EIS) measurement was carried out by using a custom-made micro-probing test station sitting on a temperature-controlled heating stage. [44,45] 100 nm thick of dense Pt electrodes with 300 μm gap of each other were prepared on the surface of PEALD YSZ films using a commercial sputter system (DAEKI HIGH Tech Co., Korea) with 100 W of direct current (DC) sputtering power at 1 Pa Ar pressure. Distance from a Pt target to the single crystal MgO was maintained 150 mm. The Gamry Potentiostats (Gamry Instruments Inc., FAS2) were employed to measure Nyquist's plots of the ionic conductivity of PEALD YSZ films in the frequency range from 300 kHz to 1 Hz under 450 °C –

550 °C temperature conditions. Measured EIS results were analyzed by using Z view software (Scribner Association Inc. USA)

In order to evaluate electrochemical characteristics of YSZ thin films, commercial nano-porous anodic aluminum oxide (AAO, Synkera, USA) template based TF-SOFCs were fabricated and examined. A 330 nm thick dense Pt anode was fabricated on a bare AAO template by using a commercial sputtering system (A-tech, Korea). 200 W of DC power was applied at 0.67 Pa Ar working pressure to prepare dense and smooth Pt anode. After deposition of anode, a 140nm thick PEALD YSZ thin film electrolyte was deposited on Pt anode. Finally, a 150 nm thick porous Pt cathode was fabricated on PEALD YSZ thin film electrolyte with 100 W of DC power at 12 Pa of Ar pressure to maximize triple phase boundaries. Electrochemical characterization was conducted in the temperature range from 450 °C ~ 550 °C by using custom-made experimental set-up. [4,6,9–11,13–15,114] 30 sccm of pure H_2 was supplied to anode as a fuel and ambient air was used at cathode as an oxidant. Electrochemical characteristics of TF-SOFCs such as open circuit voltage (OCV), current density-voltage behavior and electrochemical impedance spectroscopy (EIS) were measured by using solartron 1287/1260 (Solartron, UK) electrochemical measurement system. EIS of TF-SOFCs were examined at various voltage conditions – 1.0 V, 0.75 V and 0.5 V to evaluate detailed analysis of electrochemical losses.

Chemical composition of YSZ thin films were investigated by x-ray photoelectron spectroscopy (XPS, Theta probe base system, spot diameter: 400μm, Al Kα (1486.6 eV), Thermo Fisher

Scientific, USA). 150 eV Ar ion etching was carried out for 15 s before measurement to remove surface contaminations. Thickness and crystal structure of PEALD YSZ films on MgO substrates were evaluated by high resolution transmission electron microscopy (HRTEM, JEM-2100F, JEOL, Japan) with 200 keV operation voltage. Cross-sectional structures of TF-SOFCs were measure by using focused ion beam-scanning electron microscopy (FIB-SEM, Quanta 3D, operating voltage: 5 kV, FEI, USA).

3.3 Results and discussion

Preparation conditions of PEALD YSZ thin films are summarized in table 3.1. As shown in table 3.1., plasma duration (3 s, 8 s, and 16 s) and power (50 W and 200 W) were systematically changed to study effects of plasma conditions on properties of PEALD YSZ thin films. Plasma power and duration for the ZrO_2 deposition and the Y_2O_3 deposition were maintained identical conditions to prepare PEALD YSZ films in the specific plasma condition. In order to minimize and avoid handling errors, PEALD YSZ films were deposited on the surface of Si (chemical composition) and MgO (100) (in-plane ionic conductivity, TEM analysis) substrates at the same time.

Name	Deposition Temperature	$ZrO_2 : Y_2O_3$	Plasma Power	Plasma Duration
1	250 ˚C	7 : 1	50 W	3 s
2				8 s
3				16 s
4			200 W	3 s
5				8 s
6				16 s

Table 3.1. Deposition conditions of PEALD YSZ thin films

XPS analysis results of PEALD YSZ thin films prepared with different plasma conditions are listed in table 3.2.

Name	1	2	3	4	5	6
Plasma power	50			200		
Plasma duration	3 s	8 s	16 s	3 s	8 s	16 s
Zr	31.75	32.04	32.15	31.39	32.13	32.71
Y	3.99	4.53	4.46	4.5	4.73	4.7
O	62.62	61.62	61.51	62.58	62.18	61.55
C	1.64	1.81	1.88	1.54	0.96	1.04
Y_2O_3 mol. %	6.23	7.12	7.00	7.07	7.45	7.40

Table 3.2 Chemical compositions of PEALD YSZ films prepared by different plasma conditions.

As presented in table 3.2., all PEALD YSZ contained almost negligible (less than 2.0 atom. %) carbon impurity concentrations. These low concentrations of contaminations in YSZ film can be explained by superior reactivity of oxygen plasma species such as activated atoms, ions, and electrons. [108,110,112] Notably, PEALD YSZ thin films formed by 200 W plasma power showed relatively lower carbon contaminations (average carbon at. %: 1.18 at. %) than PEALD YSZ by 50 W (average carbon at. %: 1.78 at. %). Impurities such as carbon in ligands of Zr or Y precursors were

more effectively removed by higher plasma power (200 W), and then, chemically high quality YSZ thin films were prepared. Also, all PEALD YSZ thin films contained very similar Y atomic concentration (3.99 at. % ~ 4.73 at. %, difference of Y at. % < 1 at. %). It means that all films have similar Y_2O_3 concentrations, i.e. Y_2O_3 mol. % (6.23 mol. % ~ 7.45 mol. %).

Figure 3.1. shows in-plane oxygen ionic conductivity of 30 nm thick PEALD YSZ films on MgO (100) substrates prepared with different plasma conditions.

Figure 3.1. a) presents representative EIS plots of PEALD YSZ films with 200 W of plasma power and 16 s of plasma duration at various temperature. The in-set shows equivalent circuit model of EIS results. Solid lines were fitting results by using equivalent circuit models. As seen in figure 2.1. a), total resistances of in-plane conductivity were decreased as the measurement temperature was increased.

Figure 3.1. b) shows comparison of in-plane conductivity of PEALD YSZ with earlier researches. Dotted lines are results of previous studies. [21,28,116] As seen in figure 2.1. b), all PEALD YSZ films in this study showed very similar ionic conductivities and activation energies – incline of Arrhenius plots – compared with prior researches. [21,28,116]

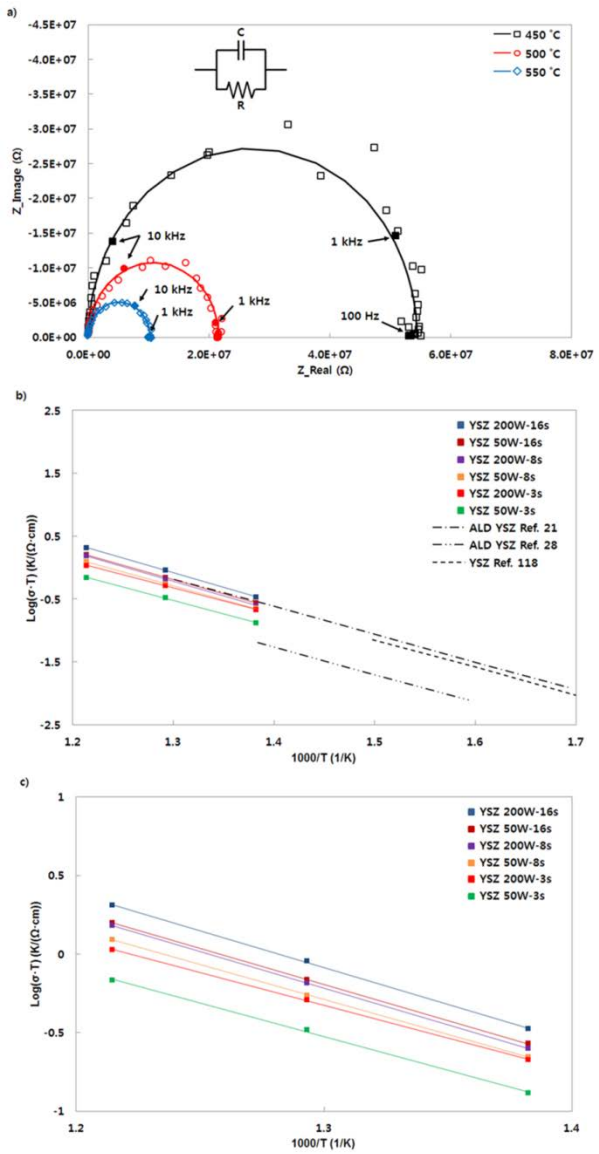

Figure 3.1. In-plane conductivity of PEALD YSZ films on MgO (100) substrates. a) representative EIS plots of PEALD YSZ with 200 W plasma power and 16 s plasma duration. b) Comparison of oxygen ionic conductivity of PEALD YSZ with prior studies. c) Arrhenius plots of PEALD YSZ films in the temperature range from 450 °C to 550 °C

Figure 3.1. c) illustrates Arrhenius plots of PEALD YSZ films in the temperature range from 450 °C to 550 °C. Interestingly, between very similar in-plane conductivities (maximum difference between conductivities is ~0.5 order in the Arrhenius plot), oxygen ion conductivities of PEALD YSZ films on MgO (100) substrate are improved as the plasma power and duration are increased regardless of the measurement temperature. Therefore, PEALD YSZ thin film fabricated by 200 W of plasma power and 16 s of duration showed the highest in-plane ionic conductivity in all temperature range compared with other PEALD YSZ thin films. We speculate that this enhancement in ionic conductivity is related with degree of crystallinity and Y_2O_3 concentration of YSZ films.

In addition, from the Arrhenius plot, activation energies for oxygen ion conduction were calculated by using followed equation.

$$\sigma T = A \cdot \exp(\frac{-E_{act}}{k_B \cdot T})$$

Where A is the pre-exponential coefficient, T is the temperature, k_B is the Boltzmann constant, E_{act} is the activation energy for oxygen ion migration.

Calculated activation energies are 0.85 eV (50 W-3 s), 0.88 eV (50 W-8 s) 0.91 eV (50 W-16 s), 0.83 eV (200 W-3 s), 0.92 eV (200 W-8 s), and 0.93 eV (200 W-16 s). In spite of slight difference in ionic conductivity of PEALD YSZ films, these activation energies for oxygen ion conduction were very similar and quite comparable with prior researches about YSZ thin films

fabricated by various thin film techniques or bulk YSZ. [21,28,103,105,115,116]

In PEALD process, thin films are highly crystallized during deposition or after treatment by bombardment of plasma species compared with films fabricated by typical thermal ALD. [108,110] In particular, films prepared by direct PEALD show much higher degree of crystallization due to higher flux of ions and closer distance between plasma generator and substrate compared with remote PEALD. In prior study, An et al. reported that degree of crystallization of oxide thin films ($BaTiO_3$, BTO) were improved by after remote plasma processing. [117] Crystal structure of almost amorphous BTO films deposited by thermal ALD was improved by after remote plasma processing. Longer plasma processing caused more crystallized films. Post plasma treatment is also improved film density and electrical characteristics. Therefore, exposure time of film surface to plasma and plasma density (i.e. plasma power) can greatly affect properties of YSZ films such as degree of crystallinity, surface roughness, and grain size.

In addition, in the case of ion conductors, degree of crystallinity and crystal structure greatly affect on conductivity of films. [39,103,105,118–120] Kim et al. reported that influences of degree of crystallinity and crystal structure (amorphous structure versus polycrystalline structure and polycrystalline structure versus single crystal structure – epitaxial growth) on proton conductivity of BYZ films fabricated by PLD. [39] BYZ films with highly crystallized and single crystal structure showed higher conductivity compared with amorphous structure and polycrystalline structure, respectively. In

YSZ films, Heiroth et al. reported similar results. [118] Polycrystalline YSZ films prepared by PLD process showed higher conductivity than amorphous YSZ films deposited by PLD due to imperfect crystallization. Guo et al. also reported that the block effect of grain boundaries of YSZ films. [119] In spite of absence of impurities, grain boundaries showed two or three orders higher resistivity compared with bulk resistivity. In addition, the blocking effect was much severe at low temperature. Yeh et al. reported effects of annealing on conductivity of reactive sputtered YSZ films. [120] Annealing dramatically enhanced ionic conductivity of YSZ films due to improved crystallinity and removal of staining dislocation at interface. Therefore, considering results of prior researches, we speculate that slightly higher ionic conductivity of 200 W−16 s PEALD YSZ films originated from enhanced degree of crystallization and improved degree of epitaxial growth caused by more additional energies from higher plasma power and long duration. Furthermore, earlier studies about relation between Y_2O_3 concentration and ionic conductivity of YSZ films reported that Y_2O_3 concentration greatly affected in−plane ionic conductivity of YSZ films. [115,121] Son et al. reported that higher Y_2O_3 concentration YSZ films (10.9 mol. % Y_2O_3) prepared by thermal ALD presented the highest in−plane oxygen ion conductivity compared with various Y_2O_3 concentration YSZ films from 4.3 mol. % to 28.8 mol. % of Y_2O_3. [115] Also, Jung et al. reported that 6.5 mol. % Y_2O_3 doped YSZ films prepared by reactive magnetron sputtering (slightly lower Y_2O_3 concentration) showed the highest conductivity over 400 °C due to extended meta−stability of cubic structure at

nanometric grains. [121] Therefore, considering earlier study about Y_2O_3 concentration of ALD YSZ films, we think that low ionic conductivity of 50 W−3 s PEALD YSZ film was partially caused by relatively slight lower Y_2O_3 concentration compared with other PEALD YSZ films.

In order to examine detailed microstructure of PEALD YSZ films on MgO (100) substrate and to confirm above speculations, TEM analysis was carried out. Figure 3.2. presents TEM images of cross sectional structure of PEALD YSZ films (50 W−3s and 200 W−16 s) on MgO (100) structure.

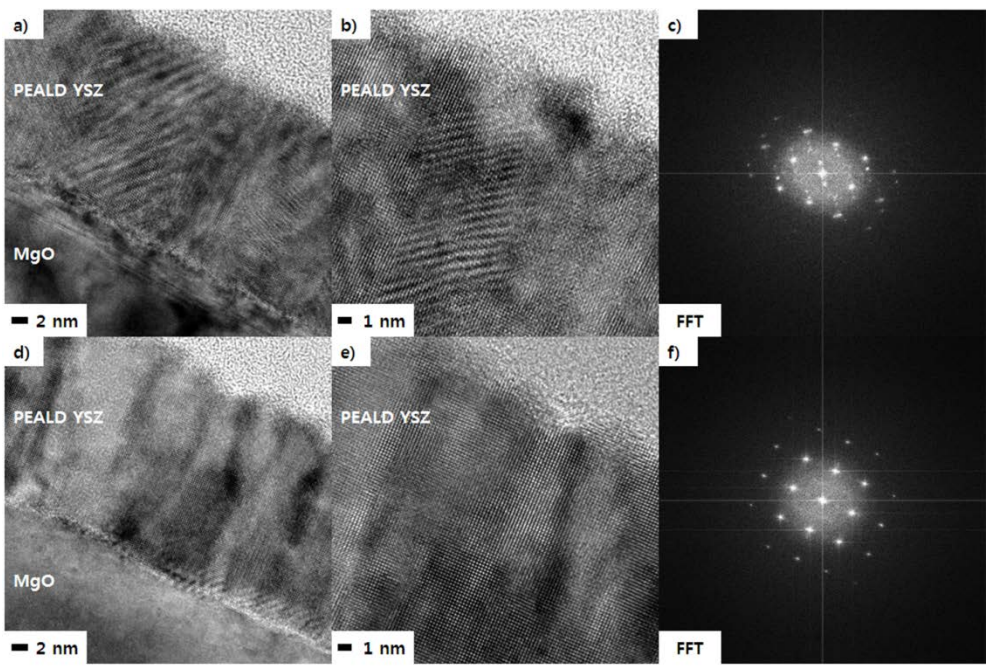

Figure 3.2. Representative TEM images of PEALD YSZ films on MgO (100) substrate. a) Cross sectional TEM image of 50 W−3 s PEALD YSZ film on MgO. b) HRTEM image of 50 W−3 s PEALD YSZ film. c) FFT of HRTEM image of 50 W−3 s PEALD YSZ film. d)

Cross sectional TEM image of 200 W−16 s PEALD YSZ film on MgO. e) HRTEM image of 200 W−16 s PEALD YSZ film. f) FFT of HRTEM image of 200 W−16 s PEALD YSZ film

As shown in figure 3.2., PEALD YSZ films showed clearly different microstructure. Cross sectional TEM images of 50 W−3 s PEALD YSZ films showed clear polycrystalline structure and FFT results also clarified well established polycrystalline structure. (figure 2.2. a), b), and c)) In contrast, TEM images of 200 W−16 s PEALD YSZ films presented slightly different microstructure. Figure 3.2. a) illustrated that well developed and nearly epitaxial microstructure guided from MgO (100) substrate. HRTEM image (figure 3.2. d)) of 200 W−16 s PEALD YSZ showed epitaxial microstructure compared with 50 W−3 s PEALD YSZ films in figure 3.2. b). FFT results also proved single crystal microstructure of 200 W−16 s of PEALD YSZ films. In summary, 50 W−3 s PEALD YSZ film had polycrystalline structure and 200 W−16 s PEALD YSZ film had nearly single crystal structure (epitaxial growth). It indicates that 50 W−3 s PEALD YSZ film had higher grain boundary densities which show severe resistivity compared with bulk density. [119] Therefore, slightly lower in−plane ionic conductivity of 50 W−3 s PEALD YSZ film caused by higher grain boundary density compared with 200 W−16 s PEALD YSZ film.

After characterization of PEALD YSZ films, an AAO based TF−

SOFC was prepared by using 200 W−16 s plasma condition due to its highest in−plane ionic conductivity. Figure 3.3. presents surface morphology and cross sectional structure of the cell.

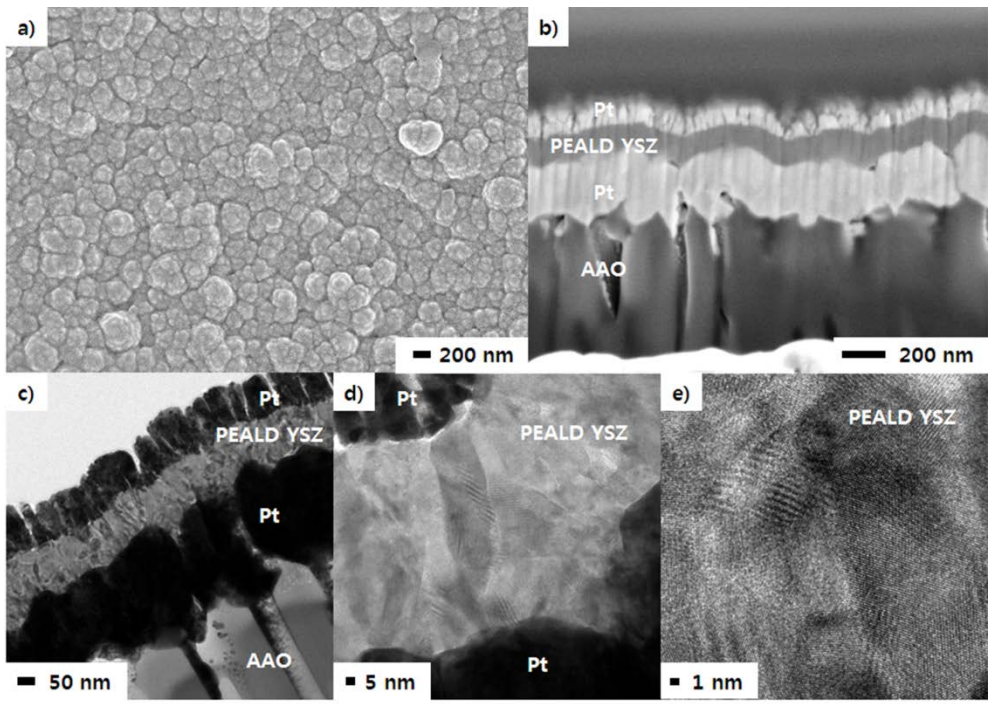

Figure 3.3. Surface morphology and cross sectional structure of an AAO based TF−SOFC based on 200 W−16s PEALD YSZ. a) Surface morphology of 200 W−16 s PEALD YSZ thin film electrolyte. b) Cross sectional structure of a TF−SOFC based on 200 W−16s PEALD YSZ. c) TEM cross sectional images of a TF−SOFC. d) TEM images of a 200 W−16 s PEALD YZS thin film electrolyte e) HRTEM images of a 200 W−16 s PEALD YZS thin film electrolyte

Figure 3.3. a) shows cathode side surface morphology of PEALD YSZ thin films electrolyte. PEALD YSZ thin film electrolyte presents pin-hole free and dense electrolyte surface. Figure 3.3. b) shows cross sectional structure of an AAO based TF-SOFC measured by FIB-SEM. As shown in figure 3.3. b), PEALD YSZ electrolyte showed fully dense and pin-hole free structure which are critical issue of thin film electrolyte. Figure 3.3. c), d), and e) presents results of TEM analysis of the cell. In spite of rough surface of Pt anode and low deposition temperature (250 °C), PEALD YSZ thin film electrolyte shows obvious polycrystalline structure. We speculate that additional energy was provided by severe bombardment during plasma steps in YSZ supercyle – high plasma power (200 W) and long duration (16 s) by plasma species. [108,110,112,117] Bombardment of plasma species provides additional energy to grains of the film, and therefore grains become crystallize to larger grains and form polycrystal structure.

Figure 3.4. presents results of electrochemical characterization of a TF-SOFC based on 200 W-16 s PEALD YSZ thin film electrolyte.

As seen in figure 3.4. a), performances of a TF-SOFC were improved as the temperature was increased from 450 °C to 550 °C. The maximum power density of a TF-SOFC was measured at 95.4 mW/cm^2 and 217.5 mW/cm^2 at 450 °C and 550 °C, respectively.

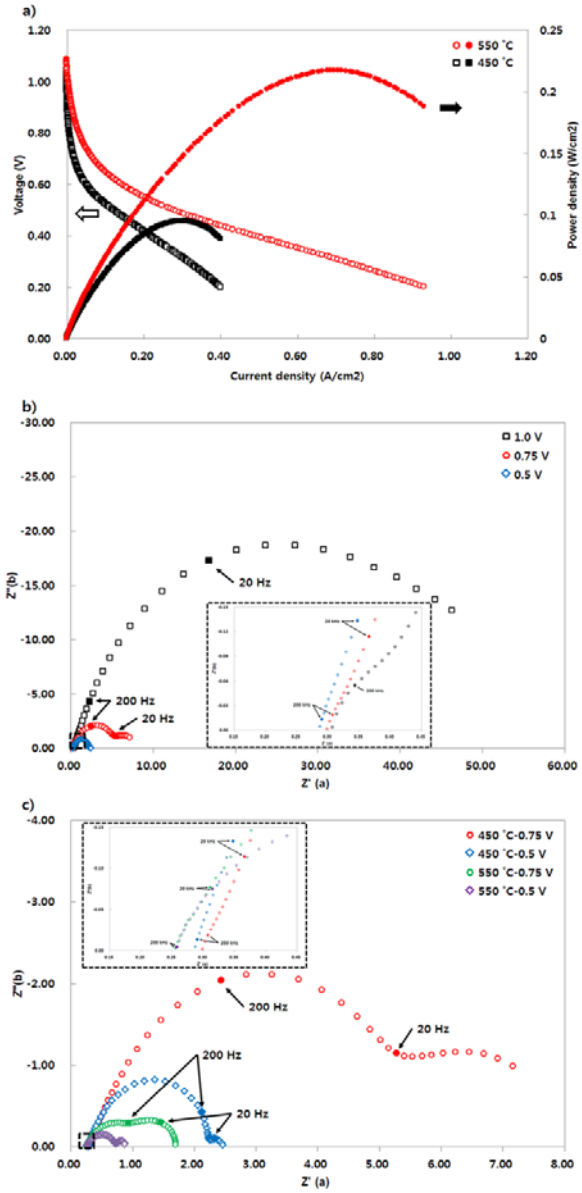

Figure 3.4. Results of electrochemical characteristics of a TF-SOFC based on 200 W- 16 s PEALD YSZ. a) Current density vs. voltage behavior of a fuel cell. b) EIS results of a TF-SOFCs under different voltage conditions at 450 °C. c) Comparison of EIS results under 0.75 V and 0.5 V measured at 450 °C and 550 °C.

As the temperature was increased, both activation loss which was the voltage drop in low current density area and ohmic loss which was the inclination of a current density – voltage curve at medium current density area were clearly improved. [1,2] These reduction of polarization and ohmic resistance were clearly showed in EIS results. Figure 3.4. b) presents representative EIS results of a TF-SOFC under different voltage conditions at 450 °C. The in-set shows high frequency area of EIS results. As shown in figure 2.4. b), radius of semicircles are clearly reduced under DC biased conditions. It means that radius of semicircle indicates polarization resistance of a TF-SOFC. Interestingly, the X-axis intercept points of EIS results showed almost identical values regardless of voltage conditions, This implies that the x-axis intercept point is the total ohmic resistance of a TF-SOFC. [1,2] Figure 2. 4. c), shows EIS results at 0.75 V and 0.5 V under different temperature conditions. The in-set presents high frequency are of EIS results. As mentioned above, polarization resistances (i.e. radius of semicircle) and ohmic resistance (i.e. X-axis intercept point at high frequency) were clearly decreased as the temperature was increased.

3.4 Conclusions

In this study, preparation and characterization of PEALD YSZ thin films are carried out for the first time. Influences of plasma power (50 W and 200 W) and plasma duration (3 s, 8 s, and 16 s) on properties of PEALD YSZ are systematically evaluated. Chemical composition is clearly independent with plasma conditions. However, in-plane conductivities of PEALD YSZ films on MgO (100) substrate are obviously related with plasma power and duration. As the plasma power and duration are increased, in-plane conductivities of YSZ films are improved. This may be caused by differences of degree of crystallinity and microstructure of PEALD YSZ films due to different plasma power and duration for bombardment of plasma species. Higher plasma power and long duration causes stronger and longer bombardment by plasma species, and then, degree of crystallinity is improved and almost epitaxial growth.

After film characterization, electrochemical properties of PEALD YSZ were evaluated as a thin film electrolyte of a TF-SOFC. An AAO based TF-SOFC with the AAO supporting substrate – dense Pt anode – PEALD YSZ thin film electrolyte – porous Pt cathode

structure was examined in the temperature range from 450 °C to 550 °C. The maximum power densities of a TF-SOFC were measured at 95.4 mW/cm^2 and 217.5 mW/cm^2 at 450 °C and 550 °C, respectively. The detailed analysis of EIS results indicate that the activation resistance and ohmic resistance were decreased as the measurement temperature was increased. Results of this study may provide significant insights about design of high performance TF-SOFCs.

CHAPTER 4 OPTIMIZATION OF Y_2O_3 DOPANT CONCENTRATION OF PEALD YSZ FOR TF-SOFCS

4.1 Introduction

For thin film electrolyte of TF-SOFCs, 8 mol. % yttria stabilized zirconia (YSZ) is widely adopted. [4-84] As mentioned in chapter 1, the YSZ is a typical electrolyte material for SOFCs due to mechanical strength, comparable ionic conductivity and superior chemical stability in both oxidized and reduced atmosphere. [1,2,5,105] However, because of poor oxygen ionic conductivity of YSZ at low temperature, from tens to hundreds nanometer thick of YSZ thin films are used as a thin film electrolyte for TF-SOFCS to minimize ohmic resistance. [4-84]

However, in TF-SOFCs, polarization loss, particularly related with oxygen reduction reactions (ORRs) is most crucial problems due to sluggish ORRs at low temperature compared with negligible ohmic resistance due to nanometer scale thick electrodes and electrolyte. [4-84,126] Therefore, many investigations have been conducted to improve ORRs of TF-SOFCs at low temperature such as insertion of cathode functional layer or improvement of cathode electrode. [24,33,37,38,41,126] In prior researches, doped ceria (i.e. gadolinia-doped ceria (GDC), yttria-doped ceria (YDC))

cathode functional layers which have lower activation energy to oxygen incorporation reactions than YSZ improved performance of fuel cells by reduction of cathodic polarization resistance. Interestingly, enhancements of ORRs caused by YSZ thin film cathode functional layer by controlling Y_2O_3 contents and its grain size are reported in prior studies. [24,41,43] Notably, most helpful YSZ cathode functional layer is not 8 mol. % Y_2O_3 stabilized ZrO_2 which is well known best ion conductivity Y_2O_3 concentration but 14−19 mol. % Y_2O_3 stabilized ZrO_2 thin films. [1,2,41,43,116] This highly concentrated YSZ cathode functional layer induced increased oxygen vacancies at interface between Pt cathode – YSZ cathode functional layer interface and then, enhanced ORRs (decreased of cathodic polarization loss). [41,43] Moreover, considering ion conductivity, there are various studies related with Y_2O_3 concentration. Jung et al. reported that among various Y_2O_3 concentrated YSZ thin films prepared by reactive sputtering method on single crystal MgO, 6.5 mol % Y_2O_3 stabilized ZrO_2 films showed best ion conductivity due to meta−stable phase of ZrO_2. [121] However, in ALD YSZ thin films, Son et al. reported that high Y_2O_3 concentrated YSZ films (100 / 200 / 300 cycle of ALD YSZ, ALD Al_2O_3 deposited quartz) 10.9 mol. % Y_2O_3 showed best ion conductivity than other Y_2O_3 concentrated YSZ films because of larger parallel ion conduction pass. [115]

However, there have been no researches about optimization of Y_2O_3 concentration of YSZ thin film electrolyte at full TF−SOFCs. In this study, therefore, we synthesized YSZ thin film by means of PEALD which has various Y_2O_3 contents and applied to TF−SOFCs

in order to clarify optimized YSZ thin film electrolyte for TF-SOFCs. Chemical and physical characteristics of YSZ thin films were studied before applied to TF-SOFCs as an electrolyte. Electrochemical characteristics of YSZ thin films with various Y_2O_3 contents were also evaluated as a thin film electrolyte of TF-SOFCs.

4.2 Experimental

A commercial showerhead type direct PEALD with capacitively coupled plasma generator (Atomic premium, CN1, Korea) was used to prepare YSZ thin films with different Y_2O_3 doping rates. A commercial tetrakis(dimethylamino)zirconium (Sigma Aldrich, USA) and tris(methylcyclopentadienyl)yttrium (Sigma Aldrich, USA) were used. 300 sccm of high purity O_2 gas (99.999%, Shinjin, Korea) and Ar gas (99.999%, Shinjin, Korea) were used for O_2 plasma and carrier gas, respectively. Stainless steel canisters for Zr and Y were kept at 50 °C and 150 °C during preparation. Also, stainless steel lines between canisters and reaction chambers were maintained 70 °C and 165 °C to prevent condensation of precursors, respectively. Deposition of YSZ thin films were conducted at 250 °C which was generally known YSZ deposition temperature. [4–6,12,17,19,21,28,32,36,38,41,114] Fabrication process of ZrO_2 thin film was as follows: Zr pules (3 s) – Ar purging (40 s) – O_2 pulse (1 s) – O_2 pulse with plasma (2 s) – Ar purging (40 s). Deposition process of Y_2O_3 was composed similar steps: Y pulse (3 s) – Ar purging (75 s) – O_2 pulse (1 s) – O_2 pulse with plasma (2 s) – Ar purging (75 s). The 1 s of O_2 pulse was inserted to stabilized O_2 partial pressure before plasma generation. Ratios between ZrO_2 process and Y_2O_3 process in the YSZ supercycle was changed from 7:1 to 1:1 to control Y_2O_3 dopant

concentration. Detailed deposition conditions were summarized in table 4.1.

Name	Plasma condition	YSZ cycle	Experiments
YSZ-1	ZrO_2 50 W 2s & Y_2O_3 50 W 2s	ZrO_2 1	Very high Y_2O_3
		Y_2O_3 1	
YSZ-4		ZrO_2 4	High Y_2O_3
		Y_2O_3 1	
YSZ-7		ZrO_2 7	Normal Y_2O_3
		Y_2O_3 1	
YSZ-10		ZrO_2 10	Low Y_2O_3
		Y_2O_3 1	

Table 4.1. Deposition conditions of PEALD YSZ thin films

In order to study influence of Y_2O_3 doping rates on electrochemical characteristics of YSZ films, commercial nanoporous anodic aluminum oxide (AAO, Synkera Co., USA) template based TF-SOFCs were fabricated and examined at 450 °C. 100 μm thick AAO templates with 80 nm diameter pores were used as substrates of TF-SOFCs. 330nm dense Pt anode was prepared on bare AAO templates by using a commercial sputtering system (A-tech Co., Korea) to remove possibility for growth of pinholes during deposition of electrolyte. 200 W of direct current (DC) power was applied to Pt target at 0.67 Pa of Ar working pressure. After preparation of anode, YSZ thin film electrolytes were prepared by using PEALD. Finally, 150 nm porous Pt cathode was fabricated with 100 W of DC power at 12 Pa to maximize triple phase boundaries (TPBs) at electrolyte-cathode interface.

Electrochemical characterizations of TF-SOFCs were carried out

at 450 °C by using a custom-made characterization set-up. 30 sccm of pure H_2 was supplied as a fuel to anode side and ambient air was used as an oxidant. A Solartron 1287/1260 potentiostat / galvanostat and frequency response analyzer system (Solartron Co., UK) were used to examine electrochemical characteristics of TF-SOFCs such as open circuit voltage (OCV), current density - voltage behavior, and electrochemical impedance spectroscopy (EIS). EIS of TF-SOFCs were measured under OCV and 0.5 V DC bias conditions with 30 mV of amplitude voltage over the frequency range from 2 MHz to 2 Hz. Zplot software (Scribner Co., USA) was used to analyze EIS results.

Chemical composition of YSZ films were studied by using an x-ray photoelectron spectroscopy (XPS, Theta Probe base system, 1486.6 eV Al Kα source, Thermo Fisher Scientific, USA). Field emission scanning electron microscopy (FESEM, SUPRA55VP, operating voltage: 2 kV, Carl-Zeiss, Germany) was used to evaluate surface morphology of TF-SOFCs. Focused ion beam-scanning electron spectroscopy (FIB-SEM, Quanta 3D, operating voltage: 5 kV, FEI, USA) was also used to examine cross-sectional structure of TF-SOFCs. More detailed cross-sectional microstructures of TF-SOFCs were measured by high resolution transmission electron microscopy (HRTEM, JEM-2100F, JEOL, Japan) with 200 keV operation voltage.

4.3 Results and Discussion

It is generally known that Y_2O_3 concentration of YSZ thin films has crucial effects on characteristics of YSZ thin film electrolyte such as oxygen ion conductivity or oxygen vacancies. [41,43,115,121] According to chapter 3, carbon contamination in YSZ films prepared by ALD also have critical influence on performance of TF-SOFCs due to low OCV caused by formation of electrical leakage current.

Chemical composition including Y_2O_3 and carbon impurity concentration in YSZ thin films were measured by XPS as a function of the ZrO_2/Y_2O_3 process ratio. In order to evaluate chemical composition of films, multi-point XPS analysis (3 points for each YSZ thin film, distance between evaluated points was more than 2 mm) was conducted. Results of multi-point XPS (calculated average values) were summarized in table 4.2 and figure 4.1.

Figure 4.1. and table 4.2. show average value of chemical composition all YSZ thin films. As seen in figure 4.1., Y_2O_3 concentrations are increased as the ZrO_2/Y_2O_3 process ratio in the YSZ supercycle is decreased. Interestingly, sudden increase in Y_2O_3 concentration in the YSZ films prepared by 1:1 YSZ supercycle (ZrO_2/Y_2O_3 = 1, 32.1 mol. %, YSZ-1) was observed. This sudden increase which was also observed in previous studies was caused by different nucleation speed of materials on different substrates.

[21,94,115] Carbon contaminations were also negligible (less than 1.0 at. %) for all YSZ films due to superior reactivity of oxygen plasma species. [108,110,112]

Name	YSZ-1	YSZ-4	YSZ-7	YSZ-10
Y at. %	17.63	6.68	4.60	3.2
Zr at. %	20.85	30.18	32.02	33.3
C at. %	0.26	0.95	0.71	0.99
Y_2O_3 mol. %	32.1	10.73	7.24	4.96

Table 4.2. Chemical composition of PEALD YSZ films.

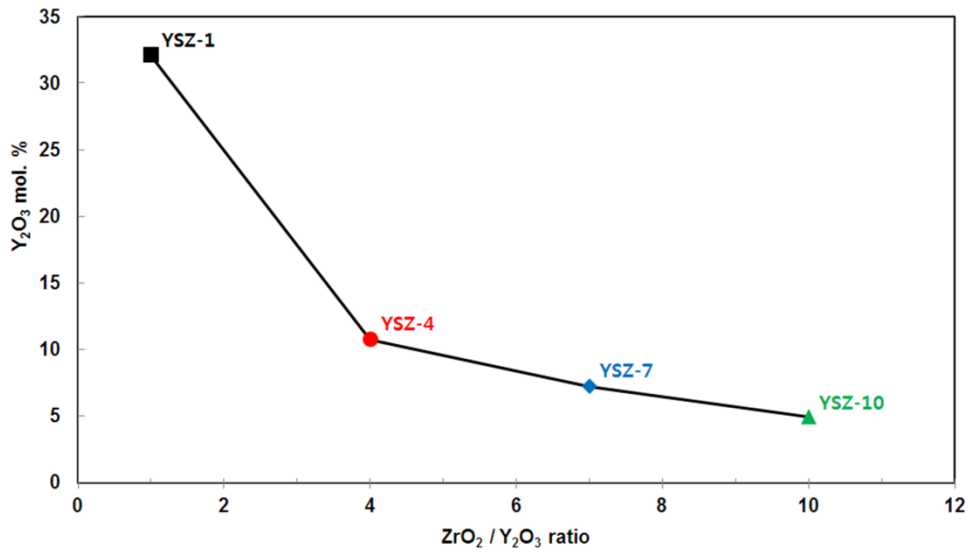

Figure 4.1. Chemical composition of PEALD YSZ

As mentioned above, we want to optimize Y_2O_3 concentration of PEALD YSZ films of TF-SOFCs. Therefore, we examined other factors which had critical influence on characteristics of TF-SOFCs, except Y_2O_3 doping concentration.

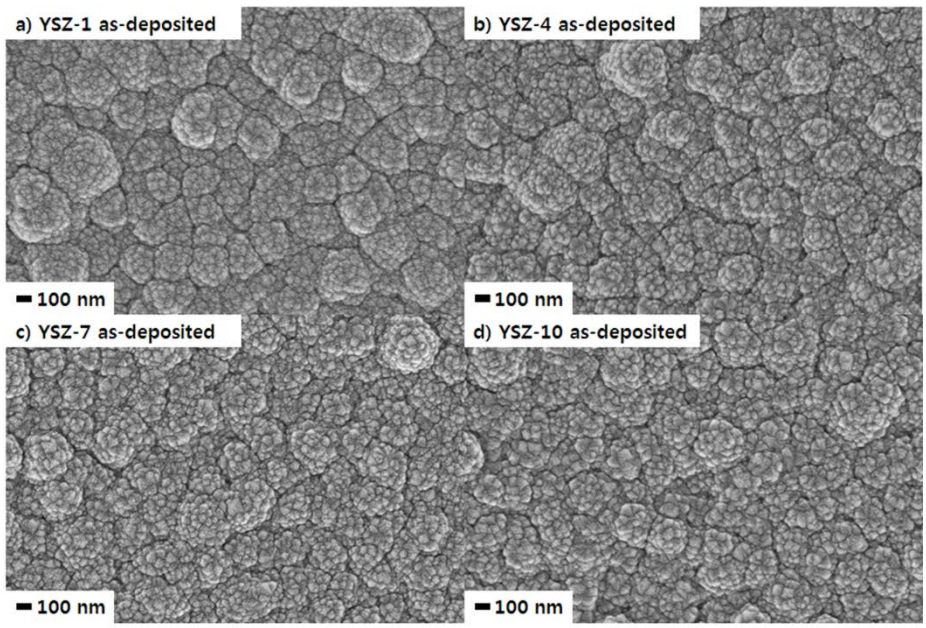

Figure 4.2. Surface morphology of PEALD YSZ thin film electrolyte of TF-SOFCs

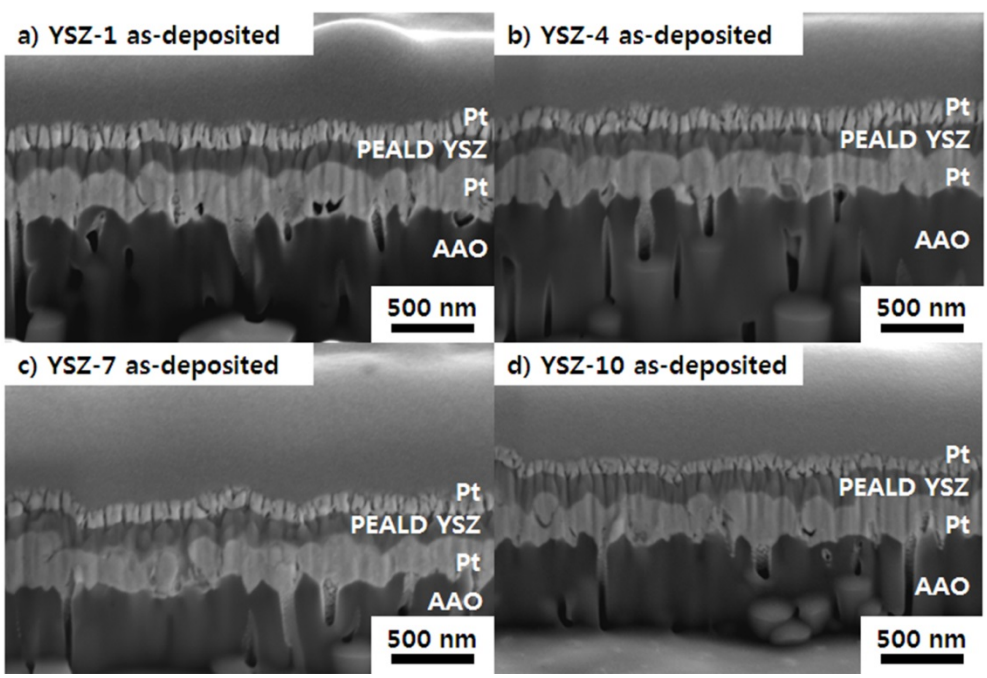

Figure 4.3. Cross sectional structure of TF-SOFCs

Surface morphologies of as-deposited YSZ thin film electrolytes on Pt anode (i.e. cathode side of YSZ electrolyte) and cross sectional structures of TF-SOFCs are presented in figure 4.2. and 4.3. According to prior studies, cathode-electrolyte interface such as average surface grain size (surface grain boundary density) or chemical composition has critical influence on performance of TF-SOFCs. [17,24,33,34,41,43,44,117] Interestingly, as seen in figure 4.2., surface of all YSZ thin film electrolytes of TF-SOFCs prepared on the top of dense Pt anode show very similar grain size and dense surface morphology regardless of Y_2O_3 concentration. It means that YSZ thin film electrolytes are well fabricated by using PEALD without defects or pinholes. In addition, Ji. et al. reported that surface grain size of PEALD YSZ thin film electrolyte was proportional to thickness of YSZ thin film electrolyte. [17] Therefore, according to figure 4.2., and results of prior study, we speculate that all TF-SOFCs in this study had very similar electrolyte thickness.

Moreover, as shown in figure 4.3., similar cross sectional structure and thickness of components (dense anode, porous cathode, and dense, pin-hole free electrolyte) of cells which also have significant impact on electrochemical behavior of TF-SOFCs are also confirmed by FIB results. All cells showed very similar microstructure and thickness. Therefore, we think that influence of interface between porous Pt cathode and YSZ electrolyte related with grains (average grain size, i.e. grain boundary density) and effects of microstructure of all TF-SOFCs are almost identical,

except Y_2O_3 concentration of PEALD YSZ thin film electrolyte.

As mentioned above, higher Y_2O_3 concentrated YSZ thin films show reduced cathodic polarization loss and better ionic conductivity. [41,43,115] Chao et al. showed that 1 nm surface modification layer (SML) of YSZ films prepared by thermal ALD process improved performance of fuel cells. [41,43] Increments of maximum power density of fuel cells were related with Y_2O_3 concentration of YSZ SMLs. Fuel cell with 14 – 19 mol. % Y_2O_3 concentrated YSZ SML showed the best performance in the temperature range from 350 °C to 450 °C. Moreover, Son et al. reported Y_2O_3 concentration dependent in-plane conductivity of YSZ films prepared by thermal ALD. [115] YSZ films with 10.9 mol. % Y_2O_3 showed the highest in-plane conductivity in the temperature range from 333 °C to 559 °C. Interestingly, in all prior studies, excessive Y_2O_3 concentration within YSZ films showed bad influence on performance or conductivity.

Therefore, we examined detailed microstructure of TF-SOFCs with YSZ-1 (32.1 mol. % Y_2O_3, excessive Y_2O_3), YSZ-4 (10.73 mol. % Y_2O_3, higher Y_2O_3) and YSZ-7 (7.24 mol. % Y_2O_3, norminal Y_2O_3) by using TEM. Figure 4.4. presents TEM images of TF-SOFCs based on YSZ-1, YSZ-4, and YSZ-7 thin film electrolyte, respectively. In order to prevent thermal annealing influences on microstructure of PEALD YSZ, TEM measurement were carried out with as-deposited samples. As seen in figure 4.4. a), b) and c), similar to FIB results (figure 4.3), all TF-SOFCs showed very similar cross sectional microstructure (AAO – dense Pt anode – PEALD YSZ thin film electrolyte – porous Pt cathode). More

detailed microstructure of PEALD YSZ thin film electrolytes are shown in figure 4.4. d), e), and f). As seen in figure 4.4. d), e), and f), all PEALD YSZ thin film electrolytes presents similar thickness and degree of crystallization. Figure 4.4. g), h), and i) illustrate HRTEM images of PEALD YSZ thin film electrolytes of cells. As shown in figure 4.4. g), h), and i), all YSZ films show almost identical degree of crystallization because of same plasma conditions (power and duration) and deposition temperature.

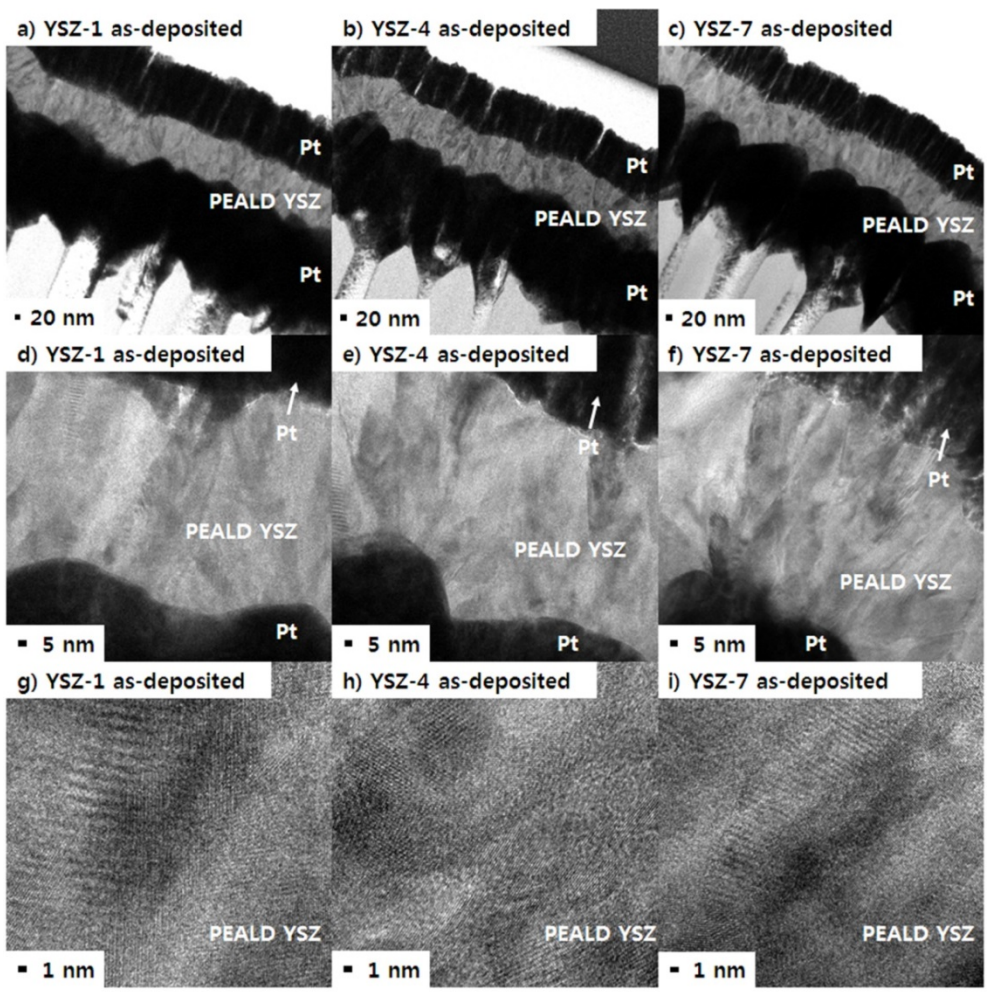

Figure 4.4. TEM images of cross-sectional structure of TF-SOFCs. a) TEM image of microstructure of TF-SOFC with YSZ-1 thin film electrolyte. b) TEM image of microstructure of TF-SOFC with YSZ-4 thin film electrolyte. c) TEM image of microstructure of TF-SOFC with YSZ-7 thin film electrolyte. d) TEM image of YSZ-1 thin film electrolyte. e) TEM image of YSZ-4 thin film electrolyte. f) TEM image of YSZ-7 thin film electrolyte. g) HRTEM image of YSZ-1 thin film electrolyte. h) HRTEM image of YSZ-4 thin film electrolyte. i) HRTEM image of YSZ-7 thin film electrolyte

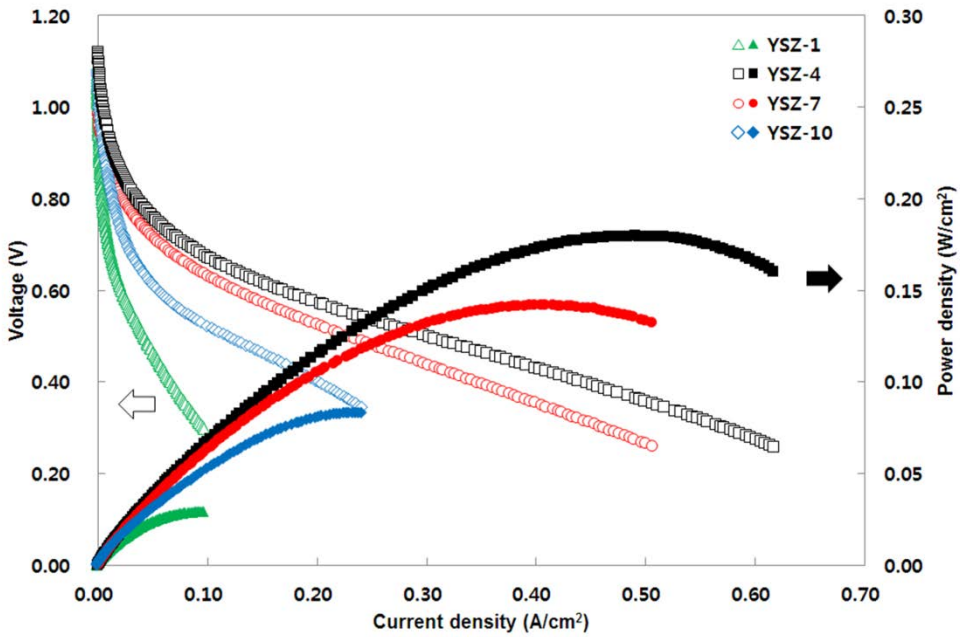

Figure 4.5. Polarization curves of TF-SOFCs

Figure 4.5 shows polarization curves of TF-SOFCs measured at 450 °C. Interestingly, maximum power density of TF-SOFC is strongly related with Y_2O_3 concentration within YSZ thin film

electrolyte. As seen in figure 4.5, TF-SOFC with 10.73 mol % YSZ (YSZ-4, higher Y_2O_3) showed the best performance 180 mW/cm^2 at 450 °C. However, TF-SOFC with the highest Y_2O_3 concentration (YSZ-1, 32.1 mol %, excessive Y_2O_3) showed only 27 mW/cm^2 at 450 °C. YSZ-7 and YSZ-10 cells (YSZ-7: 7.24 mol. %, norminal Y_2O_3 and YSZ-10: 4.95 mol. %, low Y_2O_3) measured to 143 mW/cm^2 and 83 mW/cm^2, respectively. This tendency of Y_2O_3 concentration dependent performance was in good accordance with prior researches. [41,43,115] In spite of similar thickness and structure of components – anode, cathode and electrolyte, activation loss which is generally shown at low current density region and ohmic loss which is the inclination of current voltage curve at middle current density region of TF-SOFCs showed obvious differences. It means that electrochemical properties such as oxygen ionic conductivity and activation energy of oxygen incorporation reaction of YSZ thin films are greatly affected by Y_2O_3 concentration in YSZ films.

In order to clarify detailed electrochemical losses of fuel cells, EIS measurements were carried out under various voltage conditions (OCV and 0.5 V condition) in the frequency range from 2 MHz to 2 HZ. First, in order to clarify the total ohmic resistance of fuel cells including electrolyte resistance and contact resistance, EIS Nyquist plots measured under different voltage conditions were compared. It is generally known that electrode polarization resistances of fuel cells are greatly affected by the applied voltage conditions while ohmic resistance of fuel cells are almost independent of the applied voltage. [24,28,33,34,38,44,126]

Figure 4.6. shows representative Nyquist plots of YSZ-10 measured under OCV and 0.5 V conditions at 450 °C. High frequency region of Nyquist plots are illustrated at inset.

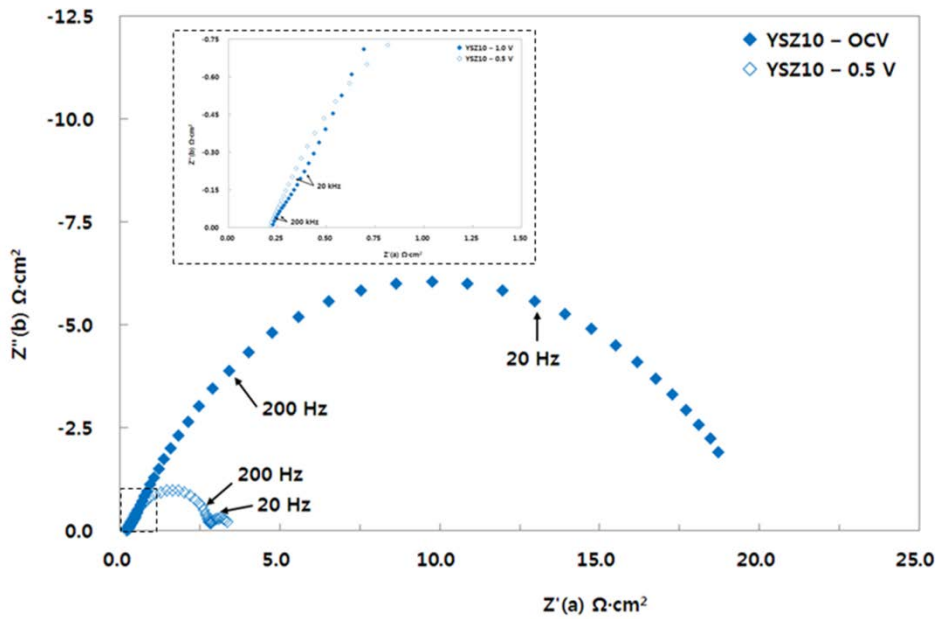

Figure 4.6. Nyquist plots of YSZ-10 under OCV and 0.5 V.

As seen in figure 4.6., semicircle of Nyquist plots are clearly affected by applied voltage conditions, while X-axis intercept points were almost identical regardless of different applied voltage conditions (showed in the in-set of figure 4.6.). It implies that X-axis intercept points represent the ohmic resistance of fuel cells including electrolyte resistance and contact resistance. [1,4,17,24,28,33,34,38,44,126] In addition, ohmic resistances of fuel cell in this study are very similar to previous studies about TF-SOFCs. [4,17]

Therefore, according to previous studies, semicircles of EIS plots

under OCV and 0.5 V conditions represent electrode polarization resistances of cells. [1,4,17,24,28,33,34,38,44,126] Nyquist plot measured under 0.5 V condition showed clear two semicircles – at middle frequency region and at low frequency region. However, Nyquist plots measured under OCV condition showed significantly depressed semicircle. It is widely known that EIS results (Nyquist plot) of fuel cells are composed of two electrode polarization components – anode polarization resistance related with hydrogen oxidation reactions (HORs) and cathode polarization resistance related with oxygen reduction reactions (ORRs). [1] Therefore, we think that significantly depressed semicircle in EIS plots measured at OCV is composed of two semicircles – anode polarization resistance and cathode polarization resistance. As mentioned above, these two semicircles – anode and cathode polarizations are greatly affected by the applied voltage, and then, are clearly divided two semicircles at 0.5 V condition.

Interestingly, semicircle at middle frequency region is much larger than semicircle at low frequency region in figure 4.6. It is generally known that anode polarization related with HORs is showed small semicircle at middle frequency and cathode polarization related with ORRs is presented large semicircle at low frequency in Nyquist plot of fuel cells due to differences in reaction kinetics. [1,2] However, in figure 4.6., semicircle of anode polarization (shown at middle frequency region) is much larger than semicircle of cathode polarization (shown at low frequency region). We speculate that this large anode polarization loss is related with microstructure of anode – 330 nm thick and dense Pt anode. In

earlier study using almost identical structured TF-SOFCs (AAO-dense Pt / PEALD YSZ (~8 mol. %) / porous Pt cathode) also showed large middle frequency semicircle and small low frequency semicircle in EIS results. [17] In addition, Park et al., reported that microstructure of anodes had great influence on performance of AAO based TF-SOFCs. [15] Porous structure of anodes improved performance of fuel cells by increasing triple phase boundaries (TPBs). Therefore, in current density versus voltage results, fuel cells with porous anode showed smaller activation loss in low current density region than TF-SOFCs with dense anode. [15] These results indicate that anode polarization related with HORs of TF-SOFCs on nanoporous AAO templates have great influence on performance.

Therefore, in order to clarify our speculation – relation between large middle frequency semicircle with HORs in anode, we examined two cells. AAO based TF-SOFCs with different anode microstructure – porous anode and dense anode were examined. All measurements were carried out at 450 °C. In order to fabricate porous Pt anode, 300 nm thick porous anode was fabricated at 12 Pa of Ar with 100 W of DC power on the top of bare AAO template like prior research. [15] PEALD YSZ electrolyte was prepared with norminal Y_2O_3 doping concentration condition (1 YSZ supercycle = ZrO_2 7 : Y_2O_3 1, YSZ-7).

Figure 4.7. illustrates comparisons of current density versus voltage behavior and EIS Nyquist plots of fuel cells with different anode microstructure.

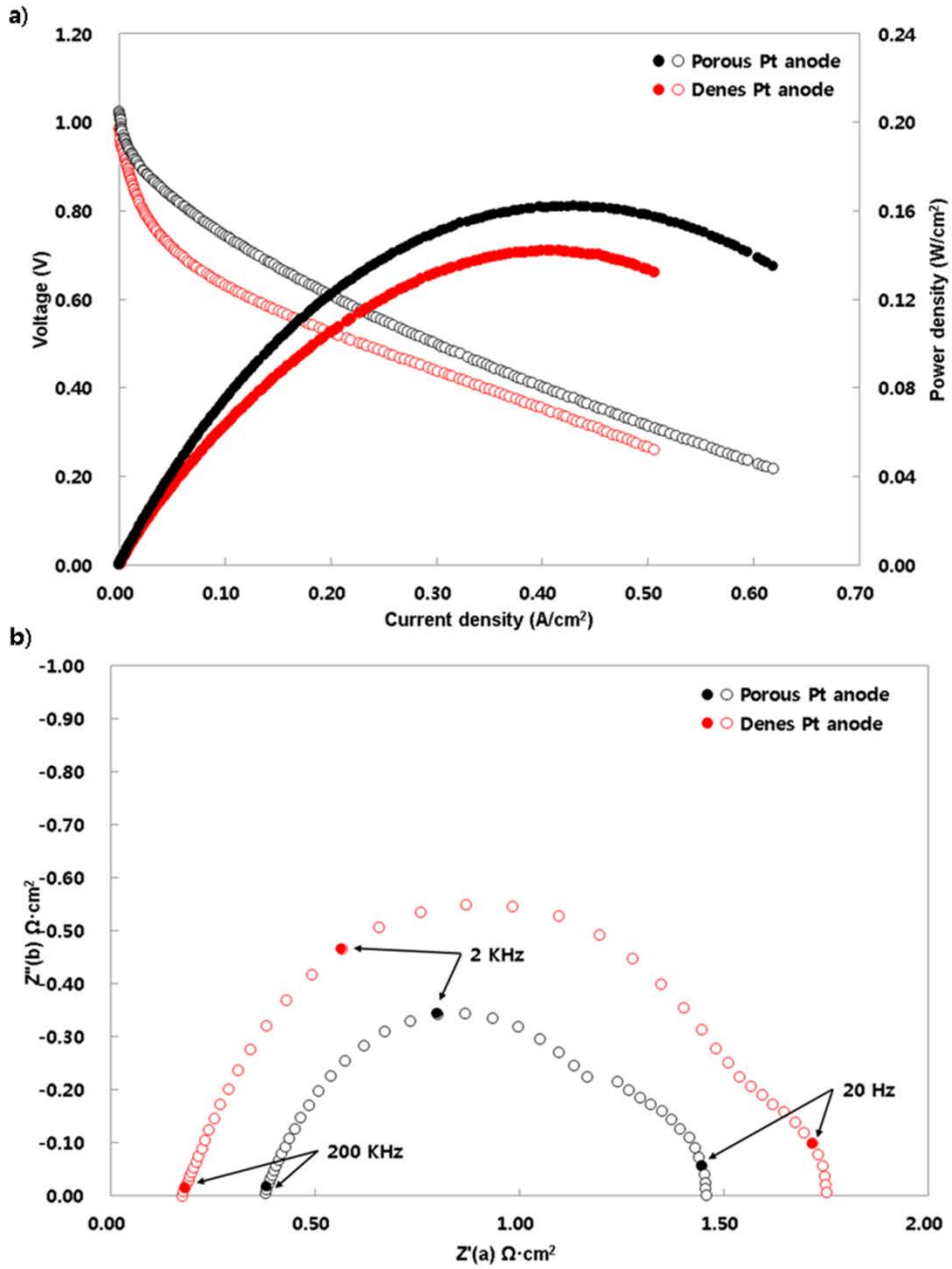

Figure 4.7. Electrochemical characteristics of fuel cells with different anode microstructure. a) Polarization curves of AAO based TF-SOFCs. b) Nyquist plots of fuel cells

As shown in figure 4.7., performance and EIS plots are obviously affected by anode microstructure. For AAO based TF-SOFCs with porous anode and dense anode, polarization curves of fuel cells present clear differences. (figure 4.7. a)) Like prior studies about anode structure of AAO based fuel cells, maximum power density of fuel cell was increased with porous anode structure due to improved fuel supplement and increment of TPBs. [15] Notably, activation loss of porous anode cell which was usually shown at low current density region was much smaller than dense anode cell.

In addition, in EIS results of fuel cells (figure 4.7. b)), radiuses of semicircles showed at the middle frequency region were decreased with porous anode microstructure – i.e. reduced anode polarization resistance by increasing anode porosity – at 0.5 V conditions while cathode polarization resistance (radius of low frequency semicircle) was almost similar. Therefore, large semicircle at middle frequency area showed in figure 4.6. was identified as the anode polarization resistance. Interestingly, in Nyquist plots, ohmic resistance – X-axis intercept point – of dense anode cell was smaller than porous anode cell due to higher in-plane electrical conductivity of dense microstructure.

Figure 4.8. illustrates Nyquist plots of AAO based TF-SOFCs under 0.5 V at 450 °C. High frequency area is showed at in-set.

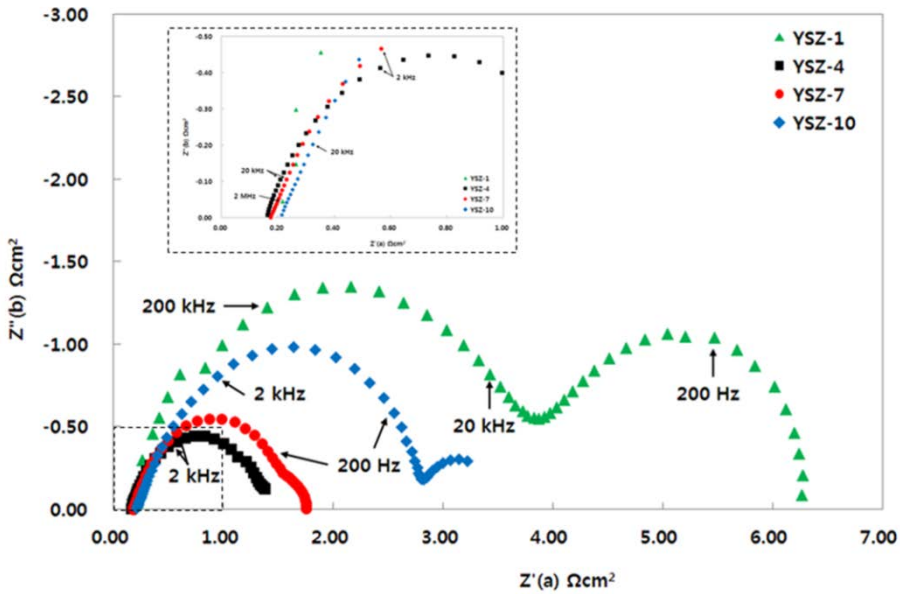

Figure 4.8. Nyquist plots of TF-SOFCs under 0.5 V at 450 ° C

As shown in figure 4.8., polarization resistances including both anode polarization and cathode polarization of fuel cells are obviously related with Y_2O_3 doping concentration of PEALD YSZ thin film electrolyte, while ohmic resistances of cells are almost identical. As mentioned above, heavily doped YSZ thin films are much helpful as a cathodic functional layer to reduce cathodic polarization resistance (14 ~ 19 mol. %) and showed much higher in-plane conductivity (10.9 mol. %) due to higher density oxygen vacancies at the cathode-electrolyte interface. [41,43,115] Therefore, differences in performance and polarization resistance from YSZ-10 to YSZ-4 (i.e. from 4.95 mol. % to 10.73 mol. %) cells are explained similar ways. For YSZ-4, higher Y_2O_3 doping concentration formed higher density of oxygen vacancies at the cathode-electrolyte interface which helped oxygen incorporation

reactions, and then, YSZ-4 showed the best performance and smallest polarization resistance in EIS. For YSZ-1 (32.4 mol. %), excessive Y_2O_3 doping concentration, was also explained similar manners. We think that too much Y_2O_3 concentration formed extremely high density of oxygen vacancies, and then, these too much oxygen vacancies interrupted each other for oxygen incorporation reactions. Thus, size of low frequency semicircles – cathodic polarization resistances – were as follows: YSZ-1 > YSZ-10 > YSZ-7 > YSZ-4. In addition, almost identical explains were also applied for HORs which were occurred at anode-electrolyte interface. Appropriately high Y_2O_3 doping concentration in YSZ thin film electrolyte helps HORs, but, too much Y_2O_3 doping concentration disturbs HORs like ORRs. Therefore, similar to cathodic polarization resistances, size of middle frequency semicircles (related with HORs) also showed identical order: YSZ-1 > YSZ-10 > YSZ-7 > YSZ-4.

4.4 Conclusions

In this study, evaluation of influence of Y_2O_3 doping concentration and optimization of Y_2O_3 doping concentration on characteristics of PEALD YSZ based TF-SOFCs were carried out. By controlling the ratio between ZrO_2 and Y_2O_3 process in PEALD YSZ supercycle, Y_2O_3 doping concentration was successfully changed. As thin film electrolytes of TF-SOFCs, surface morphology, cross sectional structure, and degree of crystallinity have no relation with Y_2O_3 concentration. (i.e. all TF-SOFCs showed almost identical surface morphology, cross-sectional structure, degree of crystallinity)

In contrast, performance of TF-SOFC was obviously dependent on Y_2O_3 doping concentration of PEALD YSZ thin film electrolyte. 10.73 mol. % Y_2O_3 doped cells showed the best performance (180 mW/cm^2 at 450 $^\circ C$) compared with other Y_2O_3 doped fuel cells. From EIS results, electrode polarization resistance including both anode polarization resistance and cathode polarization resistance were also greatly affected by Y_2O_3 doping concentration of PEALD YSZ thin film electrolyte. Therefore, extremely high Y_2O_3 concentration (32.4 mol %) cell showed the worst performance (27 mW/cm^2 at 450 $^\circ C$) and the largest polarization resistances.

CHAPTER 5 PROPERTIES OF ZrO_2 THIN FILMS PREPARED BY PEALD AT LOW TEMPERATURE (100 °C)

5.1 Introduction

Recently, flexible thin film electronics are drawing lots of attention due to their wide range of applications such as flexible display, battery, fuel cells, and solar cells. [127–130] Flexible or bendable devices generally necessitate polymer or metal foil substrates which are usually temperature sensitive. For emerging applications such as moisture permeation barrier for organic light emitting diodes, lighting applications, and corrosion resistance barrier layers for metals, temperature sensitive substrates are also widely used.[108,131–137] When such devices are fabricated on top of temperature-sensitive substrates, excessive heating may cause the permanent thermal degradation or surface oxidation of the substrates, which can significantly alter the properties of substrates and deteriorate the device performance. Therefore, the fabrication process which can deposit high quality thin films even at low temperature regime becomes important.

Plasma enhanced atomic layer deposition (PEALD) is considered as a promising candidate for depositing thin films at relatively low temperature. PEALD is a kind of energy-enhanced ALD which uses

highly reactive plasma species instead of conventional oxidants, e.g. water, oxygen, etc., for ligand exchange. [110,112,131,132,138] PEALD is known to have various advantages compared to thermal ALD: Most importantly, the reaction temperature for PEALD is known to expand significantly lower temperature regime than that of thermal ALD due to the use of highly reactive plasma species. Therefore, PEALD has been actively studied to prepare metal oxide thin films such as TiO_2, ZrO_2, or Al_2O_3 at low temperature for above emerging applications. [108,132–135,137] Additionally, PEALD typically shows higher growth rate than thermal ALD, and higher quality films with high density, enhanced stoichiometry, and low concentration of contamination because of the effective removal of ligands. The choice of precursors is also known to be more flexible.

Among metal oxide thin films prepared by PEALD, ZrO_2 is a promising high−k dielectric material which is considered as a strong candidate replacing of SiO_2. Due to the high dielectric constant related with crystal structure (~19.7 for monoclinic, ~46.6 for tetragonal, ~36.8 for cubic structure), many studies have been conducted to apply for volatile dynamic random access memory (DRAM), complementary metal oxide semiconductor, and metal oxide semiconductor field effect transistor. [139–146] ZrO_2 has good thermal compatibility with Si, wide band gap (4.6~5.8 eV) and wide band offset on Si (~1.4 eV). [142–145,147] ZrO_2 also has high melting point (2680 ° C), good oxidation resistance, and high reflective index (2.15~2.18 eV). [142,143] Furthermore, low boiling points (under 100 ° C) of commercial Zr precursors (tetrakis (dimethylamino) zirconium (TDMAZr) and tetrakis

(ethylmethylamino) zirconium) enable the film deposition at low temperature for aforementioned flexible devices.

In this study, we report the deposition of ZrO_2 thin films at low temperature (100 ° C) using PEALD with O_2 plasma. Effects of plasma parameters, i.e. power and duration on physical, chemical, and electrical properties of ZrO_2 thin films are systematically investigated and presented. Process flexibility as well as film quality controllability enabled by the use of plasma may open up new possibilities for novel applications of ALD.

5.2 Experimental

ZrO_2 thin films were deposited using a commercial direct showerhead type PEALD system with a radio frequency (RF) capacitively coupled plasma power source. (Atomic Premium, CN-1 Co., Korea) A p-type Si wafer (<100>, LG siltron Co., Korea) was used as a substrate for preparation ZrO_2 thin films. A commercial TDMAZr precursor (Sigma Aldrich, USA) was utilized for Zr source. The temperature of a bubbler type Zr canister was maintained at 50 ° C and the temperature of the canister line between chamber and canister was kept at 70 ° C to prevent condensation of a precursor. Substrate temperature was maintained at 100 ° C. High purity Ar gas (99.999%, Shinjin gas, Korea) was used as a carrier and a purging gas at a flow rate of 300 sccm. Pure O_2 gas (99.999% Shinjin gas, Korea) was used as a source for O_2 plasma at a flow rate of 100 sccm. One cycle of ZrO_2 deposition process was consisted of Zr pulsing (3 s), Ar purging (30 s), O_2 pulsing (1 s), O_2 pulsing with RF plasma (2~8 s), and Ar purging (30 s). 1 s of O_2 pulsing step was inserted before RF plasma step to stabilize the oxygen partial pressure. During O_2 pulsing step with RF plasma, 300 sccm of Ar was also supplied simultaneously to stabilize the plasma. Plasma duration and power were varied to investigate

effects on characteristics of ZrO_2 films. The thickness and surface morphology of ZrO_2 films were measured by focused ion beam electron spectroscopy (FIB-SEM, Quanta 3D, FEI Co., USA) with 5 kV of operation voltage. Chemical composition of ZrO_2 thin films were investigated by using x-ray photoelectron spectroscopy (XPS Theta probe base system, Al Kα (1486.6eV), Thermo Fisher Scientific, USA). Surface of samples were cleaned by using 150 eV Ar ion etching for 30s before measurements. Crystallinity and film density of ZrO_2 thin films were evaluated by using x-ray diffraction (XRD) with Cu Kα radiation in glancing mode and x-ray reflectivity (XRR, X' pert pro, PANalytical Co., Netherlands). Atomic force microscopy (XE150, Park system Co., Korea) was used to characterize the surface topography of 2 μm X 2 μm of as deposited ZrO_2 thin films in noncontact mode. Image processing and data analysis were conducted with XEI program. Electrical characteristics of ZrO_2 thin films were measured at room temperature under ambient air atmosphere by using HP4284A precision LCR meter. Metal-insulator-metal (MIM) structure was used to study electrical characteristics of as deposited ZrO_2 films. 300 cycles of ZrO_2 thin films were deposited on heavily doped p-type silicon wafer at 100 ° C. 50 nm thick gold top electrode was prepared on ZrO_2 thin films by thermal evaporation method. Leakage current-voltage characterizations and capacitance-voltage characteristics were characterized.

5.3 Results and Discussion

Generally, ALD thin films deposited at the temperature that is lower or higher than ALD window contain lots of impurities because of precursor condensation or thermal decomposition. [148–150] Impurities in thin films such as C can significantly affect the properties of thin films. [151,152] Figure 5.1. shows the results of XPS measurement of C and N contaminations within the ZrO_2 thin films. O_2 plasma power was changed from 25 W to 200 W and plasma duration was varied from 2 s to 8 s to investigate effects of plasma power and duration.

In spite of low deposition temperature, nearly 1 atom. % of C and negligible (<0.5 atom. %) amount of N impurities were detected from ZrO_2 thin films when the plasma power was 50 W or above regardless of duration. In case of 25 W of plasma power, negligible C and N contaminations were detected more than 4 s of plasma duration. These results can be explained by high reactivity of plasma species and physical bombardment of accelerated plasma species by plasma potential. [147,151] Because of these reasons, it is considered that ligands of precursors are perfectly removed despite of the low deposition temperature. However, in case of 25 W−2 s O_2 plasma, 3.41 atom. % of C and 1.4 atom. % of N were measured. This means that 25 W of plasma power and 2 s of duration were not enough to remove ligands.

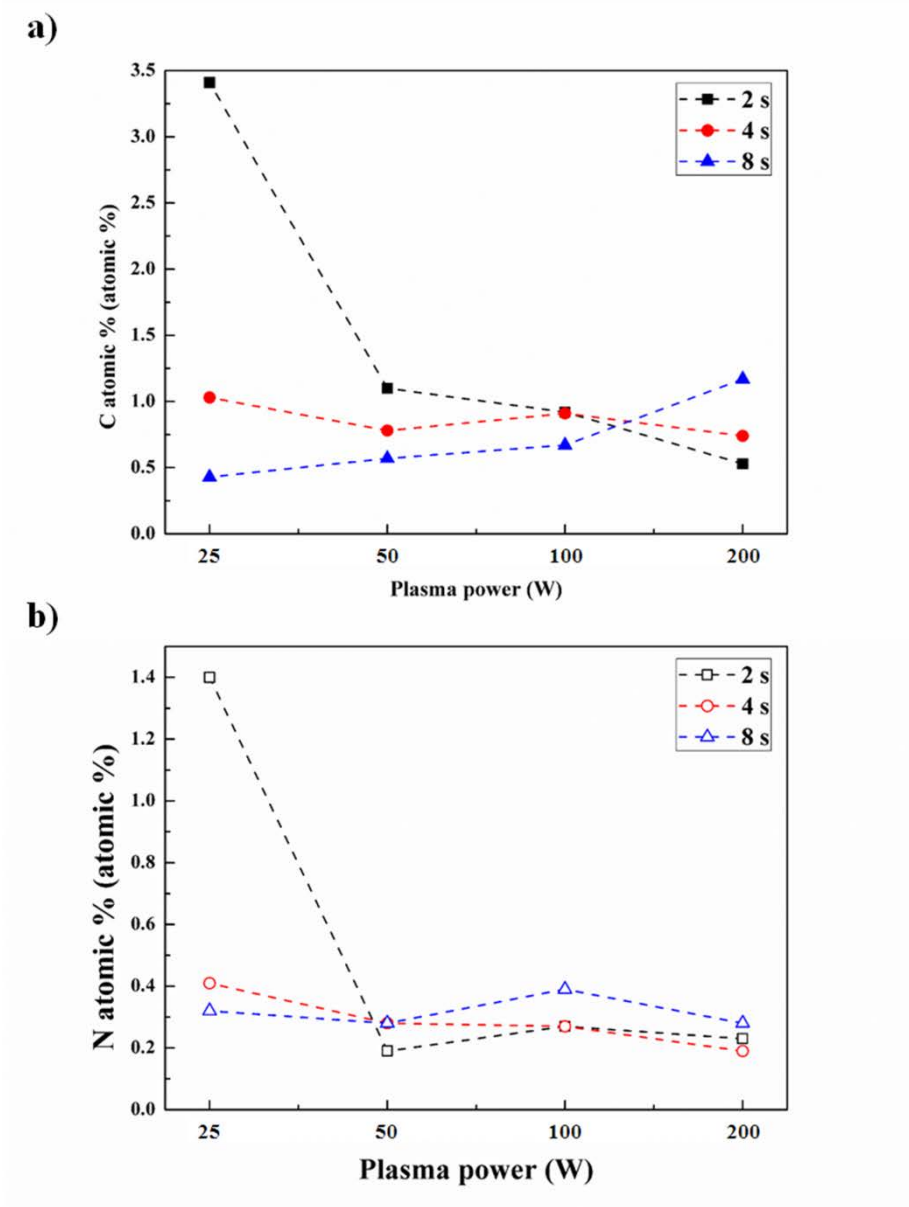

Figure 5.1. Chemical composition results of C and N impurities within the ZrO_2 thin films deposited by PEALD at 100 °C on bare Si wafer. a) C, b) N contaminations

Figure 5.2. presents the XRD results of ZrO_2 films. As previously

mentioned, the dielectric property of ZrO_2 is strongly related with the crystal structure of ZrO_2. [139–141]

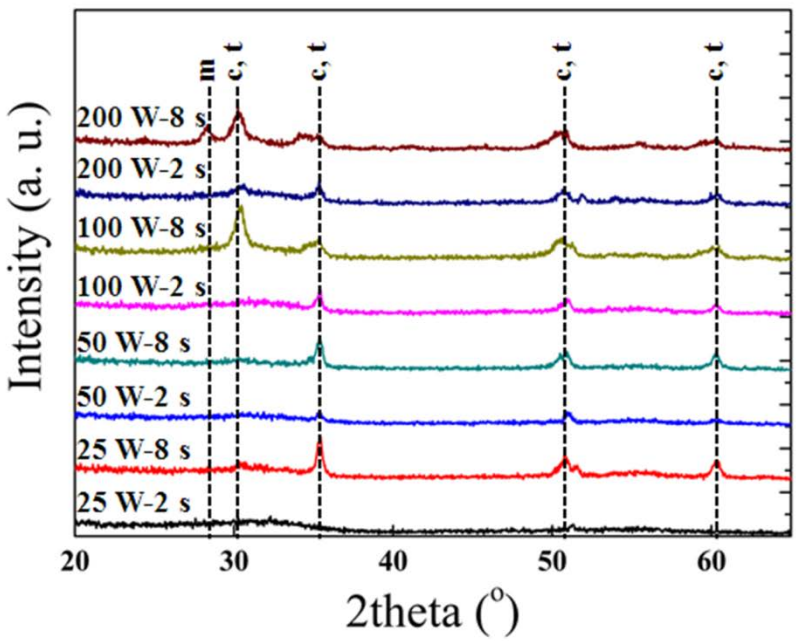

Figure 5.2. Crystallinity of ZrO_2 thin films prepared by means of PEALD at 100 ℃ on Si wafer

Generally, the crystal structure of ZrO_2 thin films by thermal ALD process largely depends on the substrate temperature. [153] On the contrary, figure 5.2., shows that the crystallinity of ZrO_2 films prepared by PEALD can be independently controlled by plasma power and duration even at the same substrate temperature. (100 ˚C) The diffraction peaks of ZrO_2 films became clearer and sharper as the plasma power increased from 25 W to 200 W. At the same power, the crystallinity of ZrO_2 films significantly improved as

the plasma duration increased from 2 s to 8 s. Relatively weak peaks were measured in all 2 s plasma duration ZrO_2 films, while clear and sharp peaks were observed in all 8 s plasma duration ZrO_2 films. This result implies that increasing plasma duration is more effective in improving the crystallinity of ZrO_2 films than increasing plasma power at low temperature. These tendencies are consistent with prior researches on the deposition of ZrO_2 film by PEALD. [151]

Despite low deposition temperature, the diffraction peaks of either cubic or tetragonal phases were clearly shown in the films with 8 s duration except 200 W-8 s ZrO_2 films that showed monoclinic phase (ICDD-JCPDS Card No. 01-080-0965, 00-027-0997, 00-036-0420). [125,141,151,153] In prior researches, ZrO_2 thin films prepared by thermal ALD with H_2O or O_3 as oxidants at relatively high deposition temperature (200 ° C~350 ° C) showed cubic or tetragonal crystal structure while those at low temperature (80 ° C) showed amorphous structure, which confirms that the crystallization of our ZrO_2 films is strongly related with the use of plasma. [125,153] Notable thing is that, in case of 200 W-8 s ZrO_2 films, monoclinic structure of ZrO_2 was observed. This may be due to large lateral grains of ZrO_2 due to high plasma power and long plasma duration. Hwang and Kim reported that ZrO_2 films prepared by CVD at high deposition temperature (above 475 ° C) formed monoclinic structure with large grains compared with tetragonal structure with small grains at low deposition temperature (350 ° C). [141] Thus, higher plasma power and longer plasma duration caused large lateral grains, then, affected the crystal

structure of ZrO_2 films.

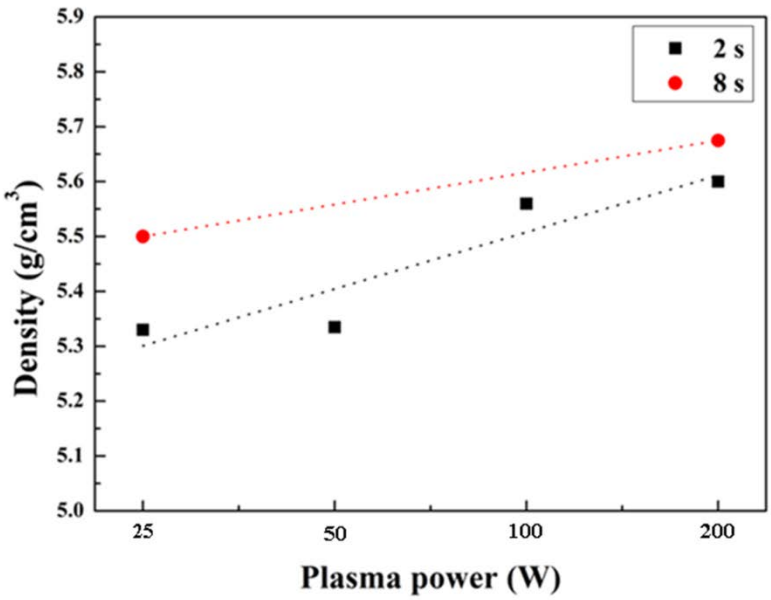

Figure 5.3. Density of ZrO_2 thin films synthesized by PEALD at 100 °C on Si wafer

Figure 5.3. shows the density of ZrO_2 thin films measured by XRR. Similar to the trend in crystallinity, the density of ZrO_2 films increased as the plasma power and duration increased. The densities of all ZrO_2 thin films were shown to be more than 90 % of the theoretical bulk ZrO_2 density (5.68 g/cm^3). In particular, the density of ZrO_2 films with 200 W−8 s of plasma power and duration was more than 95 % of the ideal density. These results could be because the additional energy provided by bombardment of plasma species has helped the surface adatoms to be more mobile. Therefore, the surface pores may have filled by the mobile adatoms

more easily increasing the density of films. [141] Additionally, more effective desorption of ligands by plasma could have led to the decrease of defects, e.g. impurities or voids and therefore, the formation of closer packed grains.

Surface morphologies of ZrO_2 films measured by using AFM are presented in figure 5.4. and summarized in figure 5.5.

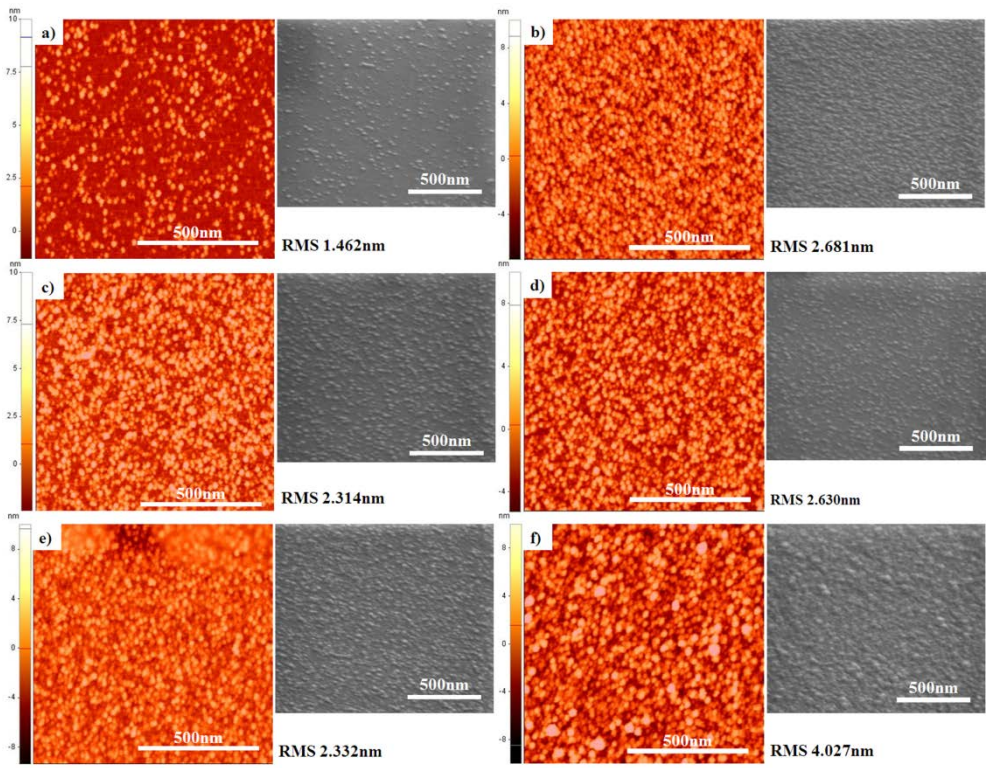

Figure 5.4. Surface characteristics of ZrO_2 films fabricated by PEALD at 100 ℃ on Si wafer. Preparation conditions of plasma power and duration are a) 25 W−2 s ZrO_2, b) 25 W−8 s ZrO_2, c) 50 W−2 s ZrO_2, d) 100 W−2 s ZrO_2, e) 200 W−2 s ZrO_2, and f) 200 W−8 s ZrO_2, respectively.

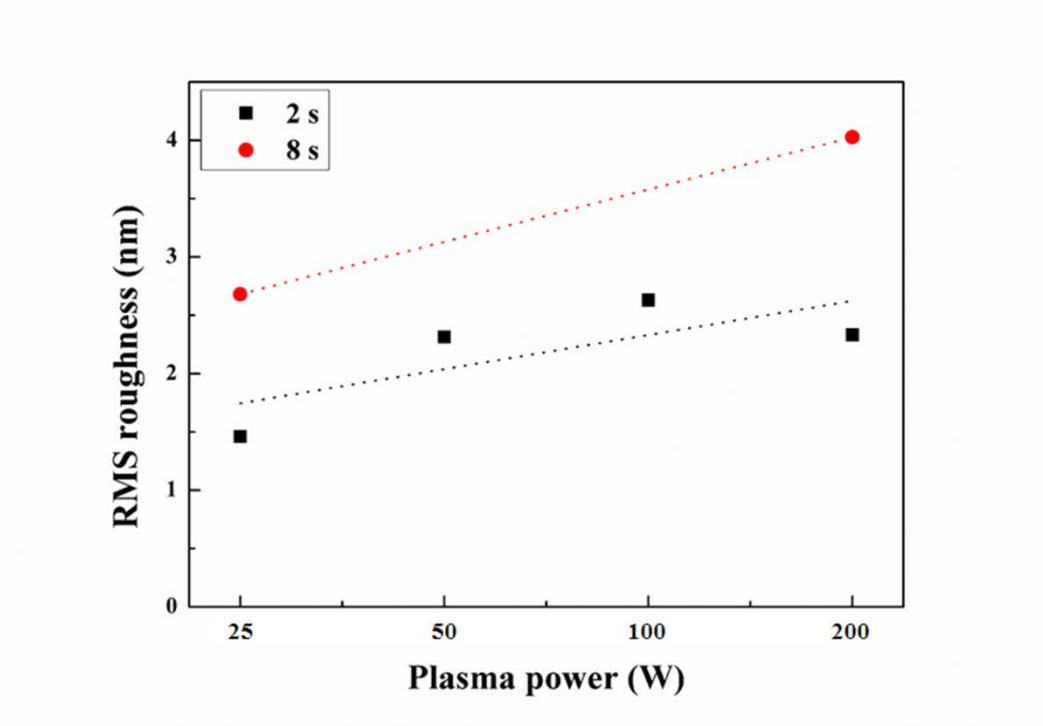

Figure 5.5. Surface RMS roughness with respect to plasma power and duration measured by AFM

RMS roughness increased when plasma power and duration increased. Despite of low deposition temperature, surface roughness of our ZrO_2 films were similar to that of ZrO_2 films reported previously. [154,155] Actually, surface roughness has been reported to increase as the deposition temperature becomes lower due to inhomogeneous gas adhesion on adsorption site. [156] In this study, however, physical bombardment of plasma species with superior reactivity seems to help to remove ligands and side products and therefore, make smooth surface ZrO_2 films. Furthermore, RMS roughness increases in accordance with the increase of plasma duration, which was also reported in prior

reports. [155] Increment of roughness seems to be caused by the enhanced crystallization, i.e. growth of facets of films at higher plasma power and longer plasma duration, which have induced the formation of rough surface. [125,153]

Electrical characterization of ZrO_2 films was conducted using MIM structure.

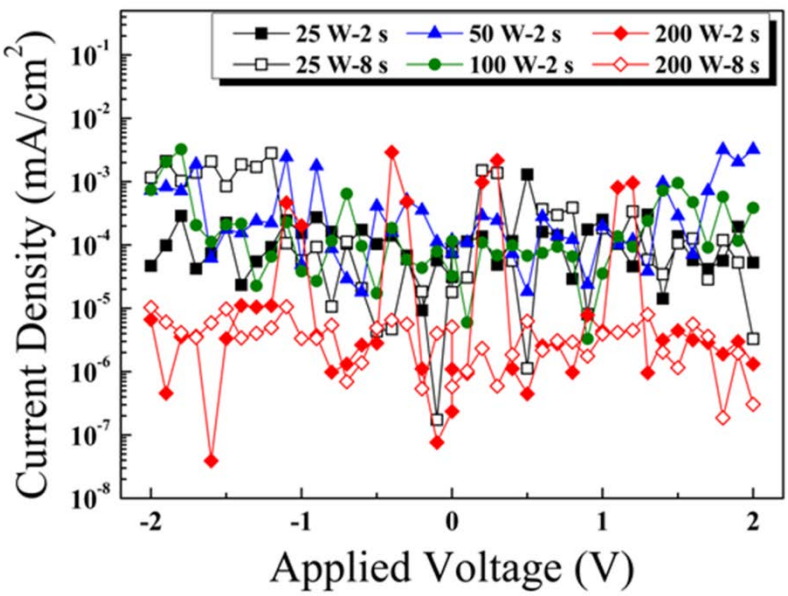

Figure 5.6. Leakage current as a function of applied voltage characteristics of ZrO_2 thin films prepared using 2 s and 8 s plasma duration and plasma power varying between 25W and 200W

Figure 5.6. shows leakage current density vs. applied voltage plot of PEALD ZrO_2 films. Leakage current density of ZrO_2 thin films were mostly in the range from 10^{-6} mA/cm^2 to 10^{-3} mA/cm^2 between −2 V and 2 V. 200 W−2 s and 200 W−8 s ZrO_2 films

showed lower leakage current density than any other ZrO_2 films. When ZrO_2 thin films are deposited with the plasma power of 200 W, the leakage current density decreased by up to one order compared with those prepared with less plasma power. We speculate that relatively low concentration of C and N impurities combined with the high film density by high power plasma may have improve the leakage current characteristics of ZrO_2 films.

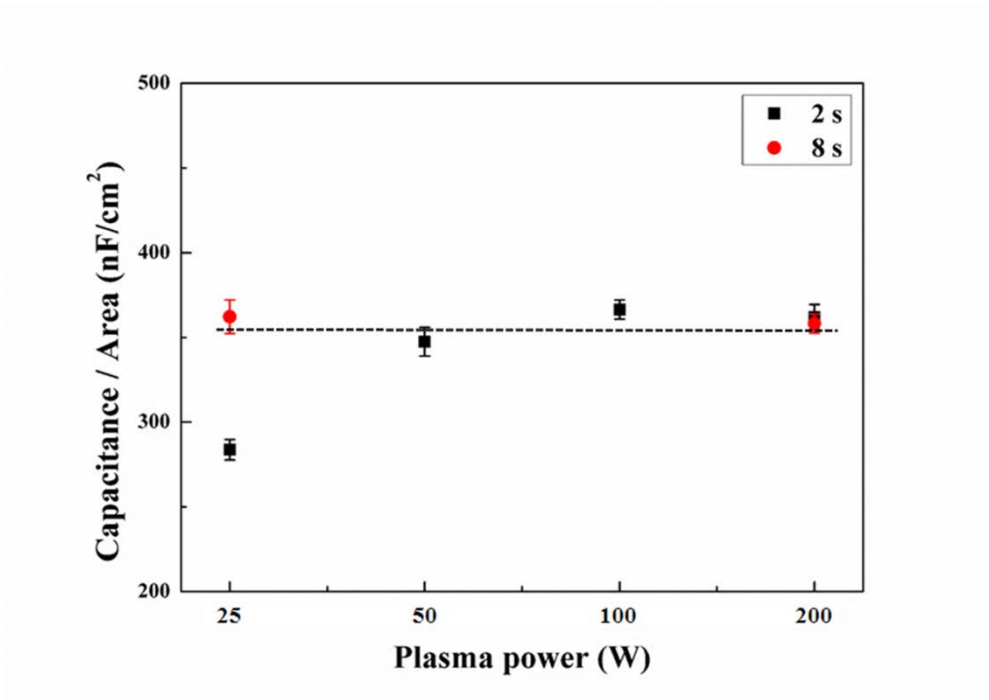

Figure 5.7. Capacitance with respect to plasma power and duration of ZrO_2 films

Capacitance – applied voltage characteristics are also presented in figure 5.7. The thicknesses of ZrO_2 thin films were consistent as 60 nm ± 5 nm. Capacitances of MIM structures were very similar

to each other except the 25 W−2 s ZrO_2 film. The 25 W−2 s ZrO_2 films demonstrated lower capacitance than other ZrO_2 films. Lower capacitance of 25 W−2 s ZrO_2 film than other films could be due to lower crystallization level and lower film density. Higher concentration of impurities combined with low plasma power and short plasma duration have prevented the film from being crystallized as was shown in figure 5.2., which significantly lowers the polarization and, therefore, the dielectric constant. Low film density also could be another reason for low dielectric constant. [141] Calculated dielectric constants based on the capacitance of ZrO_2 films including low dielectric constant (k=3.9) of SiO_2 interfacial layer were 19.26 (25 W−2 s), 24.02 (25 W−8 s), 22.93 (50 W−2 s), 24.29 (100 W−2 s), 23.96 (200 W−2 s), and 23.94 (200 W−8 s), respectively. Dielectric constant of ZrO_2 films including SiO_2 layer were consistent with dielectric constant reported in prior researches for tetragonal or cubic structured ZrO_2 thin films. [151]

5.4 Conclusions

In this study, we prepared ZrO_2 thin films through PEALD process at 100 ° C by using TDMAZr precursor and O_2 plasma.

Despite of low deposition temperature, XPS results demonstrated low impurities (C and N) concentration in ZrO_2 thin films due to highly reactive O_2 plasma species except the 25 W-2 s due to insufficient plasma power and duration. Crystallinity of ZrO_2 thin films were strongly related with plasma power and duration. As plasma power and duration increased, the crystallinity of ZrO_2 thin films improved. Also, in spite of low deposition temperature, tetragonal or cubic structured ZrO_2 films were deposited. Moreover, the density of ZrO_2 thin films also enhanced as plasma power and duration increased. Surface roughness of ZrO_2 thin films became higher as plasma power and duration increased due to improved crystallinity, but was still kept at relatively low level.

The capacitance - applied voltage as well as the leakage current density - applied voltage characteristics showed technically interesting trends that we can independently control the electrical properties of the films by varying the plasma parameters (power and duration). More importantly, using the high-power (200 W) and long-duration (8 s) plasma, we can deposit the ZrO2 films with improved leakage current density with relatively high dielectric constant.

The result reported in this paper may have implications in

widening the applications of PEALD ZrO_2 thin films by elucidating the relation between the film’s basic properties and the plasma conditions

CHAPTER 6 CHARACTERISTICS OF Y_2O_3 THIN FILMS PREPARED BY PEALD

6.1 Introduction

Y_2O_3 is an attractive material for various applications because of its especially interesting physical, chemical, and electrical characteristics. Y_2O_3 is used for buffer layers for ferroelectrics and protective coating layers due to its chemical stability and high melting point. (melting point of Y_2O_3 : 2450° C) [157–159] Y_2O_3 is also applied for optical applications such as a waveguide material due to its high refractive index and Y_2O_3 : Eu^{2+} which is well known red emitting phosphor. [157,158] $YBa_2Cu_3O_{7-\delta}$ is generally known high T_c superconductor [157,158] Moreover, Y_2O_3 is also a constituent of yttria stabilized zirconia (YSZ) which is the most typical electrolyte material for solid oxide fuel cells (SOFCs). [1,2] Above of all aforementioned applications, Y_2O_3 is generally known as promising materials for application to microelectronics such as complementary metal oxide semiconductor (CMOS) devices, thin film transistor (TFT) devices, metal–oxide–semiconductor field effect transistor (MOSFET) devices, and metal–insulator–semiconductor (MIS) devices due to its relatively high dielectric

constant (10–18), wide band gap energy (5–6eV), low lattice mismatch with silicon (a(Si) = 1.086nm, a(Y_2O_3) = 1.061nm), large conduction band offset (2.3eV), and good thermodynamic compatibility. [157–161] Therefore, Y_2O_3 is prepared by various thin film techniques such as plasma–enhanced metal organic chemical vapor deposition, sputtering, electron beam evaporation, molecular beam epitaxy, laser ablation, chemical vapor deposition (CVD), atomic layer deposition (ALD) to investigate characteristics of Y_2O_3 films or aforementioned devices. [157–161]

Among previously mentioned methods, ALD is considered as the next generation thin films techniques due to availability of precise thickness control, high uniformity, and superior step coverage. [112] Plasma enhanced atomic layer deposition (PEALD) is an energy enhanced ALD techniques which uses high reactivity of plasma species such as ions and electrons during process. PEALD usually shows higher growth rate improved physical and chemical properties of films due to superior reactivity of plasma species. [108,110,112,117] Generally, thin films which is prepared by PEALD presents higher density, improved contaminations, enhanced stoichiometry, and improved crystallinity compared with films deposited by thermal ALD. [108,110,112] And these improved and changed physical and chemical characteristics of films have influences on properties of thin films. For example, polycrystalline structure of film due to improved crystallinity by PEALD deteriorates leakage current characteristics of other oxide films.

Therefore, in this study, we synthesized and investigated Y_2O_3 thin films using commercial $(CpCH_3)_3Y$ precursor and O_2 plasma

through PEALD method to verify effects of plasma on characteristics of Y_2O_3 films. In order to corroborate characteristics of Y_2O_3 films using $(CpCH_3)_3Y$ precursor by PEALD, physical, chemical and electrical characteristics of Y_2O_3 films prepared by PEALD were investigated.

6.2 Experimental

To prepare Y_2O_3 thin films, we used a commercial showerhead type direct PEALD system (Atomic Premium, CN1 Co., Korea). To characterize growth rate of Y_2O_3 thin films, crystallinity, chemical composition, density of thin films, a commercial one side polished p type silicon wafer (100) (LG Siltron Inc., Korea) was used as a substrate. For characterization of electrical properties, Y2O3 thin films were deposited on heavily doped p type silicon wafer at different substrate temperature, 175 ° C, 250 ° C, and 325 ° C, respectively. 300 cycles of Y_2O_3 thin films was maintained. 50nm thick and 5.76mm^2 (2.4mm X 2.4mm) gold electrode was deposited on Y_2O_3 thin films by thermal evaporation method. Capacitatance – Voltage (CV) characteristics of MIM structures were measured by using a HP4284A precision LCR meter.

A tris (methylcyclopentadienyl) yttrium ($(MeCp_3)_3Y$) precursor was kept in stainless steel canister. The temperature of canister was maintained at 145 ° C and the temperature of stainless steel line between chamber and canister was maintained at 155 ° C to prevent condensation of precursor. The temperature of stage was changed from 175 ° C to 325 ° C at 25 ° C intervals to study effects of substrate temperature. High purity argon gas (99.9999%, Shinjin Gas Co., Korea) was used as a purging gas and a carrier gas. 300 standard cubic centimeter per minute (SCCM) of argon gas was

used for both carrier gas and purging gas. 100sccm of high purity oxygen gas (99.999%, Shinjin Gas Co., Korea) was supplied to chamber during the reactant step, i.e. plasma step. The PEALD process of one Y_2O_3 cycle composed of a precursor pulsing (5s), argon gas purging (60s), oxygen gas pulsing (1s), oxygen gas pulsing with radio frequency (RF) plasma (8s), argon purging (60s). In order to stabilize partial pressure of oxygen gas in a chamber, 1 second of oxgen gas pulse was used before 8 seconds of plasma step. Due to low vapor pressure of a tris (methylcyclopentadienyl) yttrium ($(MeCp_3)_3Y$) precursor, precursor pulse time was kept 5 seconds. Purging time is also maintained 60 seconds to prevent condensation of precursor. The 50W of RF plasma power and 8 seconds of duration time were maintained.

The crystallinity, density and thickness of Y_2O_3 thin films were characterized by X-ray diffraction (XRD) with the glancing scan mode and X-ray reflectivity (XRR, X' pert pro, PANalytical Co., Netherland). Chemical compositions of Y_2O_3 thin films were analyzed by X-ray photoelectron spectroscopy (XPS, Theta probe base system, Thermo Fisher Scientific Co., USA).

6.3 Results and Discussion

Figure 6.1. shows growth per cycle (GPC) of PEALD Y_2O_3 thin films on Si wafer as a function of substrate temperature.

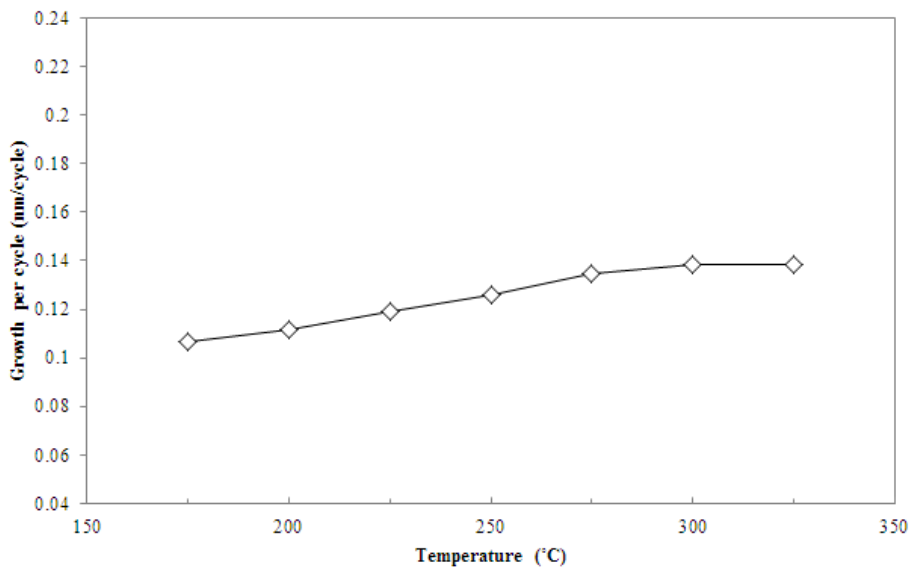

Figure 6. 1. Growth rate of Y_2O_3 thin films prepared by PEALD on Si wafer

Each Y_2O_3 thin films were deposited 300 cycles, respectively. The physical thickness of Y_2O_3 thin films were analyzed by XRR and GPC is calculated by dividing the thickness by number of cycles. As you can see from the figure, GPC is slightly increased from 0.11nm/cycle to 0.13nm/cycle as the substrate temperature is increased up to 275 ° C. After 275 ° C of substrate temperature,

GPC is almost maintained about ~0.13nm/cycle. For all range of substrate temperature, however, clear ALD window which shows constant GPC as a function of substrate temperature is not observed. Instead, GPC is improved slightly compared with GPC deposited by thermal ALD especially at low substrate temperature range. [158] Improved GPC of Y_2O_3 thin films prepared by PEALD compared with GPC of Y_2O_3 deposited by thermal ALD is due to high reactivity of plasma species which cause higher density of reactive surface sites. [108,110,112,138]

After GPC characterization, chemical compositions of Y_2O_3 thin films were analyzed.

T (℃)	175	200	225	250	275	300	325	250_O_2
Y3d	41.48	41.99	42.64	43.09	44.02	44.17	43.58	29.67
O1s	56.86	56.59	56.16	55.91	55.16	54.98	55.63	55.65
C1s	1.67	1.42	1.2	1	0.82	0.85	0.79	14.68

Table 6.1. Chemical composition of PEALD Y_2O_3 thin films on Si wafer

Table 6.1. shows chemical composition of thin films characterized by XPS. In order to compare chemical compositions, the chemical composition of Y_2O_3 thin film prepared by a thermal ALD at 250 ° C which uses oxygen gas as a reactant is also listed. Y_2O_3 deposited by a thermal ALD contains lots of carbon impurities in films, i.e. 14.68 atomic %. It is due to poor reactivity of the oxygen gas as a reactant to tris (methylcyclopentadienyl) yttrium ($(MeCp_3)_3Y$) precursor. [108,110,112,138] However, chemical composition results of Y_2O_3 thin films prepared by PEALD contains

very small amount of carbon in thin films even in low substrate temperature. These results means that ligands of tris (methylcyclopentadienyl) yttrium ($(MeCp_3)_3Y$) precursor are perfectly oxidized by high reactive plasma species and requirement of thermal energy to form thin films is decreased in PEALD process. According to decrement of carbon impurities, stoichiometry of Y_2O_3 thin films are also improved compared with Y_2O_3 prepared by thermal ALD due to excellent reactivity of plasma species.

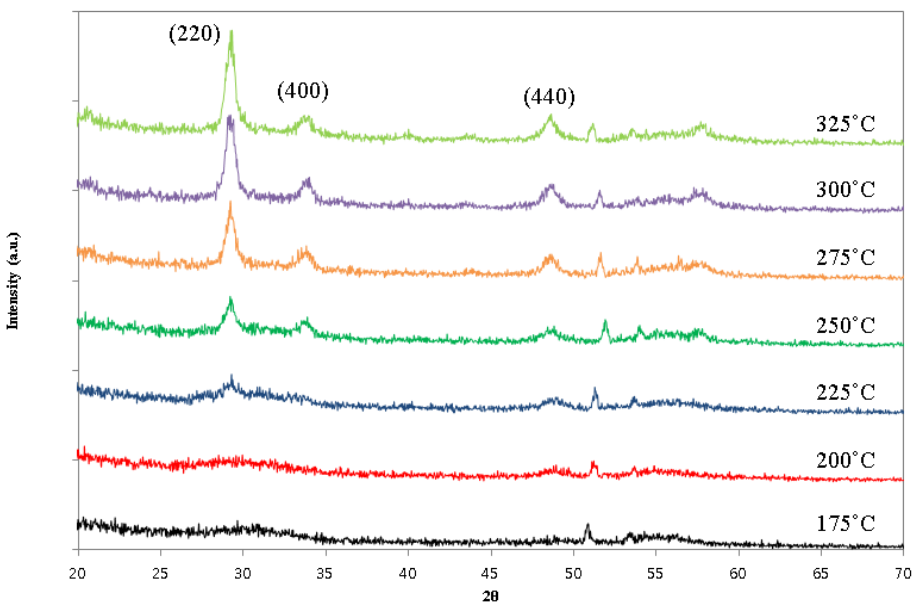

Figure 6.2. XRD results of PEALD Y_2O_3 thin films prepared on Si wafer

Figure 6.2. presents crystalline structure and crystallite orientation of Y_2O_3 thin films fabricated by PEALD onto Si (100) wafer. Thicknesses of Y_2O_3 thin films were deposited from 175 ˚C to 325 ˚C were about 40nm. Above 250 ˚C of substrate

temperature, (400) and (440) peak is appeared and (222) reflection peak is getting more clear and sharpened as the substrate temperature is increased. These results are well matched with prior research. [158] However, (222) peak is appeared more lower temperature and clear in spite of thinner Y_2O_3 films. This may be due to high reactivity of plasma species or bombardment of ions and electrons. [108,112,138,150,162]

Table 6.2. shows film density results of Y_2O_3 thin films on Si (100) wafer by XRR measurement.

T (˚C)	175	200	225	250	275	300	325
Density (g/cm^3)	4.91	4.99	4.96	4.82	5.01	5.01	5

Table 6.2. Density of PEALD Y_2O_3 thin films as a function of the substrate temperature

Ideal bulk density of Y_2O_3 is 5.03g/cm^3. As you can see from the table, density results of all Y_2O_3 films are above 95% of ideal bulk Y_2O_3 density. And density of Y_2O_3 thin films is increased to ideal value as the substrate temperature is increased, except Y_2O_3 thin films prepared at 250 ˚C. Reasons for sudden decrease of Y_2O_3 at 250 ˚C has been studied in our laboratory

Figure 6.3. depicts the capacitance – voltage curves for MIM structure where Y_2O_3 thin films were deposited by PEALD process at different temperature – 175 ˚C, 250 ˚C, and 325 ˚C for 300 cycles. As you can see from the figure 6.3., capacitance is decreased as the substrate temperature is increased due to

increment of Y_2O_3 thickness. However, capacitances of each film are maintained almost constant with respect to measured frequency. According to the GPC of Y_2O_3 as a function of substrate temperature, thickness of Y_2O_3 thin films are 32nm, 37.8nm, and 41.5nm, respectively. By using the thickness of Y_2O_3 thin films, dielectric constant k is calculated. Average dielectric constants of each Y_2O_3 thin films are 15.5, 17.2, and 16.1 at 1kHz, respectively. Dielectric constants of Y_2O_3 thin films prepared by PEALD are slightly higher than known values. [102,158] but, are not changed as a function of the substrate temperature.

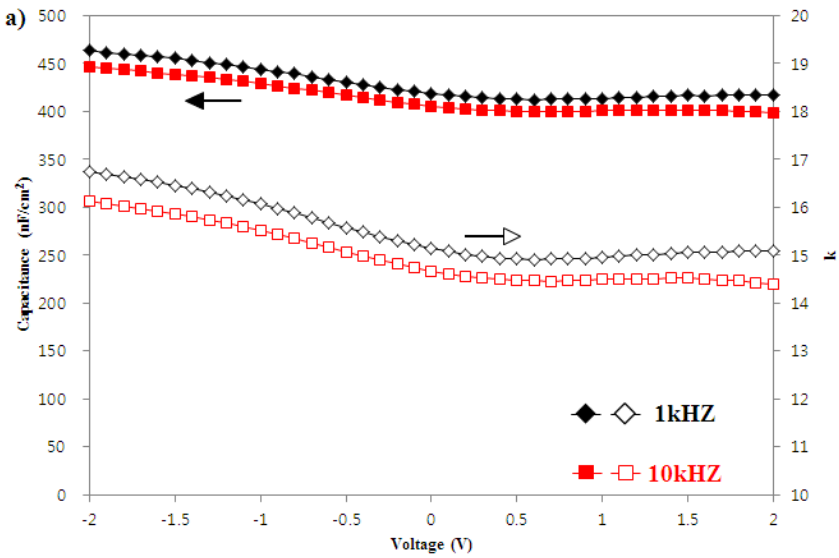

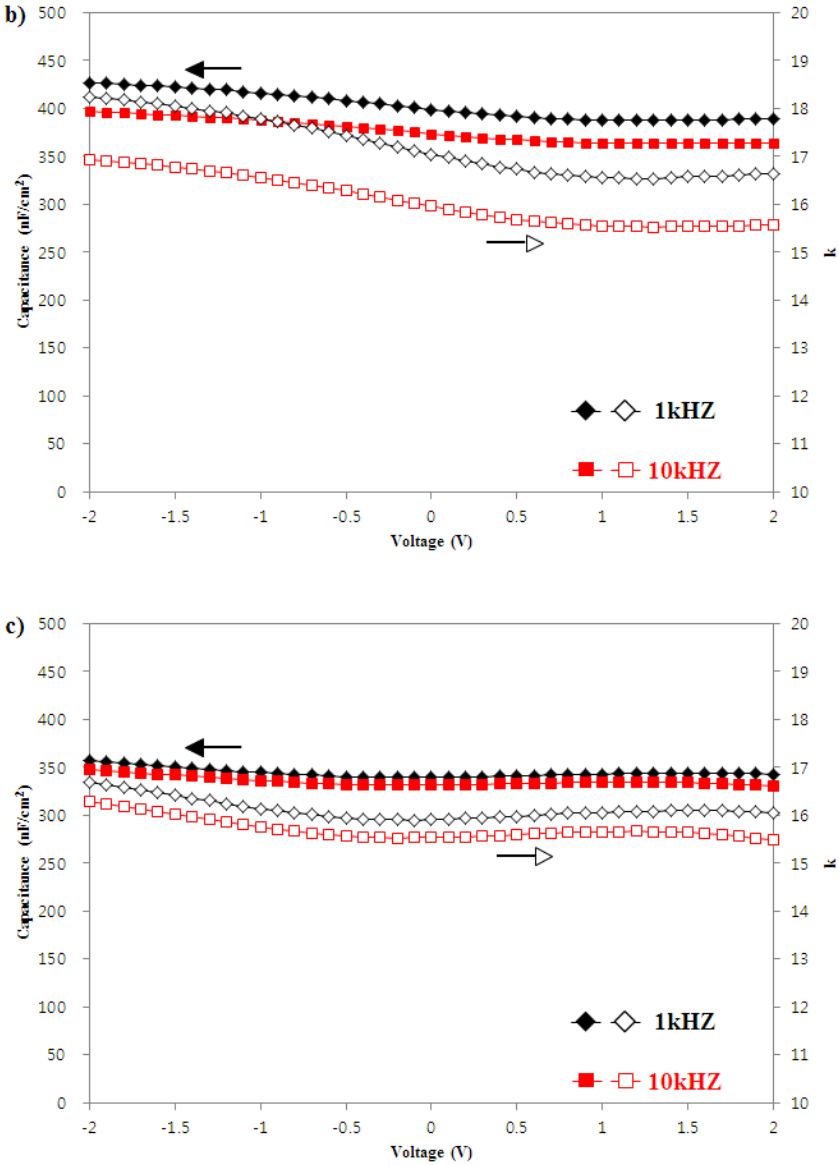

Figure 6.3. Electrical characteristics of PEALD Y_2O_3 thin films by using MIM. a) C-V characteristics of p-Si/PEALD Y_2O_3 prepared at 175°C/Au. b) C-V characteristics of p-Si/PEALD Y_2O_3 prepared at 250°C/Au. c) C-V characteristics of p-Si/PEALD Y_2O_3 prepared at 325°C/Au.

6.4 Conclusions

In this research, Y_2O_3 thin films are successfully deposited on Si (100) wafer by PEALD method. A commercial tris (methylcyclopentadienyl) yttrium ($(MeCp_3)_3Y$) precursor and oxygen plasma are used as a precursor and reactant. In spite of the unclear ALD window, growth rate per cycle is improved compared with prior researches about a thermal ALD of Y_2O_3. Carbon contaminations in Y_2O_3 thin films are drastically decreased and film stoichiometry is improved due to high reactivity of oxygen plasma species. The crystallinity of Y_2O_3 thin films are clear and increased as the substrate temperature is increased. The densities of Y_2O_3 thin films measured by XRR are above 95% of theoretical bulk Y_2O_3 density. Capacitance – voltage characteristics of Y_2O_3 thin films are measured and dielectric constants for Y_2O_3 thin films are calculated. Dielectric constants are slightly higher, 15~17, however, are almost identical with the substrate temperature.

CHAPTER 7 Concluding Remarks

7.1 Summary

This study investigated on characteristics of PEALD YSZ and showed possibility of PEALD YSZ as oxygen ion conducting thin film electrolyte of nano-porous AAO based TF-SOFCs for the first time. In addition, chemical, physical and electrical properties of ZrO_2 and Y_2O_3 thin films - well known high k materials and composition materials of YSZ thin films - prepared by PEALD process were investigated.

First, influence of preparation techniques on properties of YSZ films was investigated. PEALD YSZ showed superior chemical composition (negligible impurities) and improved crystallinity compared with sputter YSZ and thermal ALD YSZ. Compared with PEALD and thermal ALD YSZ, TF-SOFCs with 140 nm thick sputter YSZ thin film electrolyte showed perfectly short circuit due to formation of defects or pin-holes. Interestingly, TF-SOFCs based with thermal ALD YSZ showed low OCV and peak power density than TF-SOFCs based with PEALD YSZ, because of carbon contaminations of thermal ALD YSZ. High concentration of carbon impurities caused internal short circuit (leakage current through ALD YSZ thin film electrolyte), and then, reduced the OCV and performance of fuel cells.

After investigation of influence of fabrication process, effects of plasma power and duration on characteristics of PEALD YSZ were systematically studied. Chemical compositions of PEALD YSZ films (Y_2O_3 mol. %) were highly independent of plasma conditions. In contrast with chemical properties, in-plane oxygen ion conductivities of YSZ films on single crystal MgO substrates were clearly related with plasma power and duration. Increase of plasma power and duration caused enhanced in-plane oxygen ion conductivity due to improved degree of crystallinity of PEALD YSZ films. After film characterization, electrochemical properties of PEALD YSZ were examined as an oxygen ion conducting thin film electrolyte of TF-SOFC. Pt anode - PEALD YSZ thin film electrolyte - Pt cathode structure on nano-porous AAO substrate showed 95.4 mW/cm^2 and 217.5 mW/cm^2 at 450 °C and 550 °C, respectively.

In order to improve performance of TF-SOFCs with PEALD YSZ thin film electrolyte, optimization of Y_2O_3 concentration of PEALD YSZ was carried out. Y_2O_3 concentration of PEALD YSZ was controlled by changing the ratio of ZrO_2 and Y_2O_3 process in the YSZ supercycle. Effects of Y_2O_3 doping ratio on chemical and physical characteristics of PEALD YSZ films were evaluated. Y_2O_3 concentration was successfully controlled by changing the ratio of ZrO_2 and Y_2O_3 process. Crystal structure of PEALD YSZ films were very similar regardless of Y_2O_3 concentration, except 32.4 mol. % Y_2O_3 concentrated YSZ films. (ZrO_2 : Y_2O_3 = 1:1) As oxygen ion conducting thin film electrolytes, TF-SOFCs with 10.73 mol. % Y_2O_3 concentrated YSZ showed the best performance - 180

mW/cm^2 at 450 °C, which were 26.8 %, improved performance than 7.24 mol. % YSZ based cell.

As a promising high k material, ZrO_2 is considered as a strong candidate replacing of SiO_2. In order to utilize many advantages of ZrO_2 such as high dielectric constant, wide bandgap, and wide band offset on Si, on thermal sensitive substrates – flexible polymer or metal foil – ZrO_2 thin films were prepared at low temperature (100 °C) by using PEALD process and characterized. In spite of low temperature, LT PEALD ZrO_2 thin films showed negligible contaminations and clear polycrystalline structure due to superior reactivity of oxygen plasma species – activated atoms, ions, and electrons. Electrical characteristics (leakage current vs. applied voltage and capacitance vs. applied voltage) of ZrO_2 thin films were measured by using MIM structure. Using high plasma power and long duration, electrical characteristics of LT PEALD ZrO_2 thin films were improved.

Finally, PEALD Y_2O_3 thin films were prepared and characterized using the commercial tris−(methylcyclopentadienyl)−yttrium ($(MeCp_3)_3Y$) precursor. In spite of unclear ALD window of PEALD Y_2O_3, growth rate was increased than prior thermal ALD researches. Moreover, contamination of Y_2O_3 film was dramatically improved due to superior reactivity of plasma species. By using MIM structure, capacitance vs. applied voltage characteristics were measured, and then, dielectric constants was calculated.

7.2 Future Works

In this dissertation, chemical, physical, and electrochemical characterizations of PEALD YSZ thin films are described. Influence of deposition conditions of PEALD (plasma power and plasma duration), effects of deposition techniques (sputter, thermal ALD, and PEALD), and finally, influence of Y_2O_3 dopant concentration on properties of YSZ films were systematically studied. At the same time, application of PEALD YSZ as a thin film electrolyte of AAO based TF-SOFCs (Pt - PEALD YSZ - Pt) was carried out to evaluate electrochemical properties of YSZ films in the device level. After characterization and application of YSZ thin films, detailed studies about individual PEALD ZrO_2 and Y_2O_3 thin films - both are promising high k materials - were carried out, respectively.

In spite of enormous possibilities of PEALD as mentioned in chapter 1, this study only uses very small characteristics of PEALD like the tip of the iceberg. Therefore, more detailed and comprehensive studies about PEALD and thin films prepared by PEALD should be required such as process optimization (e.g. plasma power, time (duration), temperature, flow, and distance at substrate - plasma generator, volume ratio between plasma sources gas). Also, using the most critical issue of PEALD, i.e. superior reactivity of plasma species - activated atoms, ions, and electrons, attempt new precursor which have the lower melting point temperature than melting point temperature of the

tris(methylcyclopentaldienil)yttrium (150 °C) to lower the YSZ deposition temperature.

In TF-SOFCs, PEALD YSZ thin film electrolyte is utilized for the first time. In spite of much thinner PEALD YSZ thin film electrolyte than sub-micrometer scale YSZ thin film electrolyte prepared by various techniques (sputter and PLD), OCVs of TF-SOFCs have been measured near the theoretical value (calculated by the Nernst equation). This good OCV implies that PEALD YSZ shows pin-hole free and perfect gas-tightness characteristics in 100 nm level. However, thinner PEALD YSZ thin film electrolyte can lead to the increase of performance of TF-SOFCs. Therefore, optimization of PEALD YSZ thickness (as thin as possible) which secures gas-tightness and pin-hole free characteristics simultaneously is required.

This study may provide important insights in the design of high-performance TF-SOFCs, and finally, significant perception of commercialization of TF-SOFCs for various applications. At the same time, results of this thesis can enlarge the area of PEALD not only for high k oxide thin films but also next generation thin film electrochemical energy conversion devices.

REFERENCES

[1] R.P. O'Hayre, S.-W. Cha, W. Colella, F.B. Prinz, Fuel cell fundamentals, John Wiley & Sons New York, 2006.

[2] S.C. Singhal, K. Kendall, High-temperature solid oxide fuel cells: fundamentals, design and applications: fundamentals, design and applications, Elsevier, 2003.

[3] J. Larminie, A. Dicks, M.S. McDonald, Fuel cell systems explained, Wiley New York, 2003.

[4] I. Chang, S. Ji, J. Park, M.H. Lee, S.W. Cha, Ultrathin YSZ Coating on Pt Cathode for High Thermal Stability and Enhanced Oxygen Reduction Reaction Activity, Adv. Energy Mater. 5 (2015) n/a–n/a. doi:10.1002/aenm.201402251.

[5] J.Y. Paek, I. Chang, J.H. Park, S. Ji, S.W. Cha, A study on properties of yttrium-stabilized zirconia thin films fabricated by different deposition techniques, Renew. Energy. 65 (2014) 202–206. doi:10.1016/j.renene.2013.08.043.

[6] S. Ji, I. Chang, Y.H. Lee, J. Park, J.Y. Paek, M.H. Lee, et al., Fabrication of low-temperature solid oxide fuel cells with a nanothin protective layer by atomic layer deposition., Nanoscale Res. Lett. 8 (2013) 48. doi:10.1186/1556-276X-8-48.

[7] G.Y. Cho, Y.H. Lee, S.W. Cha, Multi-component nano-composite electrode for SOFCS via thin film technique, Renew. Energy. 65 (2014) 130–136.

[8] K. Bae, K.S. Son, J.W. Kim, S.W. Park, J. An, F.B. Prinz, et al., Proton incorporation in yttria-stabilized zirconia during atomic layer deposition, Int. J. Hydrogen Energy. 39 (2014) 2621–2627. doi:10.1016/j.ijhydene.2013.11.023.

[9] S. Ji, I. Chang, G.Y. Cho, Y.H. Lee, J.H. Shim, S.W. Cha, Application of dense nano-thin platinum films for low-temperature solid oxide fuel cells by atomic layer deposition, Int. J. Hydrogen Energy. (2014).

[10] S. Ji, Y.H. Lee, T. Park, G.Y. Cho, S. Noh, Y. Lee, et al., Doped ceria anode interlayer for low-temperature solid oxide fuel cells with nanothin electrolyte, Thin Solid Films. (2015) 1–5. doi:10.1016/j.tsf.2015.05.005.

[11] J. Park, I. Chang, J.Y. Paek, S. Ji, W. Lee, S.W. Cha, et al., Fabrication of the large area thin-film solid oxide fuel cells, CIRP Ann. - Manuf. Technol. 63 (2014) 513–516. doi:10.1016/j.cirp.2014.03.065.

[12] Y. Jee, G.Y. Cho, J. An, H.-R. Kim, J.-W. Son, J.-H. Lee, et al., High performance Bi-layered electrolytes via atomic layer deposition for solid oxide fuel cells, J. Power Sources. 253 (2014) 114–122. doi:10.1016/j.jpowsour.2013.12.001.

[13] S. Kang, I. Chang, Y.-B. Kim, S.W. Cha, Influence of a platinum functional layer on a Ni-Ce0.9Gd0.1O1.95 anode for thin-film solid oxide fuel cells, J. Vac. Sci. Technol. A Vacuum, Surfaces, Film. 33 (2015) 05E120. doi:10.1116/1.4927160.

[14] S. Noh, G.Y. Cho, Y.H. Lee, W. Yu, J. An, S.W. Cha, Performance Enhancement in thin film solid oxide fuel cells using metal-mixed ionic electronic conductors bilayer anode, 7 (2015) 1–6. doi:10.1166/sam.2015.2589.

[15] J. Park, Y. Lee, I. Chang, W. Lee, S.W. Cha, Engineering of the electrode structure of thin film solid oxide fuel cells, Thin Solid Films. 584 (2015) 125–129. doi:10.1016/j.tsf.2014.11.018.

[16] D.Y. Jang, H.K. Kim, J.W. Kim, K. Bae, M.V.F. Schlupp, S.W. Park, et al., Low-temperature performance of yttria-stabilized zirconia prepared by atomic layer deposition, J. Power Sources. 274 (2015) 611–618. doi:10.1016/j.jpowsour.2014.10.022.

[17] S. Ji, G.Y. Cho, W. Yu, P. Su, M.H. Lee, S.W. Cha, Plasma-Enhanced Atomic Layer Deposition of Nanoscale Yttria-Stabilized Zirconia Electrolyte for Solid Oxide Fuel Cells with Porous Substrate, 7 (2015) 2998–3002. doi:10.1021/am508710s.

[18] H. Choi, G.Y. Cho, S.W. Cha, Fabrication and characterization of anode supported YSZ/GDC bilayer electrolyte SOFC using dry press process, Int. J. Precis. Eng. Manuf. - Green Technol. 1 (2014) 95–99. doi:10.1007/s40684-014-0013-4.

[19] S. Ha, P.-C. Su, S.-W. Cha, Combinatorial deposition of a dense nano-thin film YSZ electrolyte for low temperature solid oxide fuel cells, J. Mater. Chem. A. 1 (2013) 9645. doi:10.1039/c3ta11758h.

[20] J.H. Shim, Y.B. Kim, J.S. Park, J. An, T.M. Gür, F.B. Prinz, Patterned Silver Nanomesh Cathode for Low-Temperature Solid Oxide Fuel Cells, J. Electrochem. Soc. 159 (2012) B541. doi:10.1149/2.059205jes.

[21] J.H. Shim, C.C. Chao, H. Huango, F.B. Prinz, Atomic layer deposition of yttria-stabilized zirconia for solid oxide fuel cells, Chem. Mater. 19 (2007) 3850–3854. http://www.scopus.com/scopus/inward/record.url?eid=2-

s2.0-34547653583&partnerID=40&rel=R6.5.0.

[22] J.S. Park, Y.B. Kim, J.H. Shim, S. Kang, T.M. Gür, F.B. Prinz, Evidence of proton transport in atomic layer deposited yttria-stabilized zirconia films, Chem. Mater. 22 (2010) 5366–5370. doi:10.1021/cm1017536.

[23] W. Lee, H.J. Jung, M.H. Lee, Y.B. Kim, J.S. Park, R. Sinclair, et al., Oxygen surface exchange at grain boundaries of oxide ion conductors, Adv. Funct. Mater. 22 (2012) 965–971. doi:10.1002/adfm.201101996.

[24] J.H. Shim, J.S. Park, T.P. Holme, K. Crabb, W. Lee, Y.B. Kim, et al., Enhanced oxygen exchange and incorporation at surface grain boundaries on an oxide ion conductor, Acta Mater. 60 (2012) 1–7. doi:10.1016/j.actamat.2011.09.050.

[25] S. Kang, P.C. Su, Y.I. Park, Y. Saito, F.B. Prinz, Thin-Film Solid Oxide Fuel Cells on Porous Nickel Substrates with Multistage Nanohole Array, J. Electrochem. Soc. 153 (2006) A554. doi:10.1149/1.2164769.

[26] J.H. Shim, J.S. Park, J. An, T.M. Gür, S. Kang, F.B. Prinz, Intermediate-temperature ceramic fuel cells with thin film yttrium-doped barium zirconate electrolytes, Chem. Mater. 21 (2009) 3290–3296. doi:10.1021/cm900820p.

[27] Y.B. Kim, C.-M. Hsu, S.T. Connor, T.M. Gür, Y. Cui, F.B. Prinz, Nanopore Patterned Pt Array Electrodes for Triple Phase Boundary Study in Low Temperature SOFC, J. Electrochem. Soc. 157 (2010) B1269. doi:10.1149/1.3455046.

[28] J. An, Y.B. Kim, J. Park, T.M. Gür, F.B. Prinz, Three-dimensional nanostructured bilayer solid oxide fuel cell with 1.3 W/cm2 at 450 oC, Nano Lett. 13 (2013) 4551–4555.

doi:10.1021/nl402661p.

[29] J.H. Shim, X. Jiang, S.F. Bent, F.B. Prinz, Catalysts with Pt Surface Coating by Atomic Layer Deposition for Solid Oxide Fuel Cells ALD Pt (~ 3nm), (2010). doi:10.1149/1.3368787.

[30] J. An, Y. Beom Kim, J. Sun Park, J. Hyung Shim, T.M. Gür, F.B. Prinz, Fluorine contamination in yttrium-doped barium zirconate film deposited by atomic layer deposition, J. Vac. Sci. Technol. A Vacuum, Surfaces, Film. 30 (2012) 01A161. doi:10.1116/1.3670750.

[31] J. An, Y.-B. Kim, F.B. Prinz, Ultra-thin platinum catalytic electrodes fabricated by atomic layer deposition, Phys. Chem. Chem. Phys. 15 (2013) 7520–5. doi:10.1039/c3cp50996f.

[32] P. Su, C. Chao, J.H. Shim, R. Fasching, F.B. Prinz, Solid Oxide Fuel Cell with Corrugated Thin Film Electrolyte 2008, Nano Lett. 8 (2008) 2289–2292.

[33] Y.B. Kim, J.S. Park, T.M. Gür, F.B. Prinz, Oxygen activation over engineered surface grains on YDC/YSZ interlayered composite electrolyte for LT-SOFC, J. Power Sources. 196 (2011) 10550–10555. doi:10.1016/j.jpowsour.2011.08.075.

[34] Y.B. Kim, J.H. Shim, T.M. Gür, F.B. Prinz, Epitaxial and Polycrystalline Gadolinia-Doped Ceria Cathode Interlayers for Low Temperature Solid Oxide Fuel Cells, J. Electrochem. Soc. 158 (2011) B1453. doi:10.1149/2.001112jes.

[35] H. Huang, C.-H. Hsieh, N. Kim, J. Stebbins, F. Prinz, Structure, local environment, and ionic conduction in scandia stabilized zirconia, Solid State Ionics. 179 (2008) 1442–1445. doi:10.1016/j.ssi.2008.02.061.

[36] J.H. Shim, S. Kang, S.W. Cha, W. Lee, Y.B. Kim, J.S. Park, et al., Atomic layer deposition of thin-film ceramic electrolytes for high-performance fuel cells, J. Mater. Chem. A. 1 (2013) 12695–12705. doi:10.1039/c3ta11399j.

[37] J.S. Park, Y.B. Kim, J. An, F.B. Prinz, Oxygen diffusion across the grain boundary in bicrystal yttria stabilized zirconia, Solid State Commun. 152 (2012) 2169–2171. doi:10.1016/j.ssc.2012.09.019.

[38] J. An, Y.B. Kim, T.M. G??r, F.B. Prinz, Enhancing charge transfer kinetics by nanoscale catalytic cermet interlayer, ACS Appl. Mater. Interfaces. 4 (2012) 6790–6795.

[39] Y.B. Kim, T.M. Gür, H.J. Jung, S. Kang, R. Sinclair, F.B. Prinz, Effect of crystallinity on proton conductivity in yttrium-doped barium zirconate thin films, Solid State Ionics. 198 (2011) 39–46. doi:10.1016/j.ssi.2011.07.004.

[40] Z. Fan, J. An, A. Iancu, F.B. Prinz, Thickness effects of yttria-doped ceria interlayers on solid oxide fuel cells, J. Power Sources. 218 (2012) 187–191. doi:10.1016/j.jpowsour.2012.06.103.

[41] C.-C. Chao, Y.B. Kim, F.B. Prinz, Surface modification of yttria-stabilized zirconia electrolyte by atomic layer deposition., Nano Lett. 9 (2009) 3626–3628. doi:10.1021/nl901724j.

[42] H. Huang, J.H. Shim, C.-C. Chao, R. Pornprasertsuk, M. Sugawara, T.M. Gür, et al., Characteristics of Oxygen Reduction on Nanocrystalline YSZ, J. Electrochem. Soc. 156 (2009) B392. doi:10.1149/1.3058597.

[43] C.C. Chao, J.S. Park, X. Tian, J.H. Shim, T.M. Gür, F.B. Prinz,

Enhanced oxygen exchange on surface-engineered yttria-stabilized zirconia, ACS Nano. 7 (2013) 2186–2191. doi:10.1021/nn305122f.

[44] J. Bae, S. Hong, B. Koo, J. An, F.B. Prinz, Y.B. Kim, Influence of the grain size of samaria-doped ceria cathodic interlayer for enhanced surface oxygen kinetics of low-temperature solid oxide fuel cell, J. Eur. Ceram. Soc. 34 (2014) 3763–3768. doi:10.1016/j.jeurceramsoc.2014.05.028.

[45] S. Hong, J. Bae, B. Koo, Y.-B. Kim, High-performance ultra-thin film solid oxide fuel cell using anodized-aluminum-oxide supporting structure, Electrochem. Commun. 47 (2014) 1–4. doi:10.1016/j.elecom.2014.07.008.

[46] Y. Takagi, S. Adam, S. Ramanathan, Nanostructured ruthenium – Gadolinia-doped ceria composite anodes for thin film solid oxide fuel cells, J. Power Sources. 217 (2012) 543–553. doi:10.1016/j.jpowsour.2012.06.060.

[47] H. Xiong, B.-K. Lai, A.C. Johnson, S. Ramanathan, Low-temperature electrochemical characterization of dense ultra-thin lanthanum strontium cobalt ferrite ($La_{0.6}Sr_{0.4}Co_{0.8}Fe_{0.2}O_3$) cathodes synthesized by RF-sputtering on nanoporous alumina-supported Y-doped zirconia membranes, J. Power Sources. 193 (2009) 589–592. doi:10.1016/j.jpowsour.2009.04.024.

[48] T. Cain, B.-K. Lai, S. Sankaranarayanan, S. Ramanathan, Photo-excitation enhanced high temperature conductivity and crystallization kinetics in ultra-thin $La_{0.6}Sr_{0.4}Co_{0.8}Fe_{0.2}O_{3-\delta}$ films, J. Power Sources. 195 (2010) 3145–3148. doi:10.1016/j.jpowsour.2009.11.106.

[49] C. Ko, K. Kerman, S. Ramanathan, Ultra-thin film solid oxide fuel cells utilizing un-doped nanostructured zirconia

electrolytes, J. Power Sources. 213 (2012) 343–349. doi:10.1016/j.jpowsour.2012.04.034.

[50] M. Tsuchiya, B.K. Lai, A.C. Johnson, S. Ramanathan, Photon–assisted synthesis of ultra–thin yttria–doped zirconia membranes: Structure, variable temperature conductivity and micro–fuel cell devices, J. Power Sources. 195 (2010) 994–1000. doi:10.1016/j.jpowsour.2009.08.072.

[51] B.–K. Lai, K. Kerman, S. Ramanathan, On the role of ultra–thin oxide cathode synthesis on the functionality of micro–solid oxide fuel cells: Structure, stress engineering and in situ observation of fuel cell membranes during operation, J. Power Sources. 195 (2010) 5185–5196. doi:10.1016/j.jpowsour.2010.02.079.

[52] Y. Takagi, B.–K. Lai, K. Kerman, S. Ramanathan, Low temperature thin film solid oxide fuel cells with nanoporous ruthenium anodes for direct methane operation, Energy Environ. Sci. 4 (2011) 3473. doi:10.1039/c1ee01310f.

[53] K. Kerman, B.K. Lai, S. Ramanathan, Nanoscale compositionally graded thin–film electrolyte membranes for low–temperature solid oxide fuel cells, Adv. Energy Mater. 2 (2012) 656–661. doi:10.1002/aenm.201100751.

[54] A.C. Johnson, B.–K. Lai, H. Xiong, S. Ramanathan, An experimental investigation into micro–fabricated solid oxide fuel cells with ultra–thin La0.6Sr0.4Co0.8Fe0.2O3 cathodes and yttria–doped zirconia electrolyte films, J. Power Sources. 186 (2009) 252–260. doi:10.1016/j.jpowsour.2008.10.021.

[55] K. Kerman, B.–K. Lai, S. Ramanathan, Thin film nanocrystalline Ba0.5Sr0.5Co0.8Fe0.2O3: Synthesis, conductivity, and micro–solid oxide fuel cells, J. Power Sources. 196 (2011) 6214–6218.

doi:10.1016/j.jpowsour.2011.03.049.

[56] K. Kerman, S. Xuza, S. Ramanathan, Free standing yttria-doped zirconia membranes: Geometrical effects on stability, J. Electroceramics. (2014) 91–99. doi:10.1007/s10832-014-9917-1.

[57] M. Tsuchiya, B. Lai, S. Ramanathan, Scalable nanostructured membranes for solid-oxide fuel cells, Nat. Nanotechnol. 6 (2011) 282–286. doi:10.1038/nnano.2011.43.

[58] Y. Takagi, K. Kerman, C. Ko, S. Ramanathan, Operational characteristics of thin film solid oxide fuel cells with ruthenium anode in natural gas, J. Power Sources. 243 (2013) 1–9. doi:10.1016/j.jpowsour.2013.06.002.

[59] K. Kerman, S. Ramanathan, Performance of solid oxide fuel cells approaching the two-dimensional limit, J. Appl. Phys. 115 (2014) 174307. doi:10.1063/1.4874738.

[60] K. Kerman, B.-K. Lai, S. Ramanathan, Pt/Y0.16Zr0.84O1.92/Pt thin film solid oxide fuel cells: Electrode microstructure and stability considerations, J. Power Sources. 196 (2011) 2608–2614. doi:10.1016/j.jpowsour.2010.10.068.

[61] H.-S. Noh, J.-W. Son, H. Lee, H.-S. Song, H.-W. Lee, J.-H. Lee, Low Temperature Performance Improvement of SOFC with Thin Film Electrolyte and Electrodes Fabricated by Pulsed Laser Deposition, J. Electrochem. Soc. 156 (2009) B1484. doi:10.1149/1.3243859.

[62] H.-S. Noh, J.-S. Park, J.-W. Son, H. Lee, J.-H. Lee, H.-W. Lee, Physical and Microstructural Properties of NiO- and Ni-YSZ Composite Thin Films Fabricated by Pulsed-Laser

Deposition at T â‰¤700Â°C, J. Am. Ceram. Soc. 92 (2009) 3059–3064. doi:10.1111/j.1551-2916.2009.03362.x.

[63] E.O. Oh, C.M. Whang, Y.R. Lee, J.H. Lee, K.J. Yoon, B.K. Kim, et al., Thin film yttria-stabilized zirconia electrolyte for intermediate-temperature solid oxide fuel cells (IT-SOFCs) by chemical solution deposition, J. Eur. Ceram. Soc. 32 (2012) 1733–1741. doi:10.1016/j.jeurceramsoc.2012.01.021.

[64] C.-W. Kwon, J.-I. Lee, K.-B. Kim, H.-W. Lee, J.-H. Lee, J.-W. Son, The thermomechanical stability of micro-solid oxide fuel cells fabricated on anodized aluminum oxide membranes, J. Power Sources. 210 (2012) 178–183. doi:10.1016/j.jpowsour.2012.03.020.

[65] E.-O. Oh, C.-M. Whang, Y.-R. Lee, S.-Y. Park, D.H. Prasad, K.J. Yoon, et al., Extremely thin bilayer electrolyte for solid oxide fuel cells (SOFCs) fabricated by chemical solution deposition (CSD)., Adv. Mater. 24 (2012) 3373–7. doi:10.1002/adma.201200505.

[66] H.S. Noh, J.W. Son, H. Lee, H. Il Ji, J.H. Lee, H.W. Lee, Suppression of Ni agglomeration in PLD fabricated Ni-YSZ composite for surface modification of SOFC anode, J. Eur. Ceram. Soc. 30 (2010) 3415–3423. doi:10.1016/j.jeurceramsoc.2010.07.035.

[67] H.-R. Kim, J.-C. Kim, K.-R. Lee, H.-I. Ji, H.-W. Lee, J.-H. Lee, et al., “Illusional” nano-size effect due to artifacts of in-plane conductivity measurements of ultra-thin films., Phys. Chem. Chem. Phys. 13 (2011) 6133–6137. doi:10.1039/c0cp02673e.

[68] H. Noh, J. Hong, H. Kim, K.J. Yoon, J. Lee, B. Kim, et al., Sandwiched ultra-thin yttria-stabilized zirconia layer to effectively and reliably block reduction of thin- fi lm

gadolinia–doped ceria electrolyte, (2015) 263–267.

[69] a. Evans, M. Prestat, R. Tölke, M.V.F. Schlupp, L.J. Gauckler, Y. Safa, et al., Residual Stress and Buckling Patterns of Free–standing Yttria–stabilized–zirconia Membranes Fabricated by Pulsed Laser Deposition, Fuel Cells. 12 (2012) 614–623. doi:10.1002/fuce.201200028.

[70] B.E. Buergler, a. N. Grundy, L.J. Gauckler, Thermodynamic Equilibrium of Single–Chamber SOFC Relevant Methane–Air Mixtures, J. Electrochem. Soc. 153 (2006) A1378. doi:10.1149/1.2201546.

[71] a. Bieberle–Hütter, a. J. Santis–Alvarez, B. Jiang, P. Heeb, T. Maeder, M. Nabavi, et al., Syngas generation from n–butane with an integrated MEMS assembly for gas processing in micro–solid oxide fuel cell systems, Lab Chip. 12 (2012) 4894. doi:10.1039/c2lc40809k.

[72] A. Evans, A. Bieberle–Hütter, J.L.M. Rupp, L.J. Gauckler, Review on microfabricated micro–solid oxide fuel cell membranes, J. Power Sources. 194 (2009) 119–129. doi:10.1016/j.jpowsour.2009.03.048.

[73] B. Scherrer, M.V.F. Schlupp, D. Stender, J. Martynczuk, J.G. Grolig, H. Ma, et al., On Proton Conductivity in Porous and Dense Yttria Stabilized Zirconia at Low Temperature, Adv. Funct. Mater. (2012) n/a–n/a. doi:10.1002/adfm.201202020.

[74] C. Meier, T. Hocker, A. Bieberle–Hütter, L.J. Gauckler, Analyzing a micro–solid oxide fuel cell system by global energy balances, Int. J. Hydrogen Energy. 37 (2012) 10318–10327. doi:10.1016/j.ijhydene.2012.04.009.

[75] B. Scherrer, J. Martynczuk, H. Galinski, J.G. Grolig, S. Binder,

A. Bieberle-Hütter, et al., Microstructures of YSZ and CGO Thin Films Deposited by Spray Pyrolysis: Influence of Processing Parameters on the Porosity, Adv. Funct. Mater. 22 (2012) 3509–3518. doi:10.1002/adfm.201200454.

[76] S. Heiroth, T. Lippert, a. Wokaun, M. Döbeli, J.L.M. Rupp, B. Scherrer, et al., Yttria-stabilized zirconia thin films by pulsed laser deposition: Microstructural and compositional control, J. Eur. Ceram. Soc. 30 (2010) 489–495. doi:10.1016/j.jeurceramsoc.2009.06.012.

[77] R. Frison, S. Heiroth, J.L.M. Rupp, K. Conder, E.J. Barthazy, E. Müller, et al., Crystallization of 8 mol% yttria-stabilized zirconia thin-films deposited by RF-sputtering, Solid State Ionics. 232 (2013) 29–36. doi:10.1016/j.ssi.2012.11.014.

[78] N.I. Karageorgakis, A. Heel, J.L.M. Rupp, M.H. Aguirre, T. Graule, L.J. Gauckler, Properties of Flame Sprayed Ce0.8Gd0.2O1.9-δ Electrolyte Thin Films, Adv. Funct. Mater. 21 (2011) 532–539. doi:10.1002/adfm.201001622.

[79] D. Beckel, a Bieberle-Huetter, a Harvey, a Infortuna, U.P. Muecke, M. Prestat, et al., Thin films for micro solid oxide fuel cells, J. Power Sources. 173 (2007) 325–345. doi:10.1016/j.jpowsour.2007.04.070.

[80] T. Ryll, J.L.M. Rupp, A. Bieberle-Hutter, H. Galinski, L.J. Gauckler, Characterization of thin films for solid oxide fuel cells facilitated by micropatterning, Scr. Mater. 65 (2011) 84–89. doi:10.1016/j.scriptamat.2010.09.022.

[81] A. Evans, A. Bieberle-H??tter, H. Galinski, J.L.M. Rupp, T. Ryll, B. Scherrer, et al., Micro-solid oxide fuel cells: Status, challenges, and chances, Monatshefte Fur Chemie. 140 (2009) 975–983. doi:10.1007/s00706-009-0107-9.

[82] A. Evans, A. Bieberle-Hütter, L.J. Bonderer, S. Stuckenholz, L.J. Gauckler, Micro-solid oxide fuel cells using free-standing 3mol.% yttria-stabilised-tetragonal-zirconia-polycrystal electrolyte foils, J. Power Sources. 196 (2011) 10069–10073. doi:10.1016/j.jpowsour.2011.07.087.

[83] M.V.F. Schlupp, M. Prestat, J. Martynczuk, J.L.M. Rupp, a. Bieberle-Hütter, L.J. Gauckler, Thin film growth of yttria stabilized zirconia by aerosol assisted chemical vapor deposition, J. Power Sources. 202 (2012) 47–55. doi:10.1016/j.jpowsour.2011.11.016.

[84] D. Perednis, O. Wilhelm, S.E. Pratsinis, L.J. Gauckler, Morphology and deposition of thin yttria-stabilized zirconia films using spray pyrolysis, Thin Solid Films. 474 (2005) 84–95. doi:10.1016/j.tsf.2004.08.014.

[85] Y.D. Lee, K.Y. Ahn, T. Morosuk, G. Tsatsaronis, Environmental impact assessment of a solid-oxide fuel-cell-based combined-heat-and-power-generation system, Energy. 79 (2015) 455–466. doi:10.1016/j.energy.2014.11.035.

[86] A. Buonomano, F. Calise, M.D. d'Accadia, A. Palombo, M. Vicidomini, Hybrid solid oxide fuel cells–gas turbine systems for combined heat and power: A review, Appl. Energy. 156 (2015) 32–85. doi:10.1016/j.apenergy.2015.06.027.

[87] S. Sanna, V. Esposito, A. Tebano, S. Licoccia, E. Traversa, G. Balestrino, Enhancement of ionic conductivity in sm-doped ceria/yttria-stabilized zirconia heteroepitaxial structures, Small. 6 (2010) 1863–1867. doi:10.1002/smll.200902348.

[88] S. Kim, J. Maier, Partial electronic and ionic conduction in nanocrystalline ceria: role of space charge, J. Eur. Ceram. Soc. 24 (2004) 1919–1923. doi:10.1016/S0955-2219(03)00525-

9.

[89] T. Mukai, S. Tsukui, K. Yoshida, S. Yamaguchi, R. Hatayama, M. Adachi, et al., Fabrication of Y 2 O 3 −Doped Zirconia/Gadolinia−Doped Ceria Bilayer Electrolyte Thin Film SOFC Cells of SOFCs by Single−Pulsed Laser Deposition Processing, J. Fuel Cell Sci. Technol. 10 (2013) 061006. doi:10.1115/1.4025064.

[90] J. Joo, G. Choi, Open−circuit voltage of ceria−based thin film SOFC supported on nano−porous alumina, Solid State Ionics. 178 (2007) 1602–1607. doi:10.1016/j.ssi.2007.10.006.

[91] C. Brahim, a. Ringuedé, E. Gourba, M. Cassir, a. Billard, P. Briois, Electrical properties of thin bilayered YSZ/GDC SOFC electrolyte elaborated by sputtering, J. Power Sources. 156 (2006) 45–49. doi:10.1016/j.jpowsour.2005.08.017.

[92] Y. Yamazaki, R. Hernandez−Sanchez, S.M. Haile, Cation non−stoichiometry in yttrium−doped barium zirconate: phase behavior, microstructure, and proton conductivity, J. Mater. Chem. 20 (2010) 8158. doi:10.1039/c0jm02013c.

[93] S. Ha, P.−C. Su, S. Ji, S.W. Cha, Low temperature solid oxide fuel cells with proton−conducting Y:BaZrO3 electrolyte on porous anodic aluminum oxide substrate, Thin Solid Films. 544 (2013) 125–128. doi:10.1016/j.tsf.2013.04.058.

[94] M. Putkonen, T. Sajavaara, J. Niinistö, L.−S. Johansson, L. Niinistö, Deposition of yttria−stabilized zirconia thin films by atomic layer epitaxy from β−diketonate and organometallic precursors, J. Mater. Chem. 12 (2002) 442–448. doi:10.1039/b107799f.

[95] T. Hirai, K. Teramoto, K. Nagashima, H. Koike, S. Matsuno, S.

Tanimoto, et al., Crystal and electrical characterizations of oriented yttria-stabilized zirconia buffer layer for the metal/ferroelectric/insulator/semiconductor field-effect transistor, Japanese J. Appl. Physics, Part 1 Regul. Pap. Short Notes Rev. Pap. 35 (1996) 4016–4020. doi:10.1143/JJAP.35.4016.

[96] T. Kouji, H. Hoshi, Fabrication of PbTiO 3 /Pt/Yttria Stabilized ZrO 2 Heteroepitaxial Films on Si Substrate, Appl. Phys. 39 (2000) 5399–5402.

[97] Y.J. Tian, S. Linzen, F. Schmidl, a Matthes, H. Schneidewind, P. Seidel, On ageing and critical thickness of YBa 2 Cu 3 O 7 films on Si with CeO 2 / YSZ buffer layers, Thin Solid Films. 338 (1999) 224–230. doi:10.1088/0953-2048/16/7/305.

[98] J. Qiao, C.Y. Yang, High-Tc superconductors on buffered properties and device applications silicon : materials properties and device applications, Mater. Sci. Eng. (1995) 157–202.

[99] K. Yasuda, S. Suenaga, H. Inagaki, Y. Goto, H. Takeda, K. Wada, Relationship between microstructure of plasma-sprayed 8YZ coatings and thermal fatigue life of thermal barrier coatings, J. Mater. Sci. 35 (2000) 317–321. doi:10.1023/A:1004745301833.

[100] L.S. Wang, S.A. Barnett, Deposition, Structure, and Properties of Cermeet Thin Films Composed of Ag and Y-stabilized Zriconia, J. Elect. 139 (1992) 1134–1140.

[101] P. Peshev, V. Slavova, Preparation of Yttria-stabilized Zirconia thin films by a sol-gel procedure using alkoxide precursors, Mater. Res. Bull. 27 (1992) 1269–1275.

[102] P. Majumder, G. Jursich, A. Kueltzo, C. Takoudis, Atomic Layer Deposition of Y[sub 2]O[sub 3] Films on Silicon Using Tris(ethylcyclopentadienyl) Yttrium Precursor and Water Vapor, J. Electrochem. Soc. 155 (2008) G152. doi:10.1149/1.2929825.

[103] J. Jiang, X. Hu, N. Ye, J.L. Hertz, Microstructure and ionic conductivity of yttria–stabilized zirconia thin films deposited on MgO, J. Am. Ceram. Soc. 97 (2014) 1131–1136. doi:10.1111/jace.12740.

[104] J. Jiang, D. Clark, W. Shen, J.L. Hertz, The effects of substrate surface structure on yttria–stabilized zirconia thin films, Appl. Surf. Sci. 293 (2014) 191–195. doi:10.1016/j.apsusc.2013.12.131.

[105] J. Jiang, J.L. Hertz, On the variability of reported ionic conductivity in nanoscale YSZ thin films, J. Electroceramics. 32 (2014) 37–46. doi:10.1007/s10832-013-9857-1.

[106] A. Karthikeyan, C.L. Chang, S. Ramanathan, High temperature conductivity studies on nanoscale yttria–doped zirconia thin films and size effects, Appl. Phys. Lett. 89 (2006). doi:10.1063/1.2385211.

[107] E. Navickas, M. Gerstl, F. Kubel, J. Fleig, Simultaneous Measurement of the In- and Across-Plane Ionic Conductivity of YSZ Thin Films, J. Electrochem. Soc. 159 (2012) B411. doi:10.1149/2.081204jes.

[108] H.B. Profijt, S.E. Potts, M.C.M. van de Sanden, W.M.M. Kessels, Plasma-Assisted Atomic Layer Deposition: Basics, Opportunities, and Challenges, J. Vac. Sci. Technol. A Vacuum, Surfaces, Film. 29 (2011) 050801. doi:10.1116/1.3609974.

[109] H. Kim, H.B.R. Lee, W.J. Maeng, Applications of atomic layer deposition to nanofabrication and emerging nanodevices, Thin Solid Films. 517 (2009) 2563–2580. doi:10.1016/j.tsf.2008.09.007.

[110] H. Kim, Characteristics and applications of plasma enhanced-atomic layer deposition, Thin Solid Films. 519 (2011) 6639–6644. doi:10.1016/j.tsf.2011.01.404.

[111] C. Marichy, M. Bechelany, N. Pinna, Atomic layer deposition of nanostructured materials for energy and environmental applications., Adv. Mater. 24 (2012) 1017–32. doi:10.1002/adma.201104129.

[112] N. Pinna, M. Knez, Atomic layer deposition of nanostructured materials, John Wiley & Sons, 2012.

[113] C. Kwon, J. Son, J. Lee, H. Kim, H. Lee, K. Kim, High-Performance Micro-Solid Oxide Fuel Cells Fabricated on Nanoporous Anodic Aluminum Oxide Templates, (2011) 1154–1159. doi:10.1002/adfm.201002137.

[114] W. Yu, S. Ji, G.Y. Cho, S. Noh, W.H. Tanveer, J. An, et al., Atomic layer deposition of ultrathin blocking layer for low-temperature solid oxide fuel cell on nanoporous substrate, J. Vac. Sci. Technol. A Vacuum, Surfaces, Film. 145 (2015). doi:10.1116/1.4904206.

[115] K. Sik Son, K. Bae, J. Woo Kim, J. Suk Ha, J. Hyung Shim, Ion conduction in nanoscale yttria-stabilized zirconia fabricated by atomic layer deposition with various doping rates, J. Vac. Sci. Technol. A Vacuum, Surfaces, Film. 31 (2013) 01A107. doi:10.1116/1.4755921.

[116] B.C. Steele, A. Heinzel, Materials for fuel-cell technologies.,

Nature. 414 (2001) 345–352. doi:10.1038/35104620.

[117] J. An, T. Usui, M. Logar, J. Park, D. Thian, S. Kim, et al., Plasma Processing for Crystallization and Densification of ALD BaTiO3 Thin Films., ACS Appl. Mater. Interfaces. (2014). doi:10.1021/am502298z.

[118] S. Heiroth, T. Lippert, a. Wokaun, M. Döbeli, Microstructure and electrical conductivity of YSZ thin films prepared by pulsed laser deposition, Appl. Phys. A. 93 (2008) 639–643. doi:10.1007/s00339-008-4689-6.

[119] X. Guo, J. Maier, Grain Boundary Blocking Effect in Zirconia: A Schottky Barrier Analysis, J. Electrochem. Soc. 148 (2001) E121. doi:10.1149/1.1348267.

[120] T.H. Yeh, R. De Lin, J.S. Cherng, Significantly enhanced ionic conductivity of yttria-stabilized zirconia polycrystalline nano-film by thermal annealing, Thin Solid Films. 544 (2013) 148–151. doi:10.1016/j.tsf.2013.03.134.

[121] W. Jung, J.L. Hertz, H.L. Tuller, Enhanced ionic conductivity and phase meta-stability of nano-sized thin film yttria-doped zirconia (YDZ), Acta Mater. 57 (2009) 1399–1404. doi:10.1016/j.actamat.2008.11.028.

[122] D.M. Mattox, Handbook of physical vapor deposition (PVD) processing, William Andrew, 2010.

[123] R. Pornprasertsuk, T. Holme, F.B. Prinz, Kinetic Monte Carlo Simulations of Solid Oxide Fuel Cell, J. Electrochem. Soc. 156 (2009) B1406. doi:10.1149/1.3232209.

[124] D. Chan Won, S.-W. Rhee, Effect of process temperature on the structural and electrical properties of atomic layer

deposited ZrO2 films using tris(dimethylamino) cyclopentadienyl zirconium precursor, J. Vac. Sci. Technol. B Microelectron. Nanom. Struct. 32 (2014) 03D102. doi:10.1116/1.4825109.

[125] Y. Duan, F. Sun, Y. Yang, P. Chen, D. Yang, Y. Duan, et al., Thin-film barrier performance of zirconium oxide using the low-temperature atomic layer deposition method., ACS Appl. Mater. Interfaces. 6 (2014) 3799–804. doi:10.1021/am500288q.

[126] Y.B. Kim, T.P. Holme, T.M. Gür, F.B. Prinz, Surface-modified low-temperature solid oxide fuel cell, Adv. Funct. Mater. 21 (2011) 4684–4690. doi:10.1002/adfm.201101058.

[127] H. Xu, D. Luo, M. Li, M. Xu, J. Zou, H. Tao, et al., A flexible AMOLED display on the PEN substrate driven by oxide thin-film transistors using anodized aluminium oxide as dielectric, J. Mater. Chem. C. 2 (2014) 1255–1259. doi:10.1039/C3TC31710B.

[128] Z. Wang, Z. Wu, N. Bramnik, S. Mitra, Fabrication of High-Performance Flexible Alkaline Batteries by Implementing Multiwalled Carbon Nanotubes and Copolymer Separator, Adv. Mater. 26 (2014) 970–976. doi:10.1002/adma.201304020.

[129] I. Chang, T. Park, J. Lee, M.H. Lee, S.H. Ko, S.W. Cha, Bendable polymer electrolyte fuel cell using highly flexible Ag nanowire percolation network current collectors, J. Mater. Chem. A. 1 (2013) 8541. doi:10.1039/c3ta11699a.

[130] J. Yun, W. Wang, S.M. Kim, T.-S. Bae, S. Lee, D. Kim, et al., Light trapping in bendable organic solar cells using silica nanoparticle arrays, Energy Environ. Sci. 8 (2015) 932–940. doi:10.1039/C4EE01100G.

[131] D.H. Levy, D. Freeman, S.F. Nelson, P.J. Cowdery-Corvan, L.M. Irving, Stable ZnO thin film transistors by fast open air atomic layer deposition, Appl. Phys. Lett. 92 (2008) 192101. doi:10.1063/1.2924768.

[132] S. Bang, S. Lee, S. Jeon, S. Kwon, W. Jeong, H. Kim, et al., Al $_2$ O $_3$ buffer in a ZnO thin film transistor with poly-4-vinylphenol dielectric, Semicond. Sci. Technol. 24 (2009) 025008. doi:10.1088/0268-1242/24/2/025008.

[133] C.-Y. Chang, F.-Y. Tsai, S.-J. Jhuo, M.-J. Chen, Enhanced OLED performance upon photolithographic patterning by using an atomic-layer-deposited buffer layer, Org. Electron. 9 (2008) 667–672. doi:10.1016/j.orgel.2008.04.009.

[134] M.D. Groner, F.H. Fabreguette, J.W. Elam, S.M. George, Low-Temperature Al2O3 Atomic Layer Deposition, Chem. Mater. 16 (2004) 639–645. doi:10.1021/cm0304546.

[135] D.M. King, X. Liang, P. Li, A.W. Weimer, Low-temperature atomic layer deposition of ZnO films on particles in a fluidized bed reactor, Thin Solid Films. 516 (2008) 8517–8523. doi:10.1016/j.tsf.2008.05.026.

[136] M.D. Groner, J.W. Elam, F.H. Fabreguette, S.M. George, Electrical characterization of thin Al2O3 films grown by atomic layer deposition on silicon and various metal substrates, Thin Solid Films. 413 (2002) 186–197. doi:10.1016/S0040-6090(02)00438-8.

[137] C.X. Shan, X. Hou, K.-L. Choy, Corrosion resistance of TiO2 films grown on stainless steel by atomic layer deposition, Surf. Coatings Technol. 202 (2008) 2399–2402. doi:10.1016/j.surfcoat.2007.08.066.

[138] C. Marichy, M. Bechelany, N. Pinna, Atomic Layer Deposition of Nanostructured Materials for Energy and Environmental Applications, Adv. Mater. 24 (2012) 1017–1032. doi:10.1002/adma.201104129.

[139] D. Panda, T.-Y. Tseng, Growth, dielectric properties, and memory device applications of ZrO2 thin films, Thin Solid Films. 531 (2013) 1–20. doi:10.1016/j.tsf.2013.01.004.

[140] X. Zhao, D. Vanderbilt, Phonons and Lattice Dielectric Properties of Zirconia, Phys. Rev. B. 8019 (2001). doi:10.1103/PhysRevB.65.075105.

[141] S.K. Kim, C.S. Hwang, Atomic Layer Deposition of ZrO2 Thin Films with High Dielectric Constant on TiN Substrates, Electrochem. Solid-State Lett. 11 (2008) G9. doi:10.1149/1.2825763.

[142] X. Zhao, D. Ceresoli, D. Vanderbilt, Structural, electronic, and dielectric properties of amorphous Zr O 2 from ab initio molecular dynamics, Phys. Rev. B. 71 (2005) 85107.

[143] S.M. Hwang, S.M. Lee, K. Park, M.S. Lee, J. Joo, J.H. Lim, et al., Effect of annealing temperature on microstructural evolution and electrical properties of sol-gel processed ZrO[sub 2]/Si films, Appl. Phys. Lett. 98 (2011) 022903. doi:10.1063/1.3541784.

[144] Y.-H. Wu, C.-K. Kao, B.-Y. Chen, Y.-S. Lin, M.-Y. Li, H.-C. Wu, High density metal-insulator-metal capacitor based on ZrO[sub 2]/Al[sub 2]O[sub 3]/ZrO[sub 2] laminate dielectric, Appl. Phys. Lett. 93 (2008) 033511. doi:10.1063/1.2958238.

[145] B. Králik, E.K. Chang, S.G. Louie, Structural properties and quasiparticle band structure of zirconia, Phys. Rev. B. 57

(1998) 7027.

[146] H. Search, C. Journals, A. Contact, M. Iopscience, I.P. Address, ZrO2 Gate Dielectric Deposited by Plasma-Enhanced Atomic Layer Deposition Method ZrO 2 Gate Dielectric Deposited by Plasma-Enhanced Atomic Layer Deposition Method, 3043 (n.d.). doi:10.1143/JJAP.41.3043.

[147] J. Koo, Y. Kim, H. Jeon, ZrO2 Gate Dielectric Deposited by Plasma-Enhanced Atomic Layer Deposition Method, Jpn. J. Appl. Phys. 41 (2002) 3043–3046. doi:10.1143/JJAP.41.3043.

[148] S.M. George, Atomic Layer Deposition: An Overview, Chem. Rev. 110 (2010) 111. doi:10.1021/cr900056b.

[149] Y. Yang, Y. Duan, P. Chen, F. Sun, Y. Duan, X. Wang, et al., Realization of Thin Film Encapsulation by Atomic Layer Deposition of Al2O3 at Low Temperature, (2013) 0–4.

[150] S.E. Potts, W. Keuning, E. Langereis, G. Dingemans, M.C.M. van de Sanden, W.M.M. Kessels, Low Temperature Plasma-Enhanced Atomic Layer Deposition of Metal Oxide Thin Films, J. Electrochem. Soc. 157 (2010) P66. doi:10.1149/1.3428705.

[151] S.J. Yun, J.W. Lim, J.H. Lee, Effect of Plasma on Characteristics of Zirconium Oxide Films Deposited by Plasma-Enhanced Atomic Layer Deposition, Electrochem. Solid-State Lett. 8 (2005) F47. doi:10.1149/1.2039952.

[152] G. Dutta, K.P.S.S. Hembram, G.M. Rao, U. V. Waghmare, Effects of O vacancies and C doping on dielectric properties of ZrO[sub 2]: A first-principles study, Appl. Phys. Lett. 89 (2006) 202904. doi:10.1063/1.2388146.

[153] D. Chan Won, S.-W. Rhee, Effect of process temperature on

the structural and electrical properties of atomic layer deposited ZrO2 films using tris(dimethylamino) cyclopentadienyl zirconium precursor, J. Vac. Sci. Technol. B Microelectron. Nanom. Struct. 32 (2014) 03D102. doi:10.1116/1.4825109.

[154] T. Blanquart, J. Niinisto, N. Aslam, M. Banerjee, Y. Tomczak, M. Gavagnin, et al., [Zr(NEtMe) 2 (guan-NEtMe) 2] as a Novel Atomic Layer Deposition Precursor: ZrO 2 Film Growth and Mechanistic Studies, Chem. Mater. 2 (2013) 3088–3095. doi:dx.doi.org/10.1021/cm401279v.

[155] S.J. Yun, J.B. Koo, J.W. Lim, S.H. Kim, Pentacene-Thin Film Transistors with ZrO[sub 2] Gate Dielectric Layers Deposited by Plasma-Enhanced Atomic Layer Deposition, Electrochem. Solid-State Lett. 10 (2007) H90. doi:10.1149/1.2426408.

[156] H. Ishii, A. Nakajima, S. Yokoyama, Growth and electrical properties of atomic-layer deposited ZrO 2/Si-nitride stack gate dielectrics, J. Appl. Phys. 95 (2004) 536–542. doi:10.1063/1.1629773.

[157] M. Putkonen, T. Sajavaara, L.S. Johansson, L. Niinistö, Low-temperature ALE deposition of Y2O3 thin films from β-diketonate precursors, Chem. Vap. Depos. 7 (2001) 44–50. doi:10.1002/1521-3862(200101)7:1<44::AID-CVDE44>3.0.CO;2-Q.

[158] J. Niinistö, M. Putkonen, L. Niinistö, Processing of Y2O3 thin films by atomic layer deposition from cyclopentadienyl-type compounds and water as precursors, Chem. Mater. 16 (2004) 2953–2958. doi:10.1021/cm040145v.

[159] R.J. Gaboriaud, F. Pailloux, P. Guerin, F. Paumier, Yttrium oxide thin films, Y2O3, grown by ion beam sputtering on Si, J. Phys. D. Appl. Phys. 33 (2000) 2884–2889.

[160] P. de Rouffignac, J.-S. Park, R.G. Gordon, Atomic Layer Deposition of Y2O3 Thin Films from Yttrium Tris(N,N'-diisopropylacetamidinate) and Water, Chem. Mater. 17 (2005) 4808–4814. doi:10.1021/cm050624+.

[161] G. Adamopoulos, S. Thomas, D.D.C. Bradley, M. a. McLachlan, T.D. Anthopoulos, Low-voltage ZnO thin-film transistors based on Y2O3 and Al2O3 high-k dielectrics deposited by spray pyrolysis in air, Appl. Phys. Lett. 123503 (2011) 2009–2012. doi:10.1063/1.3568893.

[162] H. Kim, H.-B.-R. Lee, W.-J. Maeng, Applications of atomic layer deposition to nanofabrication and emerging nanodevices, Thin Solid Films. 517 (2009) 2563–2580. doi:10.1016/j.tsf.2008.09.007.

국 문 초 록

본 연구에서는 최초로 플라즈마 원자막 증착기(plasma enhanced atomic layer deposition, PEALD)를 이용하여 제작한 이트리아 안정화 지르코니아(yttria – stabilized zirconia, Y_2O_3 stabilized ZrO_2, YSZ) 박막의 특성을 분석하고, YSZ를 나노 다공성 양극 산화 알루미늄(anodic oxidized aluminum, AAO)지지체 기반의 박막 고체 산화물 연료전지의 산소 이온 전도 박막 전해질로 적용하여 그 가능성을 확인하였다. 또한, PEALD를 이용하여 제작한 지르코니아(ZrO_2)및 이트리아(Y_2O_3)단일물질로 구성된 박막의 화학적, 물리적, 전기적 특성을 분석하였다.

우선, 제조 공정이 박막의 특성에 끼치는 영향을 확인하기 위하여, PEALD YSZ와 일반 열 원자막 증착기 (thermal atomic layer deposition, thermal ALD), 스퍼터를 이용하여 증착한 YSZ 박막의 특성을 비교 분석하였다. PEALD YSZ는 제작과정에서 발생하는 플라즈마 물질 – 활성화 원자, 이온, 전자 – 들의 우수한 반응성과, 플라즈마 물질들의 bombardment에 의한 에너지 공급으로 인해서 thermal ALD YSZ와 스퍼터 YSZ 박막에 비해서 우수한 결정성을 보였고, 오염물질도 거의 없는 것을 확인할 수 있었다. 각 YSZ 박막들의 전기화학적 특성을 비교해보기 위하여 AAO 기반의 박막 고체 산화물 연료전지를 만들어서 특성을 평가하였다. 140 nm 스퍼터 YSZ의 경우 결함(defects)과 핀홀

(pin-hole)로 인해 쇼트(short circuit)가 발생했다. Thermal ALD YSZ의 경우 전해질의 두께와 상관없이 일정한 개회로 전압을 보였는데(~0.8V), 이는 thermal ALD YSZ 내부에 있는 과도한 탄소 오염물질에 의한 누설전류(leakage current)효과로 인한 전압강하라고 생각된다. 반면에 50 W 플라즈마 파워와 3 s 플라즈마 공정 시간을 이용하여 제작한 PEALD YSZ 박막 전해질을 갖는 소자는 500 °C에서 개회로 전압 1.09 V에 168.2 mW/cm^2 의 성능을 보였다.

이후, PEALD 공정의 중요한 변수인 플라즈마 파워와 지속시간이 PEALD YSZ의 특성에 어떠한 영향을 끼치는지 확인해보았다. PEALD YSZ의 화학적 특성 은 플라즈마 파워 혹은 지속시관과 아무런 영향이 없는 것을 확인하였으나, 단결정 MgO (100) 기판위에 제작된 PEALD YSZ 박막의 평면방향(in-plane) 산소이온 전도도는 플라즈마 파워가 증가하고, 지속시간이 길어질수록 향상되는 PEALD YSZ 박막의 결정성으로 인해 개선되었다. 박막 특성 분석 후, PEALD YSZ의 전기화학적 특성을 분석하기 위해, Pt 연료극-PEALD YSZ 박막 전해질-Pt 공기극 구조의 AAO 기반 박막 고체 산화물 연료전지를 제작하고, 특성을 분석하였다. 박막 고체 산화물 연료전지는 각각 450도에서 95.4 mW/cm^2, 그리고 550 도에서 217.5 mW/cm^{2}의 성능을 기록하였다.

YSZ 전해질을 사용하는 박막 고체 산화물 연료전지의 성능을 향상시

키기 위하여 PEALD YSZ 박막의 Y_2O_3 몰 농도 최적화에 관한 연구를 진행하였다. YSZ 제작 공정에서 ZrO_2 와 Y_2O_3 공정의 비율을 변화시켜서 PEALD YSZ 박막의 Y_2O_3 농도를 제어하였다. 그 결과 Y_2O_3 공정 비율이 증가할수록 박막의 Y_2O_3 몰 농도가 최대 32.4 mol. % 까지 증가하였고, 서로 다른 Y_2O_3 몰 농도를 갖는 소자의 전기화학적 특성을 분석하였다. 각 소자들의 전기화학적 특성을 측정한 결과, 10.9 mol. % Y_2O_3를 갖는 박막 고체 산화물 연료전지가 450 °C에서 우수한 성능 (180 mW/cm^2)을 보였다. 이는 연료극과 전해질의 계면, 공기극과 전해질의 계면에 분포한 과량의 Y_2O_3로 인해서 발생한 많은 산소 공극 (oxygen vacancy)이 수소 산화 반응(HOR)과 산소 환원 반응(ORR)을 도와주어서 전기화학반응에서 발생하는 손실을 감소시켰기 때문으로 추측된다.

다음으로 폴리머 기판 혹은 열에 민감한 기판에 사용할 수 있도록 ZrO_2를 PEALD 공정을 이용하여 저온 (100 °C)에서 제작 후 화학적, 물리적, 전기적 특성을 분석했다. 낮은 온도에서 제작되었어도, 플라즈마의 우수한 반응성으로 인해 오염물질이 없는, 다결정 박막을 얻었다. 이후 저온 PEALD 공정으로 증착된 ZrO_2 박막의 유전상수를 금속-절연체-금속 구조를 이용하여 구하였다.

마지막으로, 최초로 PEALD 공정을 이용하여 증착된 Y_2O_3 박막의 화학적, 물리적, 전기적 특성을 평가하였다. 상용 tris

(methylcyclopentadienyl)yttrium ($(MeCp_3)_3Y$) 전구체를 이용하여 PEALD 공정을 진행하였다. 비록 명확한 ALD window가 측정되지는 않았지만, 성장률(growth rate)이 일반 thermal ALD를 이용하여 Y_2O_3를 제작할 때 보다 증가하였고, XPS 분석 결과 Y_2O_3 박막에 탄소와 같은 오염물질도 거의 없는 것을 확인하였다. 마찬가지로 금속-절연체-금속 구조를 이용하여 PEALD 공정으로 제작된 Y_2O_3의 인가 전압에 대한 캐패시턴스 특성을 확인하여 유전상수를 구하였다. PEALD Y_2O_3 의 유전상수는 15~17 의 값을 보였으며, 증착온도에 큰 영향을 받지 않는 것을 확인하였다.

주요어: 플라즈마 원자막 증착법, 원자막 증착법, 이트리아 안정화 지르코니아, 박막 고체산화물 연료전지, 박막, 양극 산화 알루미늄